Master's thesis

NTNU
Norwegian University of Science and Technology
Faculty of Engineering
Department of Geoscience and Petroleum

Karl Jørgen Abbouchy

Experimental Study of the Performance of Ball-Type Check Valves in Cyclic Fracture-to-Fracture SWEOR

Master's thesis in Petroleum Engineering
Supervisor: Milan Stanko
June 2022

NTNU
Norwegian University of
Science and Technology

Karl Jørgen Abbouchy

Experimental Study of the Performance of Ball-Type Check Valves in Cyclic Fracture-to-Fracture SWEOR

Master's thesis in Petroleum Engineering
Supervisor: Milan Stanko
June 2022

Norwegian University of Science and Technology
Faculty of Engineering
Department of Geoscience and Petroleum

NTNU
Norwegian University of
Science and Technology

Acknowledgement

This thesis written in the spring semester of 2022 indicates the fulfillment of the Master's Degree in Petroleum Production at the Department of Geoscience and Petroleum at the Norwegian University of Science and Technology (NTNU).

I would like to express my greatest gratitude to my supervisor Professor Milan Stanko for his constant guidance, support, and availability at any time throughout the semester. I would like to thank Mr. Torkjell Breivik for always being available to help in troubleshooting the software and in fixing any technical issues encountered while working with the setups. I would also like to thank Mr. Noralf Vedvik and Mr. Roger Overå for their help with mechanical issues encountered while working with the setups.

I would like to thank all my friends for supporting me and creating a great environment for me inside and outside of NTNU. Last but certainly not least, I would like to thank my family who has been my number one supporter and go-to throughout those tough yet fruitful two years. They are the reason behind me being where I am today.

(This page is left intentionally blank)

Abstract

One of the proven high recovery gas EOR techniques is the single-well fracture-to-fracture method, where injection and production of gas happens in an asynchronous, cyclic way through alternating injection and production fractures along the wellbore ($F2F_{cyc}$). Remotely activated valves or sliding sleeves placed in front of the injection and production fractures can be replaced by ball-type check valves that do not require any expensive actuation mechanisms and connectivity to the surface. This aims at reducing completion costs, giving the $F2F_{cyc}$ higher economic merits over other gas EOR methods. The valves in front of the injection fractures (injection valves) will only open during injection, and the valves in front of the production fractures (production valves) will only open during production.

The opening and closing of those floating ball-type check valves is governed by flow and pressure. There will be losses in volumetric (and therefore injection and production) efficiency due to the closing delays of and leakages across the check valves when the well is alternating between injection and production modes. This can be crucial to the utilization of the injection fluid, recovery factors, and the economics of the EOR project.

This main aim of this thesis is to study and quantify experimentally the leakage and closing performances of the injection and production ball-type check valves through leakage tests and closing rate tests respectively. The leakage test is conducted by measuring leakage rates through the closed valves at certain differential pressures. The closing rate test is conducted by measuring the rate needed to push the ball towards the valve's seat and the amount of fluid lost prior to the valve's closure. Air and nitrogen are used as the working fluids. Two setups were used: a high-pressure setup and a low-pressure setup. Both setups are used for leakage tests, but only the high-pressure one is used for closing rate tests. A dimensionless analysis was carried out to analyze the leakage test results in both setups.

Leakage rates at certain pressure differentials through the closed valves in both setups fell below the NORSOK's leak rate acceptance criteria for gas. The leaked gas prior to the closure of the valves in the high-pressure setup during the closing rate test also fell below the accepted leakage rate. The dimensionless analysis showed that the seat and ball roughness have a noticeable effect on leakage rates through the valves. Leakage rates through the high-pressure injection and production valves reached a critical differential pressure after which the valves continue to leak at a lower rate at higher differential pressures. This indicates that a good seal between the ball and the valve's seat is established at high differential pressures. This limits the volumetric losses, therefore improving the economics of the $F2F_{cyc}$ method.

(This page is left intentionally blank)

Table of Contents

List of Figures

List of Tables

Nomenclature

List of Abbreviations

EOR	Enhanced oil recovery
HnP	Huff-and-puff
F2F	Fracture-to-fracture
$F2F_{Cont}$	Fracture-to-fracture continuous
$F2F_{cyc}$	Fracture-to-fracture cyclic/asynchronous
HP	High-pressure
LP	Low-pressure
NPV	Net present value
P&ID	Piping and instrumentation diagram
P.D	Percent difference

List of Symbols

m_{air}	Mass of air inside the metallic air tank (kg)
Δm_{air}	Difference in mass of air inside the metallic air tank between times t_1& t_2 (kg)
P_m	Measured pressure inside the metallic air tank (Pa or kg.m-1.s-2)
V	Volume of metallic air tank (m3)
M_{air}	Molar mass of air (g/mol)
R	Universal gas constant (J/K.mol or kg.m2.s-2.K-1.mol-1)
T	Temperature (K)
ΔP	Differential pressure (bar)
ΔP_c	Critical differential pressure (bar)
$q_{air,LP}$	Air leakage rate in LP setup (scf/min)
$q_{air,HP}$	Leaked air rate prior to the closure of the valves in closing rate tests in HP setup (scf/min)
$q_{N_{2,ro}}$	Nitrogen leakage rate measured by the rotameter (scf/min)
$q_{N_{2,f}}$	Nitrogen leakage rate calculated through the polynomial fit (scf/min)
ρ_{air}	Air density at standard conditions (kg/m3)
Δt	Time increment (s)
P_f	Pressure calculated through a polynomial fit (bara)
P_m	Measured metallic air tank pressure (bara)

t	Time recorded by the Transparent cell software (s)
ϵ	Error (%)
ρ	Density of the fluid (kg/m^3)
q	Leakage rate through valve (sm^3/s)
μ	Viscosity of the fluid (Pa.s)
ΔP	Pressure differential across the valve (Pa)
D_b	Diameter of the ball (m)
ε_b	Roughness of the valve's ball (m)
D_a	Diameter of the valve's seat (m)
ε_a	Roughness of the valve's seat (m)
π_1	Dimensionless leak flow
π_2	Dimensionless pressure drop
π_3	Dimensionless relative roughness
E/D	Dimensionless relative roughness
π_{2_c}	Critical dimensionless pressure drop
μ_o	Reference viscosity at reference temperature T_o (cP)
T	Input temperature (degrees Rankine)
T_o	Reference temperature (degrees Rankine)
C	Sutherland's constant
δP_{HP}	Error associated to pressure measurements in the HP setup (barg or bar)
δP_{LP}	Error associated to pressure measurements in the LP setup (barg or bar)
δm_{air}	Error associated to the calculated mass of air (kg)
$\delta m_{air,t_1}$	Error associated to the calculated mass of air at a time t_1 (kg)
$\delta m_{air,t_2}$	Error associated to the calculated mass of air at a time t_2 (kg)
$\delta q_{air,LP}$	Error associated to calculated air leakage rates in LP setup (scf/min)
δq_{ro}	Error associated to measurements through rotameter (scf/min)
δq_{gf}	Error associated to measurements through gas flow meter (scf/min)
$\delta \pi_1$	Error associated to the dimensionless leak flow
$\delta \pi_2$	Error associated to the dimensionless pressure drop

1. Introduction

1.1. Background

The U.S. Energy Information Administration estimated that the technically recoverable tight oil is of around 418.9 billion bbl globally, which is roughly 10% of all types of oil reserves in the world (EIA, 2015). The U.S tight oil production in 2021 amounted to 2.64 billion barrels (7.22 million barrels/day), nearly 65% of the total U.S. crude oil production in that year (EIA, 2021). While that number seems high, the recovery factor in tight oil producing wells is very low, typically between 3 to 10% (Jacobs, 2015). Thermal and chemical EOR methods have deemed to be technically and economically unattractive in tight oil formations (Azhar, 2016). On one hand, Water injection, usually an efficient method in conventional reservoirs, is not practical in tight oil formations due to their low permeability. A more favorable approach to improve the oil recovery in tight oil formations is the injection of miscible gas, also known as gas EOR (Zhu et al., 2015).

There are several approaches to gas EOR in tight formations: well-to-well gas injection (separate wells are used for injection and production and the injection gas sweeps the oil between both), single well huff-and-puff (HnP, there is cyclic injection and production in the same well) and single well fracture-to-fracture (F2F, gas is injected through injection fractures and oil is produced from production fractures located in an alternating pattern along the wellbore).

All these methods have limitations. For example a pilot project performed in the Bakken formation applying well-to-well gas injection showed low recovery factors due to short circuits between the production and injection wells (Luo et al., 2021). The performance of single well huff-and-puff tends to declines over time. The reason behind the decreasing incremental oil recovery factor is due to the longer distances the injection gas must traverse with each cycle, (Sanchez-Rivera et al., 2015).

Regarding the fracture-to-fracture, Luo et al. (2109) indicated that, if applied continuously, the risk of short circuits – direct communication between injection and production fractures – is high, resulting in bypassed oil. Luo et al. (2021) discuss a variation of the F2F method to overcome this issue, where injection and production happen in asynchronous, cyclic way. This single-well EOR method is labelled as $F2F_{cyc}$. The alternating injection and production fractures have remotely activated valves or sliding sleeves placed in front of them. The injection and production zones are in zonal isolation from each other by the use of packers.

The valves in front of the injection fracture will only open during injection, and the valves in front of the production fractures will only open during production.

Although $F2F_{cyc}$ yields higher recoveries than HnP over the lifetime of an EOR project (Luo et al., 2021), completion costs are usually higher. Hence, decreasing completion costs and simplifying the completion would make this EOR method more attractive. One way of decreasing the cost of the $F2F_{cyc}$ method is to replace remotely activated valves or sliding sleeves by floating ball-type check valves that do not require any external actuation (**Figure 1.1)**. These ball-type check valves simply consist of a ball and a seat, and are controlled by flow and pressure. The terms tubing and liner will be used interchangeably throughout this thesis.

The desired flow during injection is from the liner into the formation, and the desired flow during production is from the formation into the liner. In the event of flow in the desired direction, the valve will open as the flowing fluid pushes the ball away from the valve's seat. In the event of flow in the undesired direction, the ball is pushed towards the seat, and it establishes a differential pressure across it.

There will be losses in volumetric (and therefore injection and production) efficiency due to the closing delays of and leakages across the check valves. For example, when the well is set from production to injection, there will be some flowback into the production fractures prior to their valve closure. After the production the valve is closed, there will be some flow into the production fractures due to the valve leakage (that depends on the pressure differential across the check valve). The unwanted loss of injection fluid can be detrimental to the injection fluid's utilization plan in an EOR project. More injection fluid will then be needed to reach a target recovery factor, and the accessibility to the extra injection fluid needed may also become a project limitation. Hence, this may affect the economics of the EOR project.

Similarly, when the well is set from injection to production, an amount of the fluid injected will flow back into the liner prior to the injection valve's closure. After the injection valve is closed there could be some leak flow from the injection fractures into the liner, due to the pressure differential across the valve. This will negatively affect the pressure maintenance in the injection fractures during the production cycle and more injection fluid will be needed in future injection periods in order to increase the pressure of the injection fractures. This in turn will negatively affect the recoveries, hence the economics of the EOR project.

In this thesis, the performance of the floating ball-type production and injection check valves is assessed experimentally, using air and nitrogen as the working fluids.

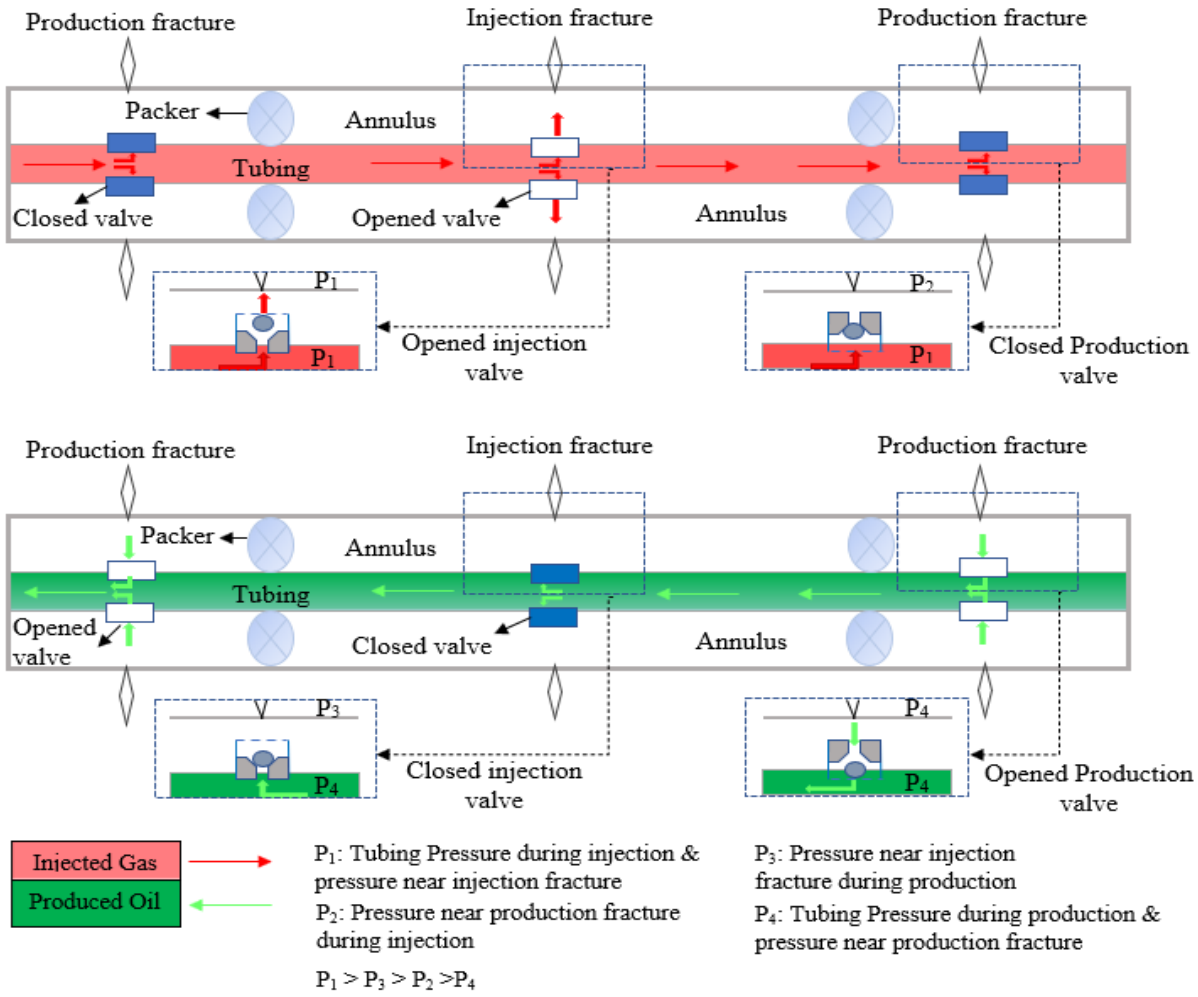

Figure 1.1: Cyclic fracture-to-fracture well configuration and pressure profile using ball-type check valves during injection *(top)* and production *(bottom)*

Firstly, the leakage rates through the production and injection valves are measured under different differential pressures while in the closed position. This test is labelled as the leakage test. Secondly, the fluid rate needed to push the ball towards the valve's seat prior to its closure is measured, and the amount of fluid lost prior to the valve's closure is determined. This test is labelled as the closing rate test. Thirdly, a dimensionless analysis was performed to determine the effect of the seat and ball roughness on valve flow performance.

Results were compared against another study on ball-type check valves: Zarea et. Al (1999).

Two experimental setups were used: a high-pressure and a low-pressure setup. Both of the setups are used to determine leakage rates under different differential pressures, but the closing rate test is carried in the HP setup only. The LP setup is designed to withstand a maximum pressure of 20 bar (operated at 7.13 bar in this thesis), and the valve seats are made of acrylic plastic. The high-pressure setup is designed to withstand a maximum pressure of 300 bar

(operated at 150 bar in this thesis), and valve seats are metallic.

1.2. Objective

The main aim of this thesis is to study and quantify the closing and leakage performance of the ball-type check valves to be employed in the $F2F_{cyc}$ EOR. There are four objectives derived from the main aim.

The first objective is to study and quantify experimentally the performance of the injection and production check valves with silicon nitride ball and metallic seat using nitrogen as a working fluid in high pressure conditions.

The second objective is to study and quantify experimentally the performance of the injection and production check valves with metallic ball and acrylic plastic seat using air as a working fluid in low pressure conditions.

The third objective is to compare leakage rates at the same pressure differentials between the HP and LP setup. The goal is to assess the effect of the valve material on its sealing capability.

The fourth and final objective is to perform a dimensionless analysis that helps determine the effect of the seat and ball roughness and expand the scope of the study to different working fluids and ball and seat dimensions.

There will also be a familiarization with the layout and the operation of both experimental setups.

This work advances further the work by Zarea et al. (1999). The results of the work could enable to perform efficient and cost-effective completion designs for $F2F_{cyc}$ EOR applications.

1.3. Scope of Work

Chapter two discusses the concept of the single-well fracture-to-fracture cyclic ($F2F_{cyc}$) EOR method, and discusses its importance and the advantages it has when compared to other single-well gas EOR methods in regards to recovery factors and economics. The behavior of ball-type check valves in the $F2F_{cyc}$ and their performance is also discussed in details in this chapter, and a study on ball-type check valves is presented.

Chapter three introduces the layout of the setups, details about their operation, instrumentation, and measurements. The methodology of the tests performed is also discussed.

Chapter four shows how the experimental parameters (differential pressures, closing rates, and leakage rates) were measured or calculated to serve the purpose of the objectives. Error propagation calculations for experimental parameters have also been shown in this chapter.

Chapter five interprets the test results and the literature study is used as a source for analyzing, comparing, and interpreting the results. Leakage rates through the valves using a gas are analyzed and discussed, and the effect of surface roughness is shown. It also shows the correspondence between the test results and the $F2F_{cyc}$ method.

The final chapter concludes the main findings of the experiments conducted. Some recommendations for future work are listed too.

2. Single-well cyclic fracture-to-fracture EOR

The $F2F_{cyc}$ EOR method is a single-well gas EOR method that relies on cyclic injection and production of gas from alternating fractures along the wellbore (**Figure 2.1**). Since both the injection and production fractures share the same tubing, check valves are placed in front of each corresponding fracture (or group of fractures). Check valves placed in front of injection fractures are referred to as injection valves, and those placed in front of the production fractures are referred to as production valves. Injection or production valves will allow flow only in each corresponding mode (injection or production). The injection and production sections should be in zonal isolation from each other. One way of achieving this is by using packers.

There are other completion techniques to achieve dedicated production and injection, but they are not considered in the present work. For example, Luo et al. (2021) shows a completion configuration of the $F2F_{cyc}$ method during an injection mode and a production mode, using remotely activated sliding sleeves in front of injection and production fractures (**Figure 2.2**). In the injection mode, the sleeves in the injection section are opened to allow the flow of the injection fluid into the formation through the injection fractures, while the sleeves in the production section are closed. In the production mode, fluid flow through the production fractures is enabled by opening the corresponding sleeves in the production section, while the sleeves in the injection section are closed.

2.1. Fracture-to-fracture cyclic vs. HnP EOR target volume

Like the $F2F_{cyc}$ EOR method, the HnP method is also a single-well gas based cyclic EOR method that has been used in tight oil unconventional reservoirs for many years. HnP has proved to yield good incremental recoveries. The HnP method consists of two periods, the injection period (huff), the production period (puff), and a soaking period after the injection period to prolong the effects of molecular diffusion, an important phenomenon in miscible gas injection. Diffusion governs the amount of mixing between the oil and the injected gas. The amount of mixing between the reservoir oil and the injection gas per each cycle dictates the incremental recovery for an HnP process (Mydland et al., 2020). During hydraulic fracturing, a “rubblized zone” (i.e. a volume of shattered rock near the hydraulic fractures) is created. During injection, the gas starts to fill up the fractures, and the pressure gradient created between the fractures and the pieces of shattered rock will force the gas into rubblized zone where it pushes the oil inward. The diffusion phenomenon will cause considerable mixing only if the size of the pieces of rock are small. If the size of the shattered rocks is large, then the injected

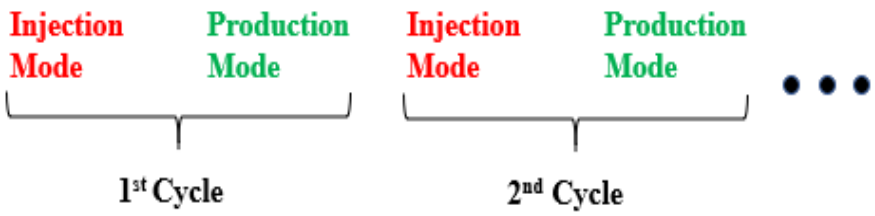

Figure 2.1: A cycle in the single well fracture-to-fracture method

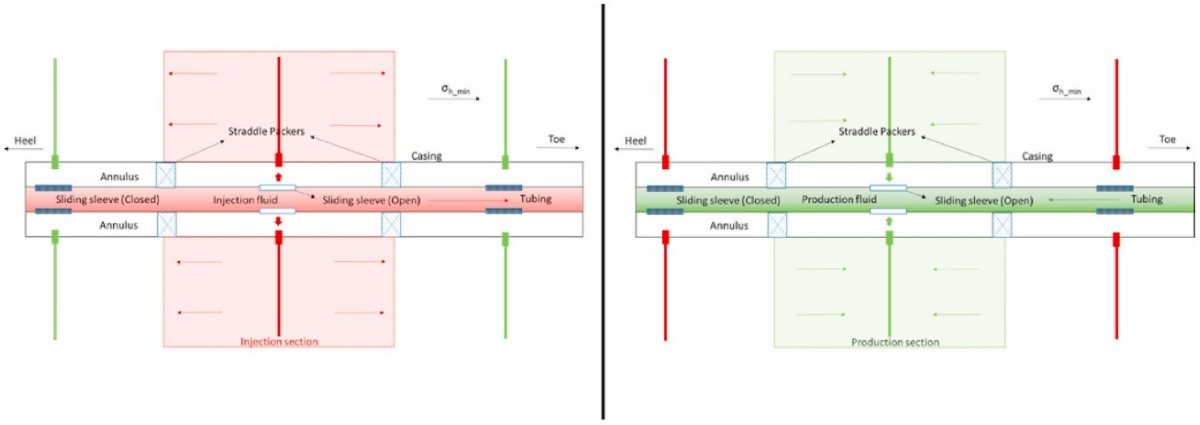

Figure 2.2: Completion configuration of F2Fcyc in injection mode *(left)* & production mode *(right)* from (Luo et al., 2021)

gas will only push the oil inwards and little to no mixing is achieved. This yields low incremental recovery factors. Therefore, the shattered rock volume is the basis for attaining incremental oil recovery by the HnP process, and little recovery is achieved outside this rock volume (i.e. the non-shattered parts of the rock matrix between the hydraulic fractures and the rock volume beyond the hydraulic fracture tips) (Mydland et al., 2020). Hence, a large volume of bypassed oil is left behind.

In the $F2F_{cyc}$ process, the injection gas moves from the injection fractures in the direction perpendicular to the production fractures. This conventional miscible-displacement mechanism allows for a much higher EOR target volume than the one in HnP. The target volume for the $F2F_{cyc}$ is the whole rock volume between the injection and production fractures, which is larger than that for the HnP. Hence, a higher recovery can be achieved.

Luo et al. (2021) performed a reservoir simulation using CO_2 as the injection gas for both HnP and $F2F_{cyc}$ methods. After 20 cycles of injection and production, it can be clearly seen (**Figure 2.3**) how the CO_2 has traversed deeper into the reservoir in the $F2F_{cyc}$ in comparison to the HnP. This further shows how the EOR volume covered by the $F2F_{cyc}$ is greater than that covered by the HnP.

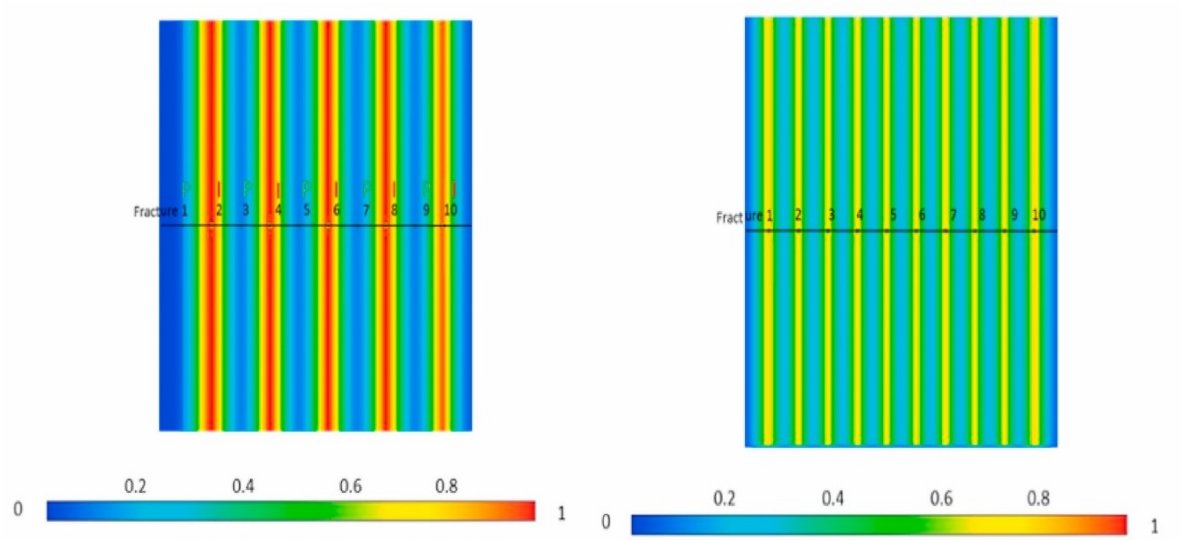

Figure 2.3: CO2 concentration traversing into reservoir in the F2Fcyc *(left)* vs. the HnP *(right),* modified from Luo et al. (2021)

2.2. Fracture-to-fracture cyclic vs. continuous

The $F2F_{cont}$ method is a variation of the $F2F_{cyc}$ method. Unlike the $F2F_{cyc}$ which consists of cyclic injection and production, the $F2F_{cont}$ has a dual conduit completion (**Figure 2.4)** which allows for continuous injection and production through the alternating injection and production fractures along the wellbore. The injection and production sections are in zonal isolation from each other through the use of packers. Due to the continuous nature of injection and production in the $F2F_{cont}$ method, all injection and production fractures are active along the wellbore. Therefore, there is a high risk of short-circuiting between injection and production fractures through highly conductive secondary fractures or cement leaks, negatively affecting recoveries. Short-circuits have little to no effect when using $F2F_{cyc}$. During the injection mode, the production fractures are non-active, since the production valves are closed. Therefore, any type of short-circuit between the production and injection fracs will have limited effect because there is no leakage of fluid to the tubing and the pressure of the production fracture increases rapidly (**Figure 2.5**). During the injection cycle, the short-circuit path is pressurized and helps push the injected fluid into the unswept areas, and the production fracture connected to the short-circuit acts as an injection fracture too. During the production mode, this production fracture starts to produce, so the region close to the short-circuit and the production fracture acts as an HnP zone (Luo et al., 2021). The $F2F_{cyc}$ is therefore "self-healing", and thus serves as a better alternative to the $F2F_{cont}$.

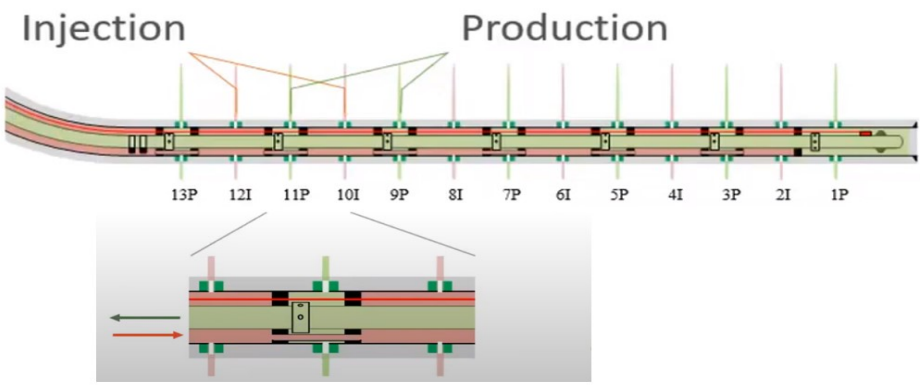

Figure 2.4: Continuous fracture-to-fracture ($F2F_{cont}$) completion configuration, from Whitson Webinar (2020)

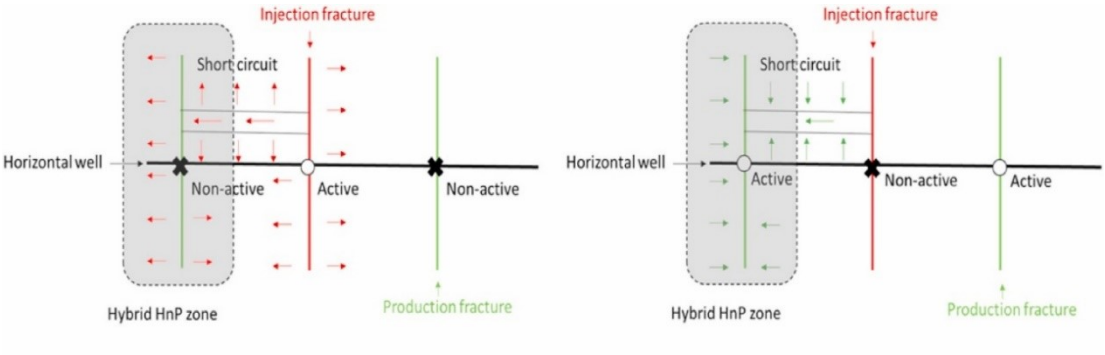

Figure 2.5: Short-circuits in $F2F_{cyc}$ during injection mode *(left)* and production mode *(right),* modified from Luo et al. (2021)

2.3. Economics of single-well gas EOR methods

Out of the three single-well gas EOR methods (HnP, $F2F_{cyc,}$ $F2F_{cont}$), the HnP involves the lowest capital investments. No additional completion components are required in order to convert a producing well into an HnP well. The highest capital investment required is for the $F2F_{cont}$, since it involves a dual-conduit completion and the need for monitoring and control devices to detect short-circuiting effects and ensure the effective utilization of the injected fluid (Luo et al., 2019). Luo et al. (2021) conducted an economic analysis on the three single-well gas EOR methods based on the injection gas's cost (CO_2 utilization) and the oil revenue. The net present value approach (NPV) was used as an economic indicator to rank the different methods against one another. The NPV of the three methods was assessed in two separate cases. In one case: the reservoir is less heterogenous than in the second case. This was simulated by varying the intensity of the secondary fractures (primary fractures being the hydraulic fractures). All the methods were simulated over a five-year period after a primary production that has depleted the reservoir to a pressure of 1500 psi, and the production and injection

periods for both the HnP and the $F2F_{cyc}$ have the same duration. In both cases, the $F2F_{cyc}$ showed a higher NPV. This shows that this method is a cost-effective method that increases recovery from tight oil formations.

2.4. Ball-type check valves

The NPV analysis discussed in **section 2.3** by Luo et al. (2020) does not include the capital costs of completion for each method used, but they state that this will not change the validity of their conclusions. Nonetheless, the proven efficiency of the $F2F_{cyc}$ makes this single-well gas EOR method worthy of further development. By means of further reducing its completion costs, it will have higher economic merits over other methods.

As discussed in **section 2**, all alternating injection and production fractures share the same tubing. Thus, on-off valves, check valves, or sleeves must be placed in front of alternating injection and production fractures to allow flow during the injection and production modes respectively. The use of self-acting valves, for example, ball-type check valves could be advantageous because they do not require expensive hydraulic or electric actuation mechanisms and connectivity to surface, regular well intervention, thus entail lower operational and capital costs.

The ball-type check valve, also known as the ball-and-seat check valve (**Figure 2.6**), employs a ball that seals when contacting a conical seat. When the ball-and-seat check valve is experiencing flow in the desired direction, the valve will open as the flowing fluid will push the ball away from the valve's opening (**Figure 2.7**). In the event of undesired fluid flow across the valve, the ball would be pushed towards the valve's seat. The ball would then push against the seat of the valve in order to maintain a seal. Hence, a differential pressure across the valve is attained depending on the downstream pressure, the upstream pressure, and the effectiveness of the seal (**Figure 2.7**).

The opening and closing of those floating ball-type check valves is governed by flow and pressure; When closed, the leakage rate depends on the pressure differential acting across the valve. When open, their closing performance will depend on the backflow rates and pressure differentials.

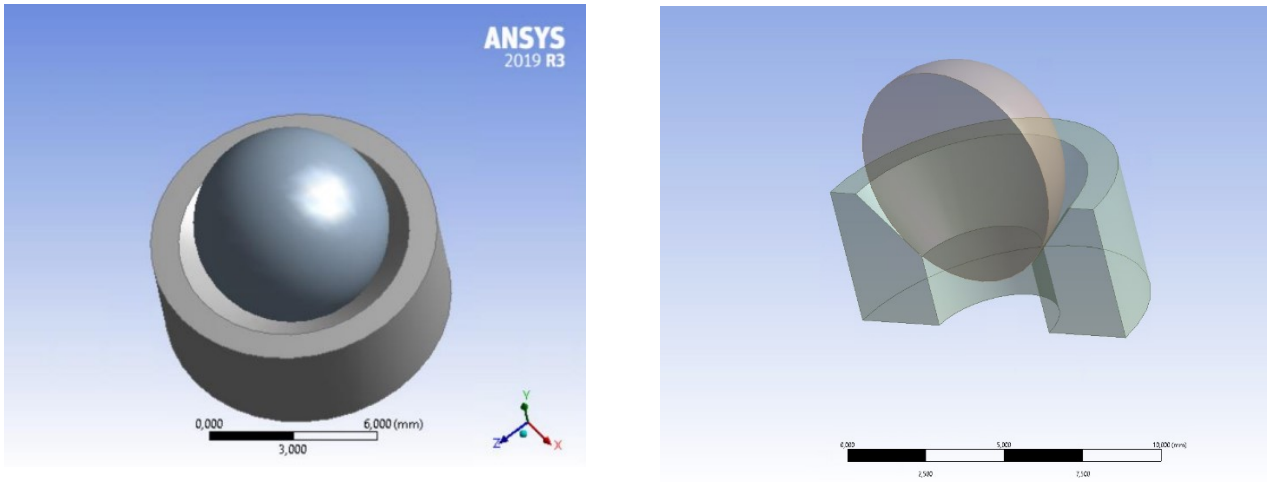

Figure 2.6: Top view *(left)* and cross-section *(right)* of ball-type check valve using Ansys Workbench

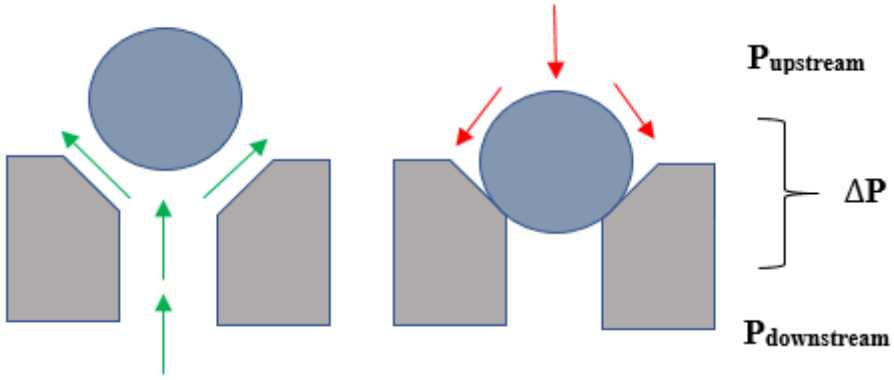

Figure 2.7: Sketch of ball-and-seat check valve in its opened *(left)* and closed position *(right)*

2.4.1. Considerations when employing a ball-type check valve in $F2F_{cyc}$ injection mode

A simulation study by Luo et al. (2021) of the $F2F_{cyc}$ method using CO_2 as the injection fluid shows the pressure profile for the production and injection sections during the injection period (**Figure 2.8**). For the simulation, the reservoir has been primarily produced until a pressure of 1500 psi (bubble point pressure) is reached. The maximum injection pressure allowed during the injection period after the primary production is 6000 psi (the fracturing pressure). This pressure profile during the injection period of the alternating production and injection fractures 5,6, & 7 (highlighted in **Figure 2.8**) has been used in a conceptual sketch of the $F2F_{cyc}$ configuration to assist in explaining the behavior of the ball-type check valves that is influenced by flow and pressure differentials across them (**Figure 2.9**).

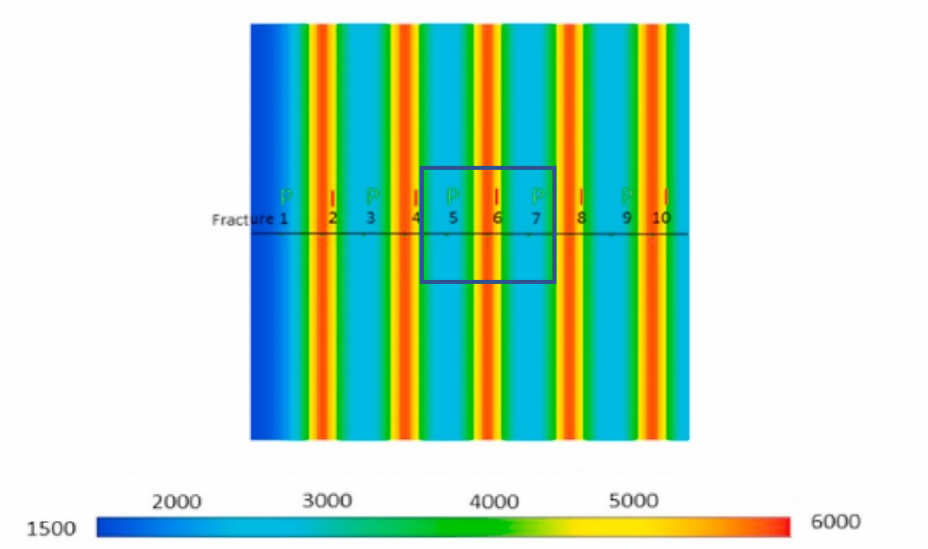

Figure 2.8: Pressure profile for injection and production sections during injection period, modified from Luo et al. (2021)

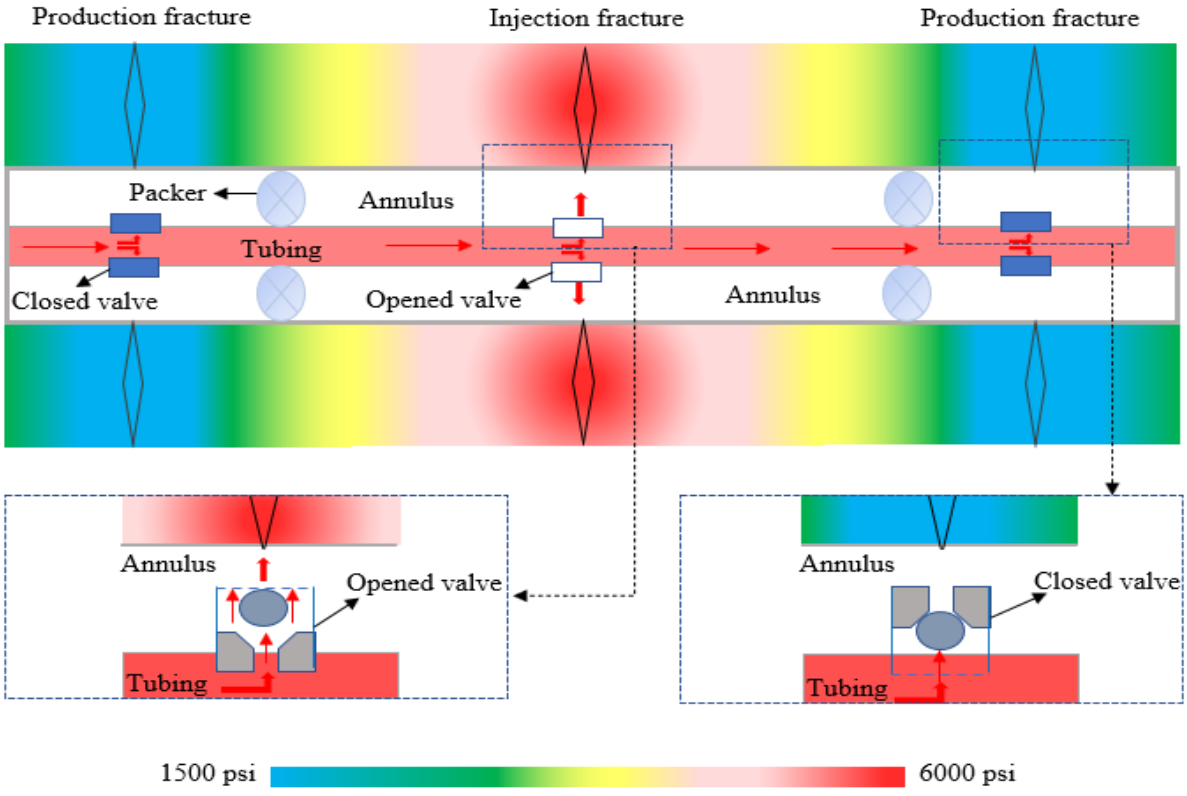

Figure 2.9: Conceptual sketch of F2F$_{cyc}$ configuration with the pressure profile in the injection period, and the behavior of the ball-type check valves

During the injection period, the injection valve opens when the injected fluid pushes the ball away from the valve's seat. The production valve closes as the ball in the production valve gets pushed by the injected fluid against the valve's seat to maintain a seal. Note that the pressure differential across the production valve is positive in the direction that pushes the ball against

the valve's seat (**Figure 2.9**).

2.4.2. Ball-type check valve in $F2F_{cyc}$ production mode

The same simulation study by Luo et al. (2021) of the $F2F_{cyc}$ method shows the pressure profile for the production and injection sections during the production period after the injection period that has been discussed in **section 2.4.1** (**Figure 2.10**). Once again, the pressure profile of the alternating production and injection fractures 5,6, & 7 (highlighted in **Figure 2.10**) during the production period has been used in a conceptual sketch of the $F2F_{cyc}$ configuration to aid in explaining the behavior of the ball-type check valves (**Figure 2.11**).

During the production mode, the production valve in the production section opens as fluid flow from the reservoir pushes the ball away from the valve's seat. In the injection section, the positive differential pressure between the injection fracture and the tubing, along with the injected fluid that tends to flow back, push the ball towards the valve's seat, closing the injection valve (**Figure 2.11**).

2.4.3. Performance of ball-type check valves

As mentioned in **section 2.4**, the performance of the valve is assessed by its closing performance and the leakage rates at certain pressure differentials across the closed valve. The closing delays and leakage rates across the check valves result in volumetric (and therefore injection and production) efficiency losses.

When the well is set from production to injection, there will be some flowback into the production fractures prior to the production valves closure. The backflow rate needed to close the production valve should be assessed, and the amount of injected fluid lost into the production fracture prior to its closure needs to be determined. After the production valve is closed, there will be some flow into the production fracture due to the valve leakage. The leakage rate depends on the pressure differential (**Figure 2.9)** across the check valve.

The injection fluid's utilization is an important factor in EOR projects. Unwanted loss of the injected fluid will result in a higher utilization to attain a target recovery factor. This in turn will negatively impact the economics of the project, and the availability of the extra injection fluid may be a project limitation.

When the well is set from injection to production, a volume of the injected fluid will flow back into the tubing, prior to the closing of the injection valve. Hence, the flowback rate needed to

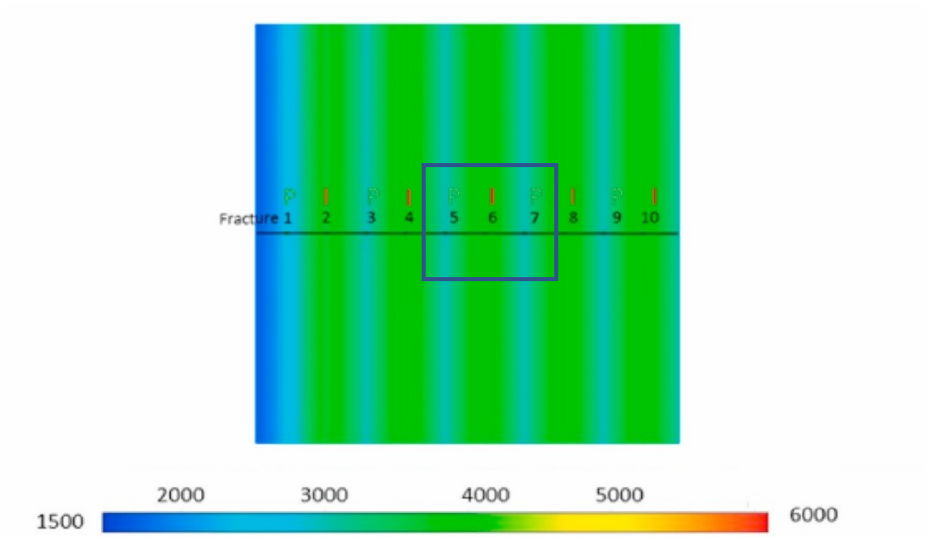

Figure 2.10: Pressure profile for injection and production sections during production period, modified from Luo et al. (2021)

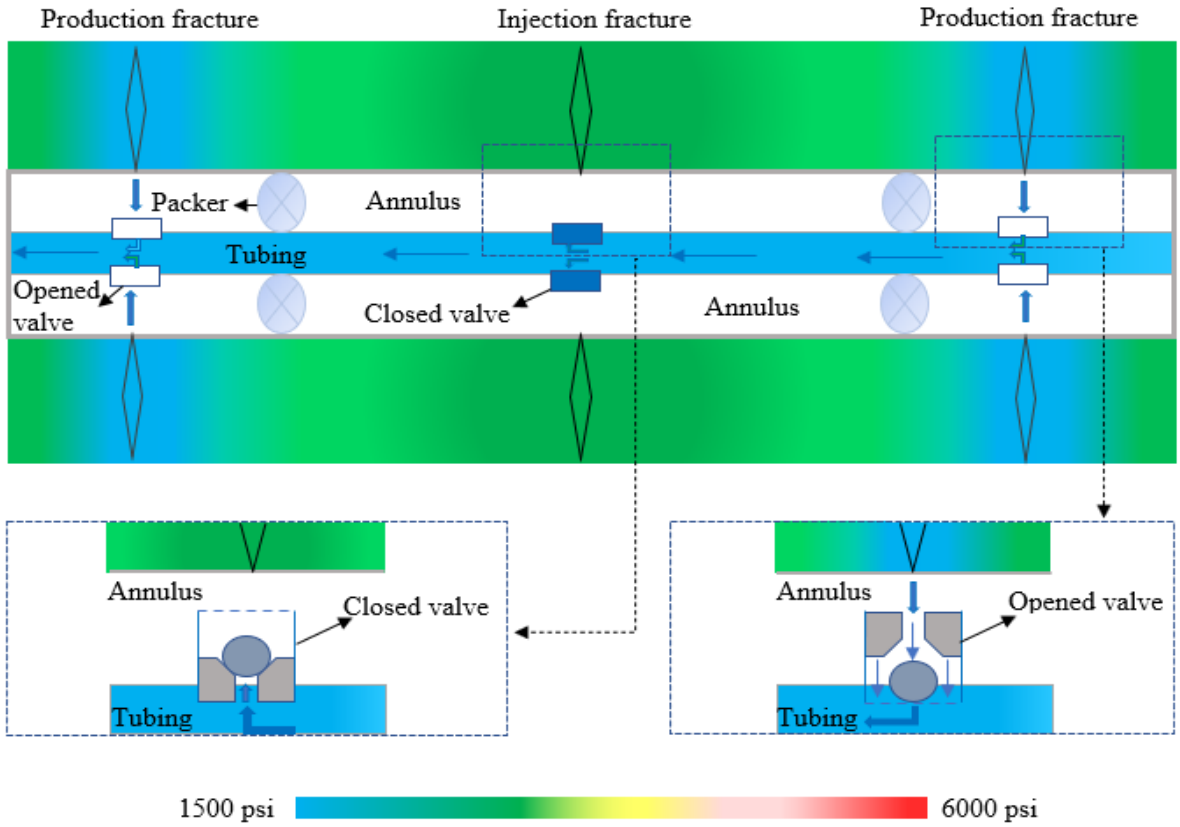

Figure 2.11: Conceptual sketch of F2F$_{cyc}$ configuration with the pressure profile in the production period, and the behavior of the ball-type check valves

close the valve should be assessed, and the amount lost should be determined. After the injection valve is closed, there will be some flow from the injection fractures into the tubing (the leakage rate depends on the pressure differential across the check valve (**Figure 2.11**).

The pressure maintenance will therefore be negatively affected during the production period, and the injection fluid's utilization in upcoming injection periods will increase in order to increase the pressure of the injection fractures. This will negatively affect the recoveries, hence the economics of the EOR project.

2.4.4. Work of Zarea et al. (1999) on ball-type check valves

Zarea et al. (1999) studied experimentally the ball-and-seat check valves, that are used in the mechanical pump unit used in the sucker rod pump artificial lift method. The purpose of this study was to demonstrate that the accepted API "vacuum test" was too severe when evaluating and using it as acceptance criteria for ball-and-seat check valves in use. According to the API "vacuum test", the maximum pressure drop across the valve that is acceptable is 14.7 psi. Zarea et al. (1999) showed that valves that fail this test still have significant sealing capabilities.
Two test setups were designed to evaluate the leakage rates through the ball-type check valves. One setup was designed for air as the working fluid, and the other was designed for liquids. The setup for testing the valves with air was limited to 100 psig only, while the one for liquid permits pressures up to 5000 psig. Four working fluids were used: air (low viscosity), water (medium viscosity), and two types of high viscosity oils (34.24 cp and 263.86 cp). For a single working fluid and a valve seat diameter and roughness, several ball roughness were tested. This was repeated for four valve seat roughness and diameters. This procedure was repeated for the three other working fluids left. Leakage rates (in ml/h) were then measured at different pressure differentials (in psi) imposed against the valve by changing the pressure upstream the valve. The pressure downstream the valve was kept at atmospheric pressure.

When air was used as the working fluid, all cases had shown a similar monotonic trend (**Figure 2.12)** for leakage rates versus pressure differentials across the valve. When the differential pressure increases, the leakage rate also increases. Leakage rates through the valves were higher for higher values of the valve's mean roughness (sum of the roughness of the seat and the ball) (this result has not been shown graphically in the paper, it was just stated).
Figure 2.13 shows a comparison between leakage rates for the three liquids of different viscosity and density at the same pressure differentials, for one specific case of ball roughness and diameter and a valve seat's roughness and diameter. The result shows that leakage rates under the same pressure differential decrease as the fluid viscosity increases. Notice that at a certain pressure drop (called the "critical differential pressure"), the leakage rates stop increasing with differential pressure and start declining. This could be due to a reduction in the

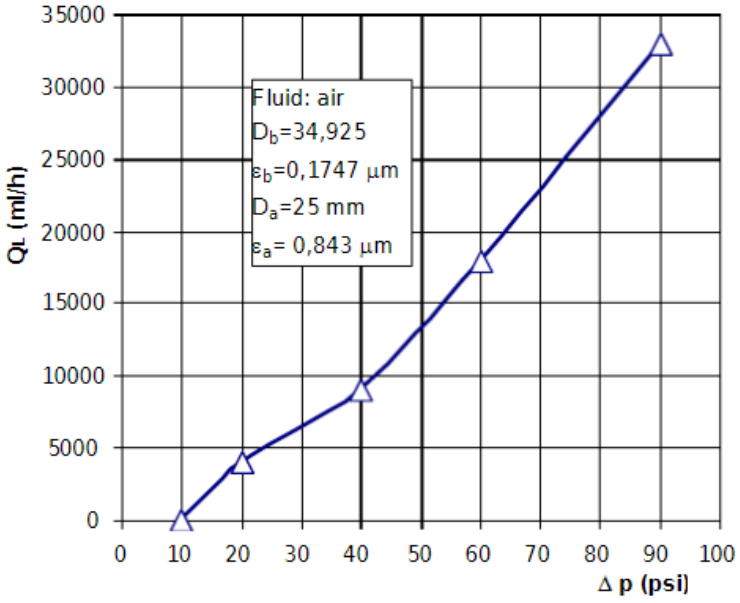

Figure 2.12: Variation of air leakage rate through the ball-type check valve vs. pressure drop using air, from Zarea et al. (1999). Ball had a roughness and a diameter of 0.1747 µm and 34.925 mm respectively and the valve seat had and a diameter of 0.843 µm and 25 mm respectively

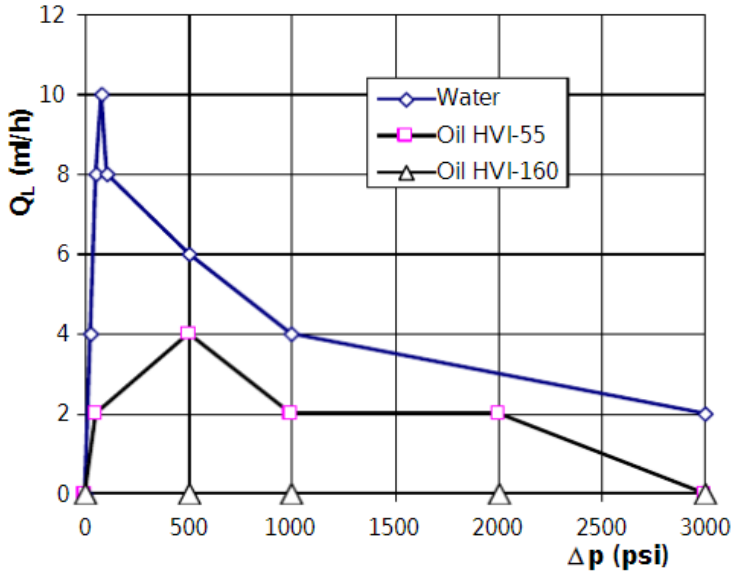

Figure 2.13: Variation of leakage rate through the ball-type check valve vs. pressure drop using different types of increasing liquid viscosities, from Zarea et al. (1999)

leak path due to the deformation of the ball and seat and subsequent increase of the seal surface. Zarea et al. (1999) carried out a dimensionless analysis to generalize the results (**Figure 2.14**). Dimensionless parameters presented in this paper are the following:

$$\text{Dimensionless leakage flow} = \frac{\rho Q}{\mu D_b} \tag{2.1}$$

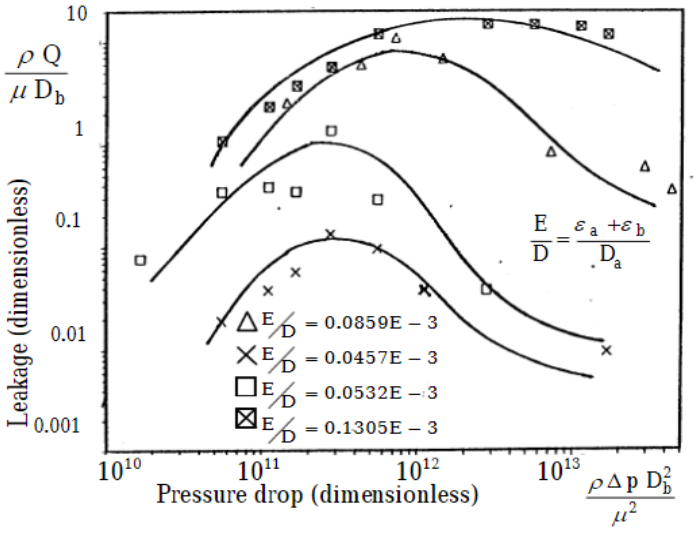

Figure 2.14: Variation of dimensionless leakage rate vs. dimensionless pressure drop, from Zarea et al. (1999)

$$\text{Dimensionless differential pressure} = \frac{\rho \Delta P D_b^2}{\mu^2} \tag{2.2}$$

$$\text{Dimensionless relative valve roughness} = \frac{\varepsilon_a + \varepsilon_b}{D_a} \tag{2.3}$$

In which:

ρ : density of the fluid

Q : leakage rate through valve

μ : viscosity of the fluid

ΔP : pressure differential across the valve

D_b : diameter of the ball

ε_b : roughness of the valve's ball

D_a : diameter of the valve's seat

ε_a : roughness of the valve's seat

The units were not presented in the paper. The dimensionless plot shows that the leakage rate through the valve increases as relative roughness of the valve increases, and the critical differential pressure is also a function of the valve's mean roughness.

An important point taken from this study is that the gas did not exhibit the leakage rate reduction effect with higher pressure differentials. However, this issue could be due to the fact that the maximum pressure differential used in these experiments (with gas as the working fluid) was of 100 psig, which is low.

3. Equipment and test methodology

The behavior of the ball-type production and injection check valves, which is influenced by flow and pressure differentials across them, depends on the mode the $F2F_{cyc}$ project is operating in. Their behavior in injection and production modes are discussed thoroughly in **sections 2.4.1** & **2.4.2** respectively.

It is then important to study and quantify the leakage and closing performance of the ball-type check valves (refer to **section 2.4.3**). Firstly, the leakage performance is assessed by measuring the leakage rates through the check valves under different differential pressures in their closed positions. Secondly, the closing performance is evaluated by measuring the fluid rate needed to push the ball towards the valve's seat before its closure and the amount of fluid lost before the valve's closure.

In order to experimentally evaluate the performance of the ball-type check valves, a high-pressure setup and a low-pressure setup were used. Both the HP and the LP setups are used to determine leakage rates across the closed valves under different differential pressures. The closing rate test is done in the HP setup only.

In this thesis, standard conditions refer to 1 bara and 15 degrees Celsius.

3.1. High-pressure setup

The HP setup is made of stainless steel and can withstand pressures up to 300 bar**.** The rig has a pressure relief valve that is automatically activated once the pressure within the setup reaches 206 bar for safety reasons**.** The HP setup allows for both leakage and closing rate tests. The working fluid in that setup is nitrogen air (N_2) for leakage tests, and air from the lab facility air supply for closing rate tests.

3.1.1. Test equipment

Figure 3.1 shows the high-pressure setup. It includes the following parts:

- A pressure cell
- A set of manually activated valves used to direct the flow of air into the pressure cell
- Two gauge pressure transmitters with a calibrated range of 0-250 bar and an accuracy of $\pm$ 0.1% of the calibrated range
- 0-3 L/min gas flow meter with an accuracy of $\pm$ 5 % of full scale
- Injection valve: Inconel valve seat, 6.25 mm grade 5 silicon nitride ball, stainless steel hex-hole lid

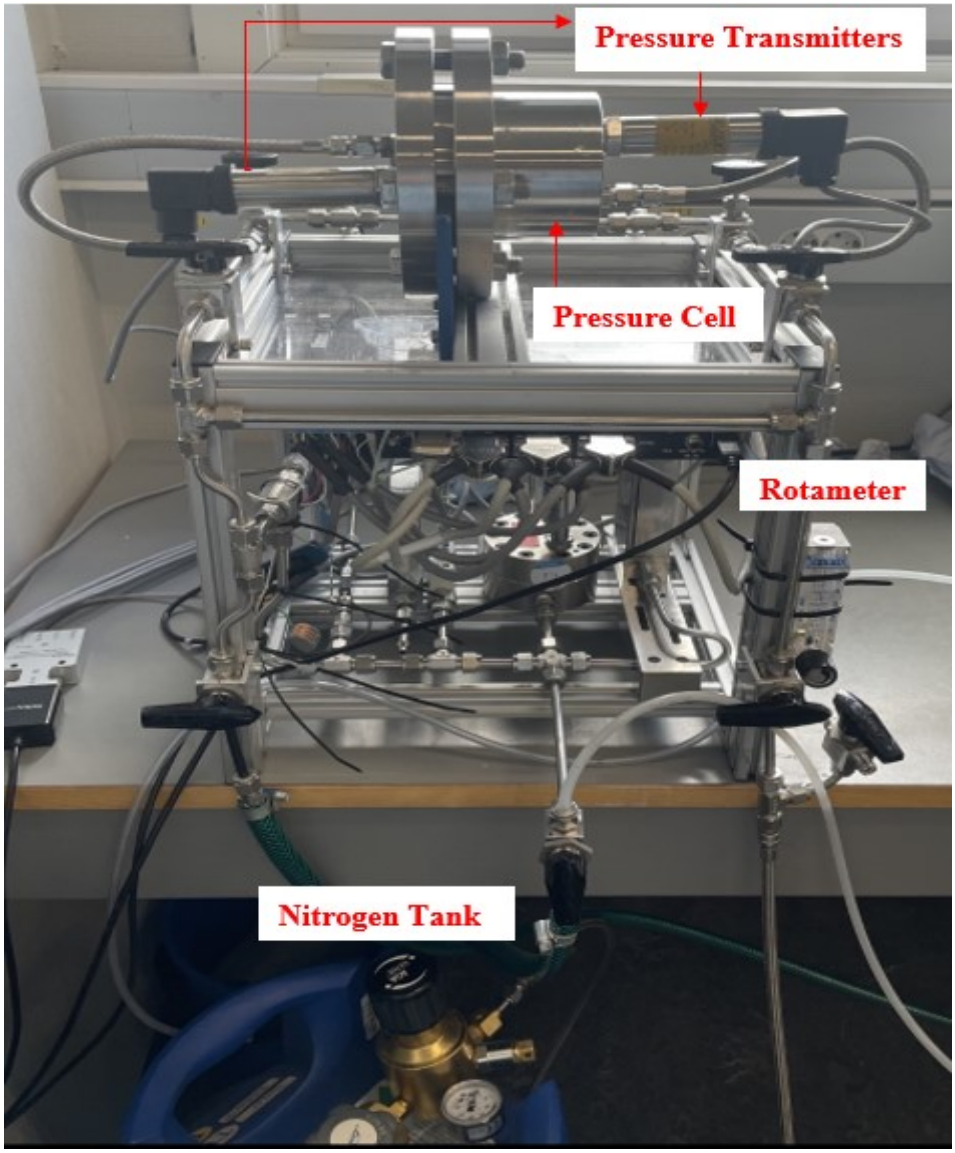

Figure 3.1: High-pressure setup

- Production valve: Inconel valve seat, 6.25 mm grade 5 silicon nitride ball, stainless steel hex-hole lid
- Nitrogen tank with a pressure gage and a regulator
- Gas rotameter with a range of 0.4 L/min to 5 L/min and an accuracy of $\pm$ 5 % of full scale.

The pressure cell consists of two parts (**Figure 3.*2***), one that goes inside the other. One part is the valve holder that goes into the outside enclosure (*Appendix 1*). The valve holder has a threaded opening where the injection and production valves can be screwed into. The injection valve (**Figure 3.3**) and the production valve (**Figure 3.4**) have a conical seat (geometry of the valves can be found in *Appendix 2 & 3*). When the valve is closed, the ball is in contact with

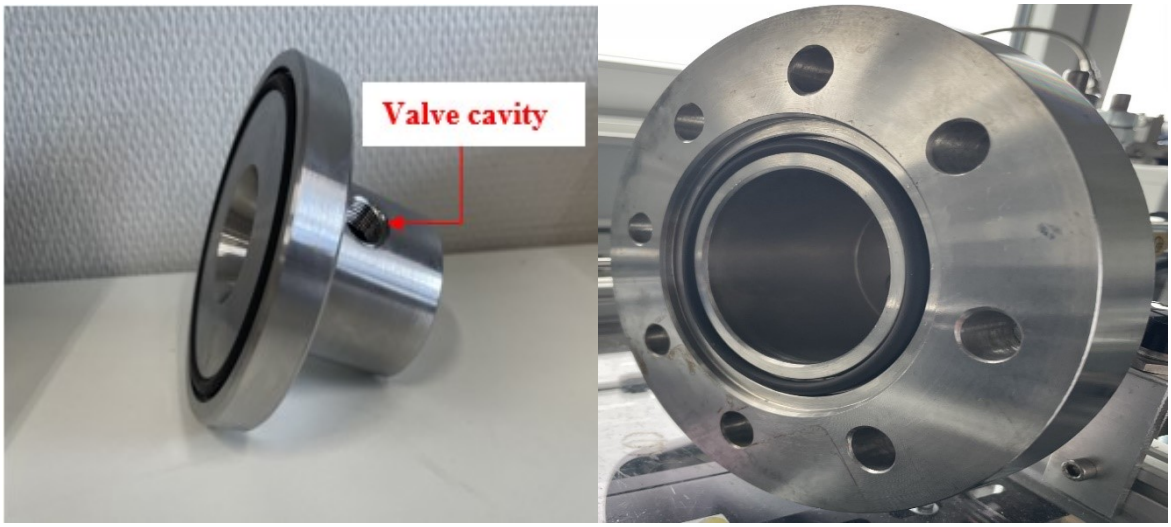

Figure 3.2: Valve holder *(right)* and the outside enclosure *(left)* that make up the pressure cell

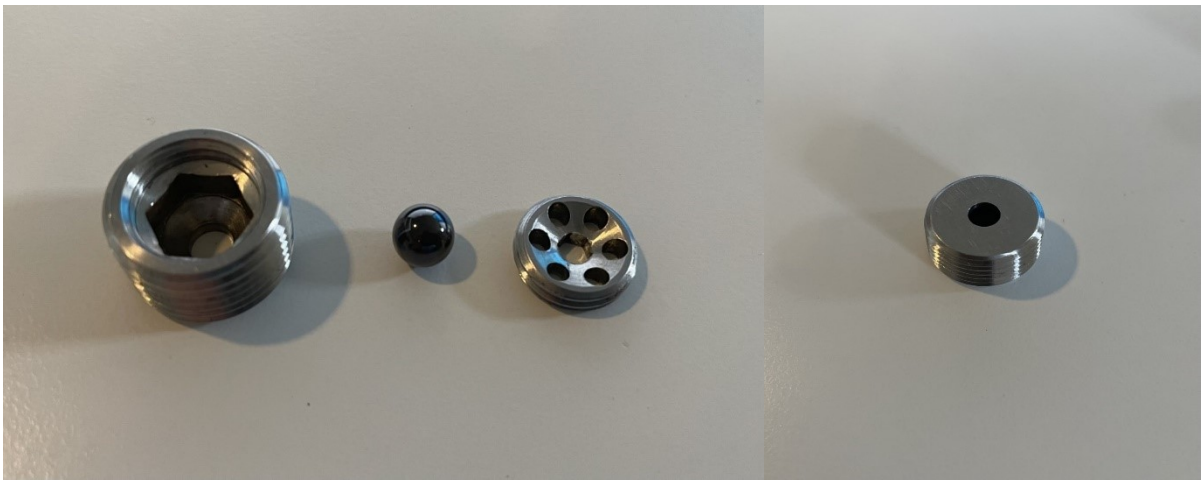

Figure 3.3: Injection valve's top view, ball, lid, and injection valve's bottom view (*left to right*)

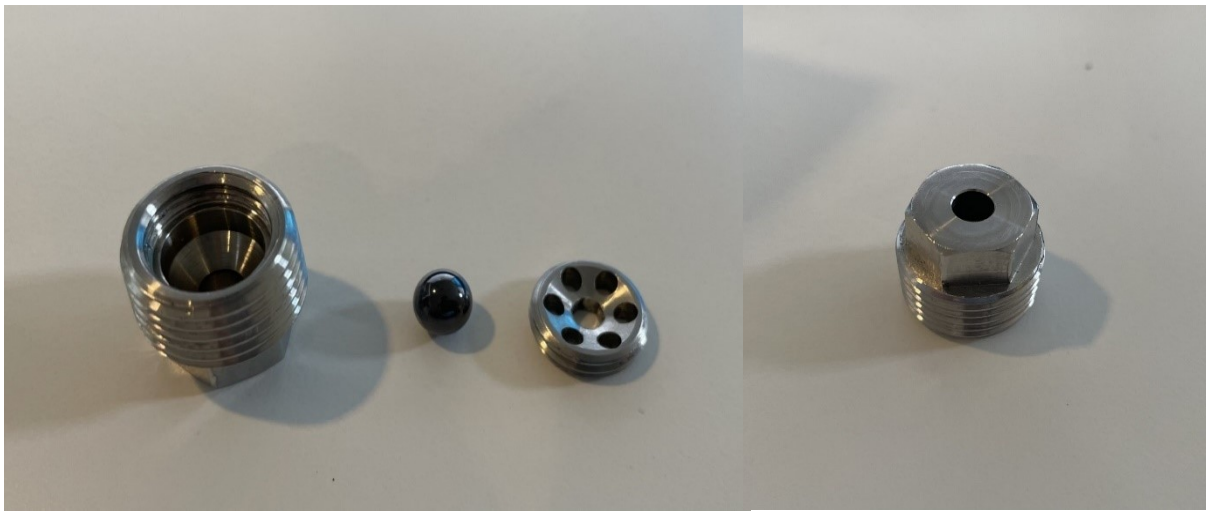

Figure 3.4: Production valve's top view, ball, lid, and production valve's bottom view *(left to right)*

the valve's seat. The hex-hole lid is screwed onto the top of the valve in order to prevent the ball from falling out when the valve is in its open position (when the ball is pushed away from the valve's seat).

3.1.2. Setup limitations

The high-pressure setup had two liquid and two gas flow meters located downstream the pressure cell:

1. Low-rate liquid flow meter: 0-300 mL/hr
2. High-rate liquid flow meter: 0.1-7 L/min
3. Low-rate gas flow meter: 0-11.76 mL/min
4. High-rate gas flow meter: 2-100 L/min

Leakage tests on the valves could not be performed using nitrogen as the working fluid, since the leakage rates through the valves could not be detected by any of the gas flow meters. The leakage rate was higher than the maximum limit of the low-rate gas flow meter (11.76 mL/min) and lower than the minimum limit of the high-rate one (2 L/min).

Therefore, a gas rotameter was used downstream the pressure cell to detect the leaked gas downstream the cell. However, the rotameter has an accuracy of $\pm$ 5 % of full scale. The gas rotameter can only detect flow ranging from 0.4 L/min to 5 L/min (rates below 0.4 L/min cannot be measured). The full-scale value of the rotameter is 5 L/min, so the error associated to all values measured through the rotameter is $\pm$ 0.25 L/min. Therefore, as one goes further away from the full scale, the error as a percentage of flow increases. For example, the error as a percentage of flow for a detected flow of 5 L/min is (0.25/5) *100 = 5 %, while the error as a percentage of flow for a detected flow of 0.4 L/min is (0.25/0.4) *100 = 62.5 %. As a result, low gas flow rates detected by the rotameter have higher errors associated with them.

A gas flow meter with a range of 0-3 L/min was ordered. It was installed towards the end of the project, but analysis on leakage tests had already been conducted using rotameter measurements. Leakage tests using the gas flow meter and the rotameter were compared, and results showed that the rotameter was an adequate tool for measuring the leakage rates in the setup.

The high-pressure setup was designed to withstand pressures up to 300 bar, but a pressure relief valve that has been installed activates as soon as the pressure within the setup reaches 206 bar. Experiments in this thesis have been limited to a maximum of 150 bar in order to have an extra margin of safety when dealing with highly pressurized gas. Therefore, leakage tests have been

performed until a differential pressure of 150 bar across the valves. Unfortunately, the pressure regulator of the nitrogen tank does not allow for small step pressure selections (*Appendix 4*). For example, it is neither possible to increase the pressure provided by the tank incrementally from 0 to 7 barg, nor increase the pressures easily and accurately by increments of 5 bar.

3.1.3. Monitoring program

The data gathering, monitoring and control program for the HP setup is done using the Labview2018 (**Figure 3.5**).

To record the data, the run button is clicked, followed by the start button. The flow rate data is recorded in the units relative to the flow meter units' specifications. The pressure is recorded in barg. The pressure transmitters, one upstream and one downstream the pressure cell, and the gas flow meter are recording data every 0.1 second when the experiment is running. Hence, three sets of data are recorded. The data is saved and can be exported to an Excel file for further analysis.

When the rotameter is used, only the pressure data is recorded using the monitoring program. The flow rate values are recorded manually by visual inspection and written by hand.

3.1.4. HP setup layout

Figure 3.6 shows the piping and instrumentation diagram (P & ID) for the high-pressure setup. The numbering on the diagram provides a guide for the experimental procedure in relation to operating the manually activated valves for each test. Using the numbering provided, the reader can also use the P & ID of the HP setup to locate the place of the valves in the real setup (**Figure 3.7**).

The water tank and the "Quizix Pump" shown in the P & ID are not used in this thesis, since nitrogen air from the N_2 tank is the working fluid used for the experiments conducted in this setup. Therefore, valve 4 is always closed. The line (shown in red on the P & ID) connecting those two components is not in use. The rotameter is located downstream the pressure cell.

The gas flow meter and rotameter downstream the pressure cell do not withstand high pressures, so the pressure downstream the cell is always kept at atmospheric pressure. This is done by keeping Valve 7 in an open position. Thus, the pressure transmitter downstream the pressure cell should always read atmospheric pressure on the monitoring program. The differential pressure across the valve is therefore dictated by the upstream pressure which is regulated by the nitrogen tank pressure regulator.

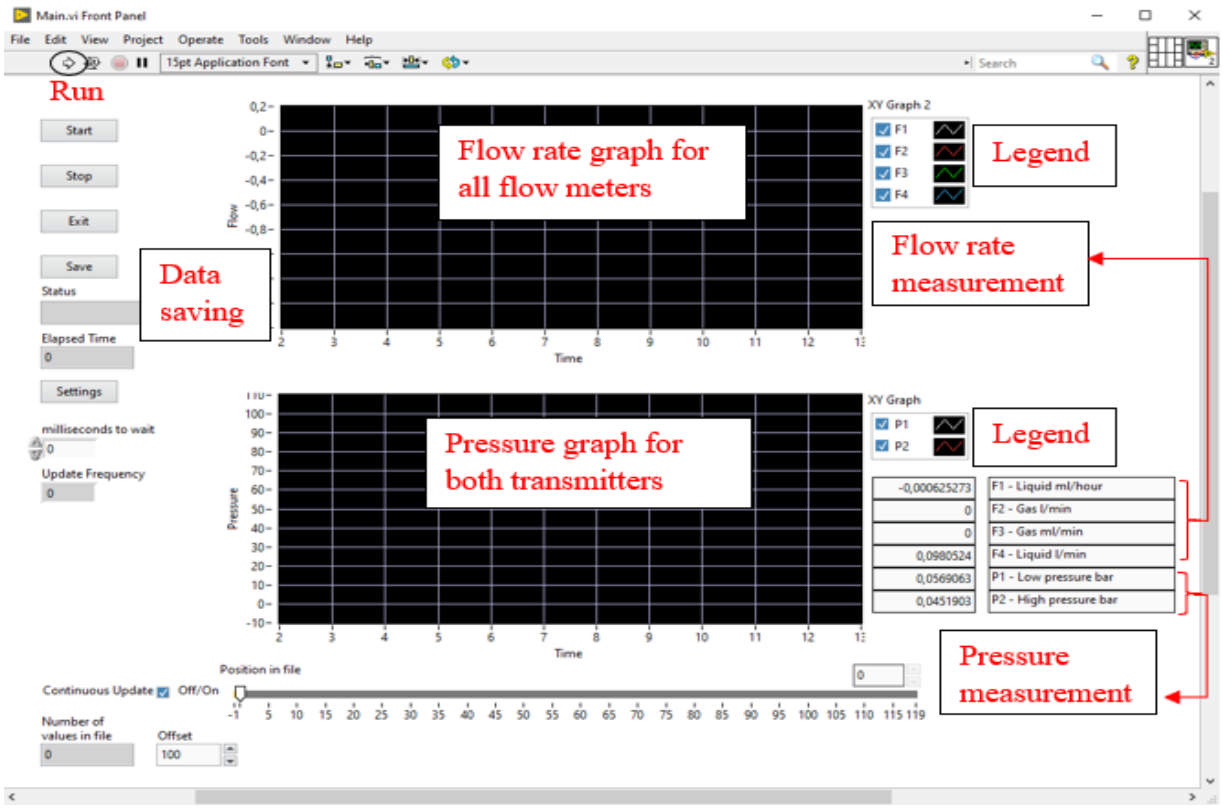

Figure 3.5: Monitoring program for the HP setup

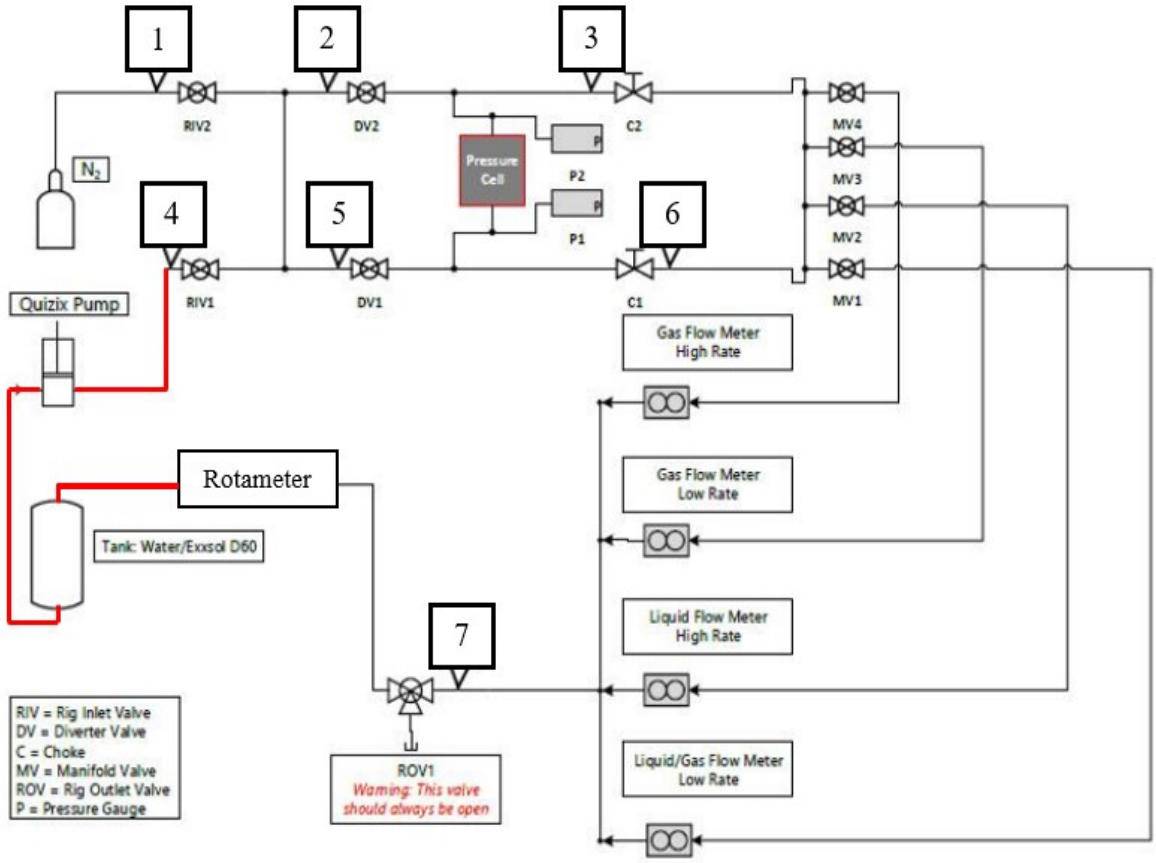

Figure 3.6: Piping and instrumentation diagram for the HP setup

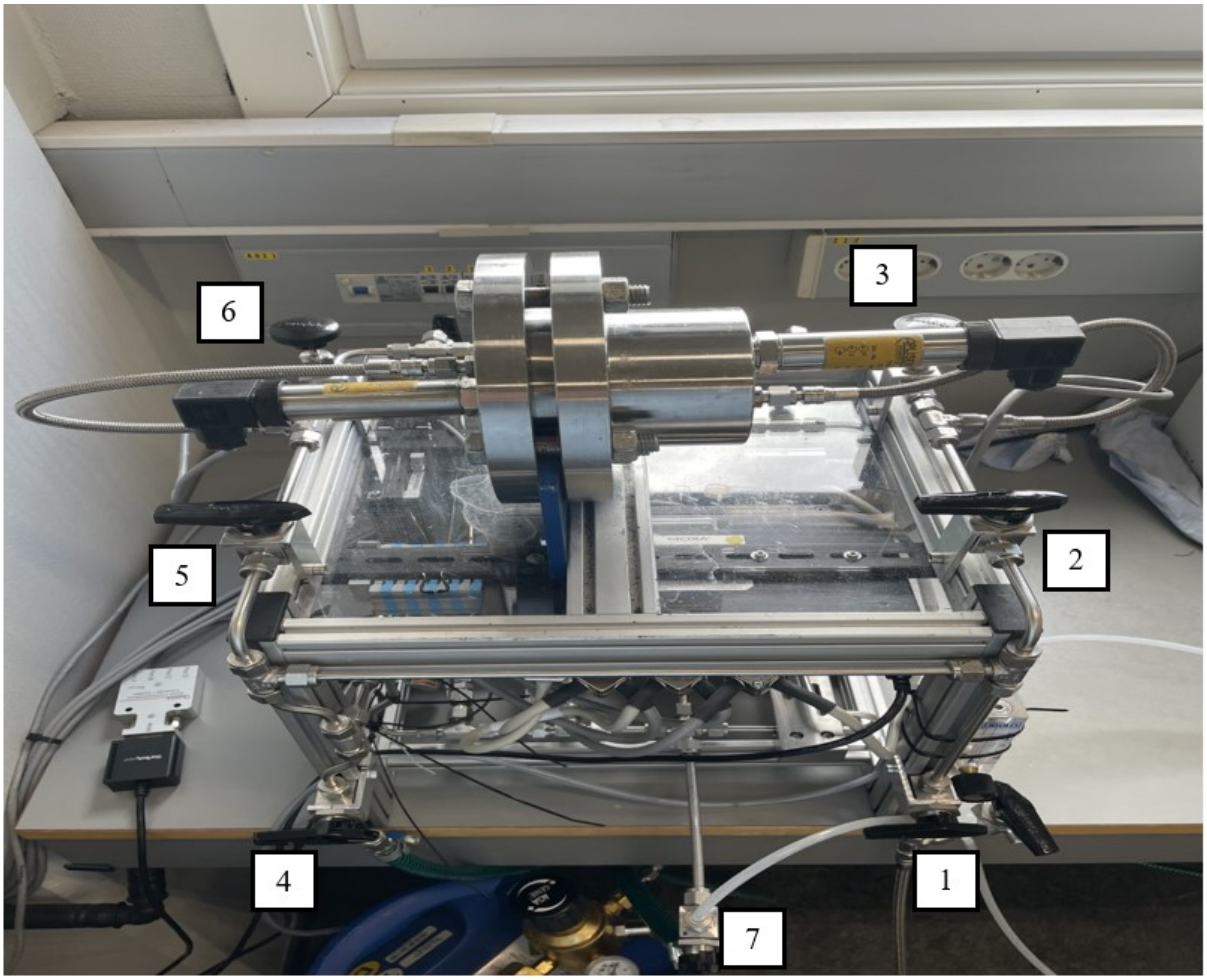

Figure 3.7: Valve numbering on the HP setup

3.1.5. Correspondence between valve leakage performance in the HP setup and the F2F$_{cyc}$ method

During injection, the production valve is closed by the gas flowback into the production fracture (**Figure 3.8**). The pressure in the tubing is higher than the pressure in the formation near the production fracture ($P_1 > P_2$). The leakage performance of this valve is evaluated by the sealing capability the ball has in its closing position when subject to different differential pressures.

Figure 3.9 shows how the production valve is placed inside the valve holder in order to test the leakage performance of that valve in its closed position **(**the ball of the production valve is in contact with the valve's seat). Once the valve is subject to gas flow, the leakage rate across the valve (indicated by the red arrows downstream the valve) is measured through the rotameter situated downstream the pressure cell at a certain differential pressure across the valve. **Figure 3.9** also illustrates how the pressure cell can represent part of the subsurface completion around the production valve during injection.

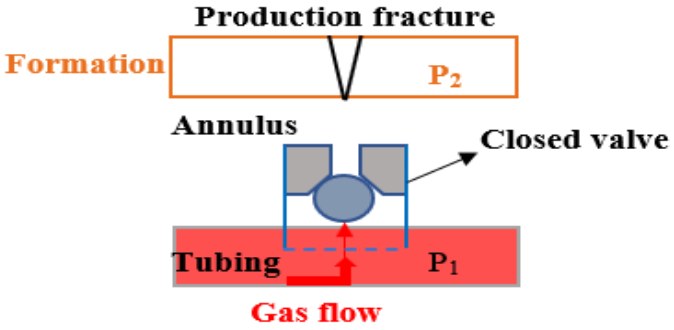

Figure 3.8: Configuration of the closed production valve and the pressure profile in the F2F$_{cyc}$ method during injection

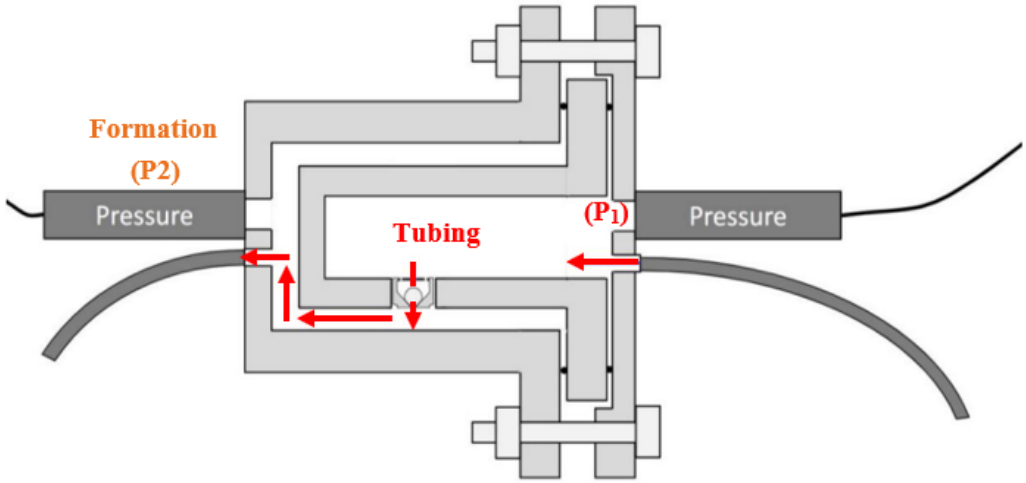

Figure 3.9: Leakage test on production valve in the pressure cell and an illustration of how the pressure cell can represent the subsurface completion of an F2F$_{cyc}$ method

As mentioned in **section 3.1.4**, the pressure downstream the cell is kept at atmospheric conditions. Thus, the pressure transmitter downstream the production valve (P_2 in that case) reads 0 barg on the monitoring program, and the pressure differential across the valve is dictated by P_1. In the F2F$_{cyc}$ method, the differential pressure that exists across the production valve is the difference between the tubing pressure and the formation pressure near the production fracture. In this case, this is represented by P_1-P_2. The pressure P_2 will typically be different than zero.

When the well is set from injection to production, an amount of injected gas will flow back from the injection fracture to the tubing, closing the valve. The pressure near the injection fracture is greater than the pressure in the tubing ($P_2 > P_1$) (**Figure 3.10**). The leakage performance of this valve is evaluated based on the amount of gas that leaks through it when the ball is in contact with the valve's seat in its closing position at different differential pressures.

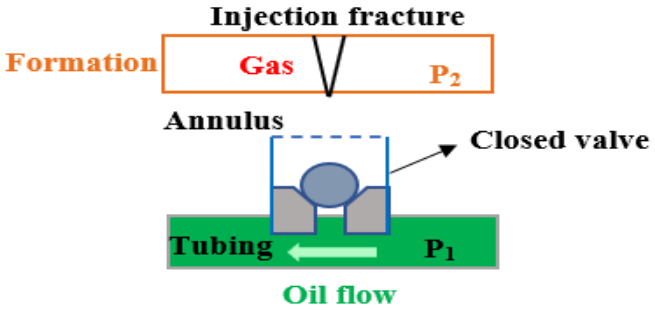

Figure 3.10: Configuration of the closed injection valve and the pressure profile in the F2F$_{cyc}$ method during production

Figure 3.11 illustrates how the injection valve is placed inside the pressure cell in order to test the leakage performance of that valve in its closed position. Once the valve is subject to gas flow, the leakage rate across the valve at a certain differential pressure is assessed through the rotameter placed downstream the pressure cell.

The pressure downstream the valve (P_1 in that case) reads 0 barg on the monitoring program, since the pressure downstream the cell is always kept at atmospheric conditions. The pressure differential across the production valve is then dictated by P_2. The differential pressure that exists across the valve is the difference between formation pressure near the injection fracture and the tubing in the F2F$_{cyc}$ method. In this case, this is represented by P_2-P_1.

As discussed in **section 3.1.1**, the injection and production valves are screwed into the valve holder that goes into the outside enclosure. However, the way both valves are screwed is different. **Figure 3.12** shows this difference.

During the leakage tests, the valves should be initially in a closed position (ball against the conical seat). Therefore, the valve holder must be placed with a different orientation for the production and the injection valve to ensure this is always the case.

Leakage test methodology and experimental procedure

The working fluid for the leakage tests conducted in the HP setup is nitrogen air from the nitrogen tank. The nitrogen tank has a pressure gage and a pressure regulator that allows for changing the pressure at which nitrogen flows out of the tank. The performance of both valves in the leakage test has been studied under pressure differentials of: 7,10, 20, 50, 75, 100, 125 and 150 bar. The pressure transmitter upstream the pressure cell reads the pressure at which nitrogen flows at from the tank, while the pressure transmitter downstream the transparent cell always reads 0 barg. Hence, the pressure differential across the valve is dictated by the pressure

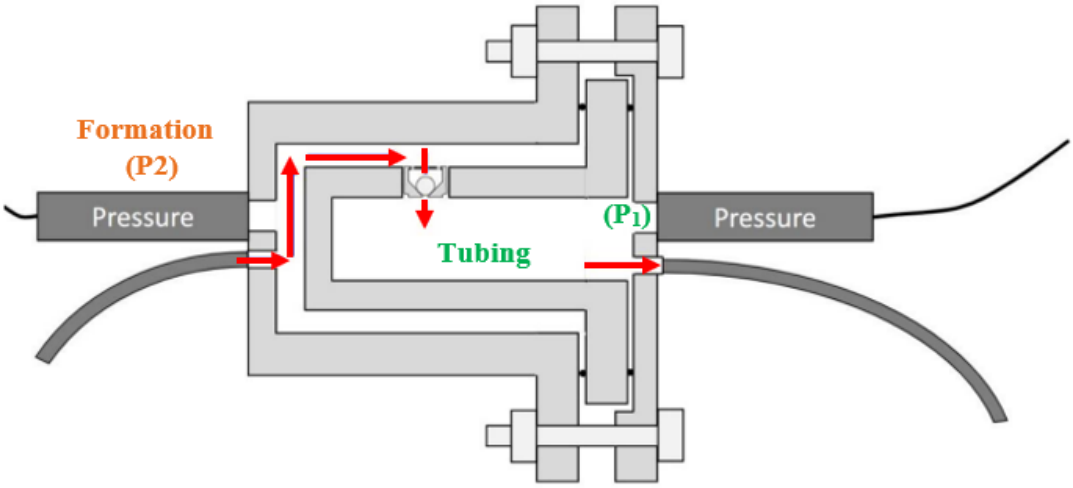

Figure 3.11: Leakage test of the injection valve in the pressure cell and an illustration of how the pressure cell can represent the subsurface completion of an F2F$_{cyc}$ method

Figure 3.12: Valve holder with the injection valve (*left*) and production valve (*right*)

coming out of the nitrogen tank. The rotameter or gas flow meter downstream the pressure cell measures the leakage rates across the valves. The leakage rates are always measured at standard conditions.

When the rotameter is used, the leakage rate is read in the rotameter when the differential pressure across the injection or production valve stabilizes at the value of interest.

Note that several trials were made to increase the nitrogen pressure accurately from 0 to 7 barg (refer to **section 3.1.2**). After successfully increasing the pressure to 7 barg and reading the leakage rate in the rotameter, it is not possible to directly increase the pressure from 7 barg to

10 barg using the pressure regulator on the nitrogen tank (it is not possible to increase the pressure in small increments). Therefore, the setup is bled out of the nitrogen gas, and the pressure is increased from 0 to 10 barg. The pressure regulator can then be regulated to directly increase the nitrogen pressure from 10 to 20 barg and so on (the pressure regulator allows to accurately increase the pressure by large increments).

Due to the way the high-pressure cell is built, the desired path for the flow of nitrogen into the cell changes between the tests done on the injection and production valves. The path of the flow of nitrogen into the pressure cell is dictated by the valves shown in **Figures 3.6 & 3.7**. **Table 3.1** shows the positions the manually activated valves should be in to properly carry out the leakage tests for the injection and production valves.

Table 3.1: Position of the manually activated valves during the leakage test for the injection and production valves

	Leakage test						
Valve type	**Valve 1**	**Valve 2**	**Valve 3**	**Valve 4**	**Valve 5**	**Valve 6**	**Valve 7**
Injection	Open	Open	Closed	Closed	Closed	Open	Closed
Production	Open	Closed	Open	Closed	Open	Closed	Closed

3.1.6. Correspondence between the valve closing performance in the HP setup and the $F2F_{cyc}$ method

When the well is set from production to injection, the injected gas flows back into the production fracture before the production valve's closure (**Figure 3.13**). The closing performance of the valve is then evaluated by the gas rate needed to close the production valve and the amount of gas lost into the production fracture prior to the valve's closure.

When the well is set to produce, the injected gas tends to flow back into the tubing prior to the injection valve's closure (**Figure 3.14)**. The closing performance of the valve is then assessed by the gas rate required to close the injection valve and the amount of gas lost into the injection fracture before the valve's closure.

Figures 3.15 & 3.16 show the placement of the production valve and the injection valve respectively inside the pressure cell to carry out the closing rate test. The ball of each of the two valves valve should be initially away from the valve's seat. The valve holder is positioned

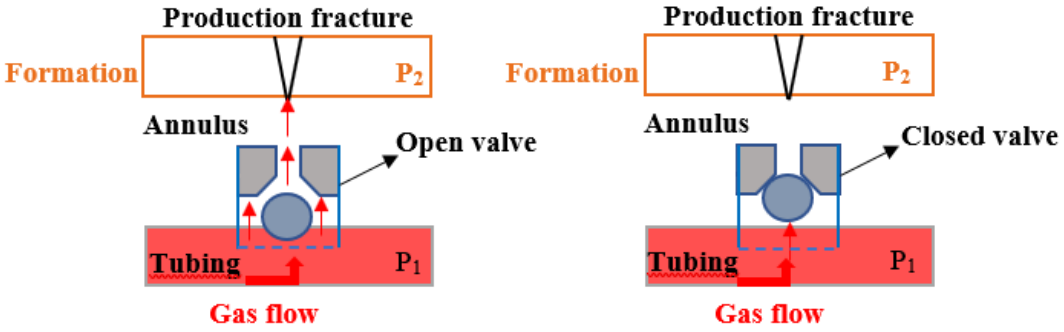

Figure 3.13: Production valve configuration before closure (*left*) showing leaked gas into production fracture, and after its closure (*right*) in the F2F$_{cyc}$ method during injection

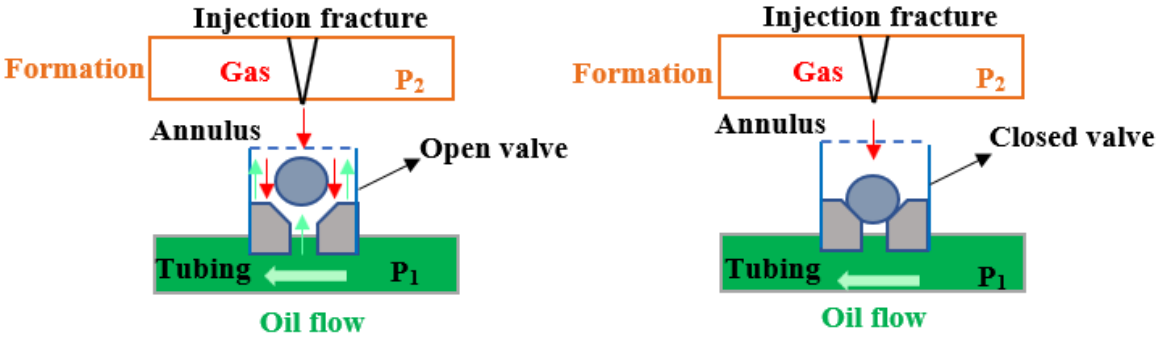

Figure 3.14: Injection valve configuration before closure (*left*) showing leaked oil into the injection fracture and leaked gas into tubing, and after its closure (*right*) in the F2F$_{cyc}$ method during production

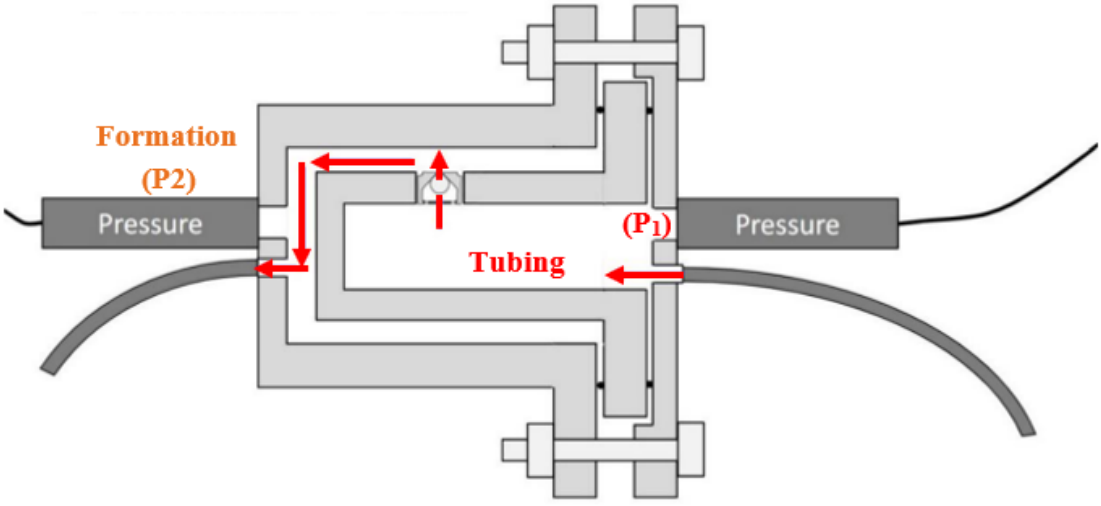

Figure 3.15: Closing rate test of the production valve in the pressure cell and an illustration of how the pressure cell can represent the subsurface completion of an F2F$_{cyc}$ method

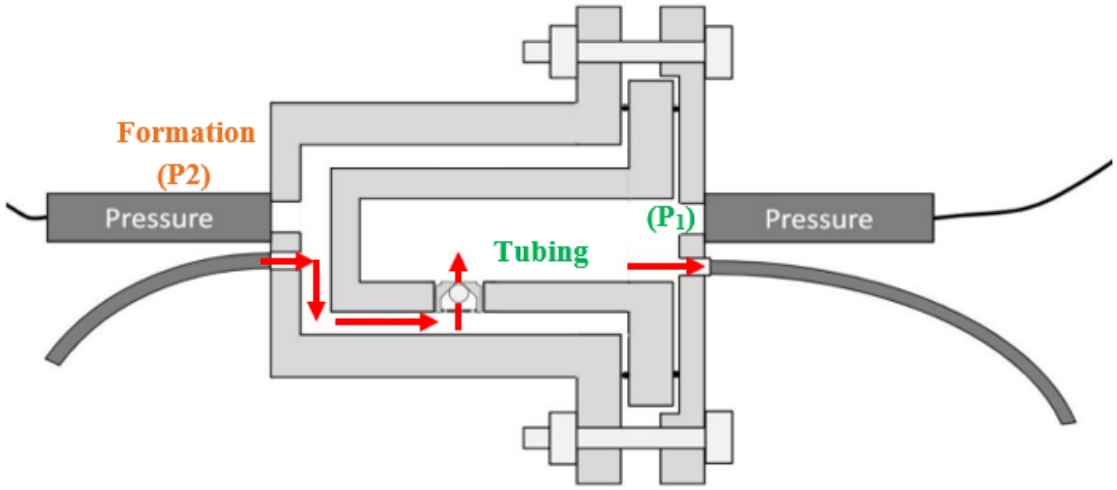

Figure 3.16: Closing rate test of the injection valve in the pressure cell and an illustration of how the pressure cell can represent the subsurface completion of an F2F$_{cyc}$ method

in a way that places the production valve at the upper side of the pressure cell and the injection valve at the lower part of the cell. These positions move the ball away from the valve's seat. Gas entering the cell at a certain rate pushes the ball towards the valve's seat, closing the valve. The rotameter situated downstream the pressure cell measures the gas lost prior to the valve's closure (indicated by the red arrows downstream the valve).

Closing rate test methodology and experimental procedure

The working fluid for the closing rate tests is air from the lab facility air supply. The nitrogen tank does not deliver a rate which is high enough to push the ball towards the valve's seat and close the valve. The rate delivered from the lab facility is at 5 L/min. This rate is the same for the closing rate tests done for the injection and production valves. The pressure at which air is delivered is at 7.13 barg. The pressure transmitter upstream the pressure cell reads a maximum of 7.13 barg, while the pressure transmitter downstream the cell should always read 0 barg. The gas flow meter situated downstream the pressure cell measures the gas leaked prior to the closure of both valves at standard conditions.

Due to the difference in positioning of the valve holder inside the pressure cell, the path for the flow of air into the cell changes between the tests done on both valves. The path of the flow of air into the pressure cell is controlled by the valves shown in **Figures 3.6 & 3.7**. **Table 3.2** shows the positions the manually activated valves should be in to properly carry out the closing rate tests for the injection and production valves.

Table 3.2: Position of the manually activated valves during the closing rate test for the injection and production valves

Closing rate test							
Valve Type	**Valve 1**	**Valve 2**	**Valve 3**	**Valve 4**	**Valve 5**	**Valve 6**	**Valve 7**
Injection	Open	Open	Closed	Closed	Closed	Open	Closed
Production	Open	Closed	Open	Closed	Open	Closed	Closed

3.2. Low-pressure setup

This setup is made of acrylic plastic. The setup can withstand pressures up to 20 bar. The LP setup is built to represent the interior of a production liner that is connected to an injection fracture and a production fracture. This setup allows for leakage rate tests to be conducted only. The working fluid in that setup is air which is supplied from the lab facility air supply.

3.2.1. Test equipment

The low-pressure setup includes the following parts:

- Transparent pressure cell
- One-liter metallic air tank
- Three solenoid valves
- Three gauge pressure transmitters with a calibrated range 0-10 bar and an accuracy of $\pm$ 0.1% of the calibrated range
- High-rate air flow meter: 2-100 L/min with an accuracy of 3%
- Injection valve: Acrylic valve seat, 7 mm grade 25 stainless steel ball, and an acrylic hex-hole lid
- Production valve: Acrylic valve seat, 7 mm grade 25 stainless steel ball, and an acrylic hex-hole lid
- Lab facility air supply

Figure 3.17 shows the LP setup. The three solenoid valves are operated through the controlling program built specifically for this low-pressure setup. The injection and production valves are built within and as part of the transparent cell (the geometry of the transparent cell can be found in *Appendix 5 & 6*). The hex-hole lids are screwed into the threads of both the injection and production valves to support the valve's ball in its open position. Both the injection and

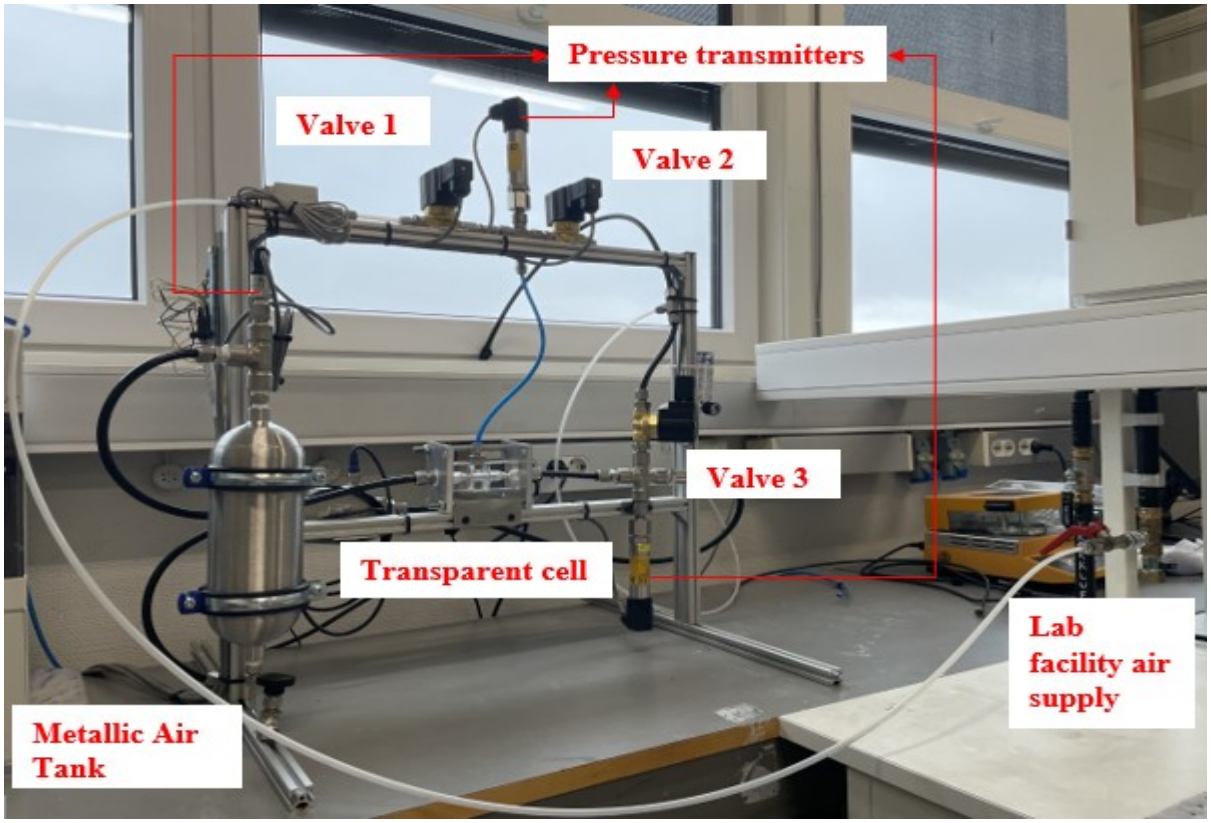

Figure 3.17: Low-pressure setup

production valves have a conical seat. The aim of building the LP setup is to represent the interior of a production liner that is connected to an injection and a production fracture, with an injection and production valve placed in front of the respective fractures (**Figure 3.18**).

3.2.2. Setup limitations

The purpose of this setup is to mimic the downhole completion of the $F2F_{cyc}$ method and measure leakage rates through the valves at certain pressure differentials. However, this setup is not built in a way that allows for gas flow meters to be installed downstream the injection and production valves.

The low-pressure setup can withstand pressures up to 20 bar, but the maximum pressure delivered by the lab wall is 7.13 barg. As a result, any differential pressure created across the valves will be equal to or less than 7.13 bar.

3.2.3. Controlling program

The controlling program for the LP setup is a “Transparent Cell” software installed on the laboratory’s PC (**Figure 3.19**).

The solenoid valves (valves 1,2, & 3) are opened and closed through this program. There exists two “valve modes” that can be chosen, and each of those modes allow the user to open and

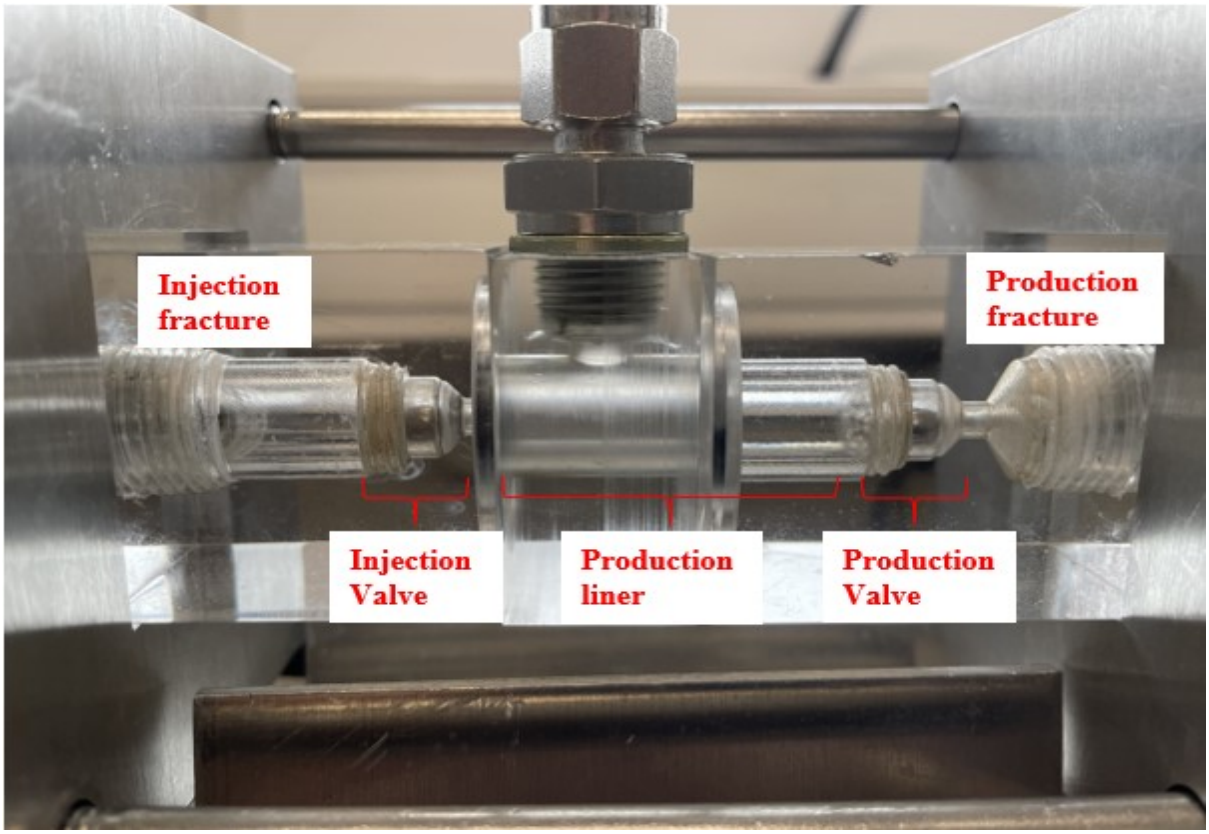

Figure 3.18: Transparent cell's injection and production valves, and an illustration of the transparent cell's representation of the F2F$_{cyc}$ completion

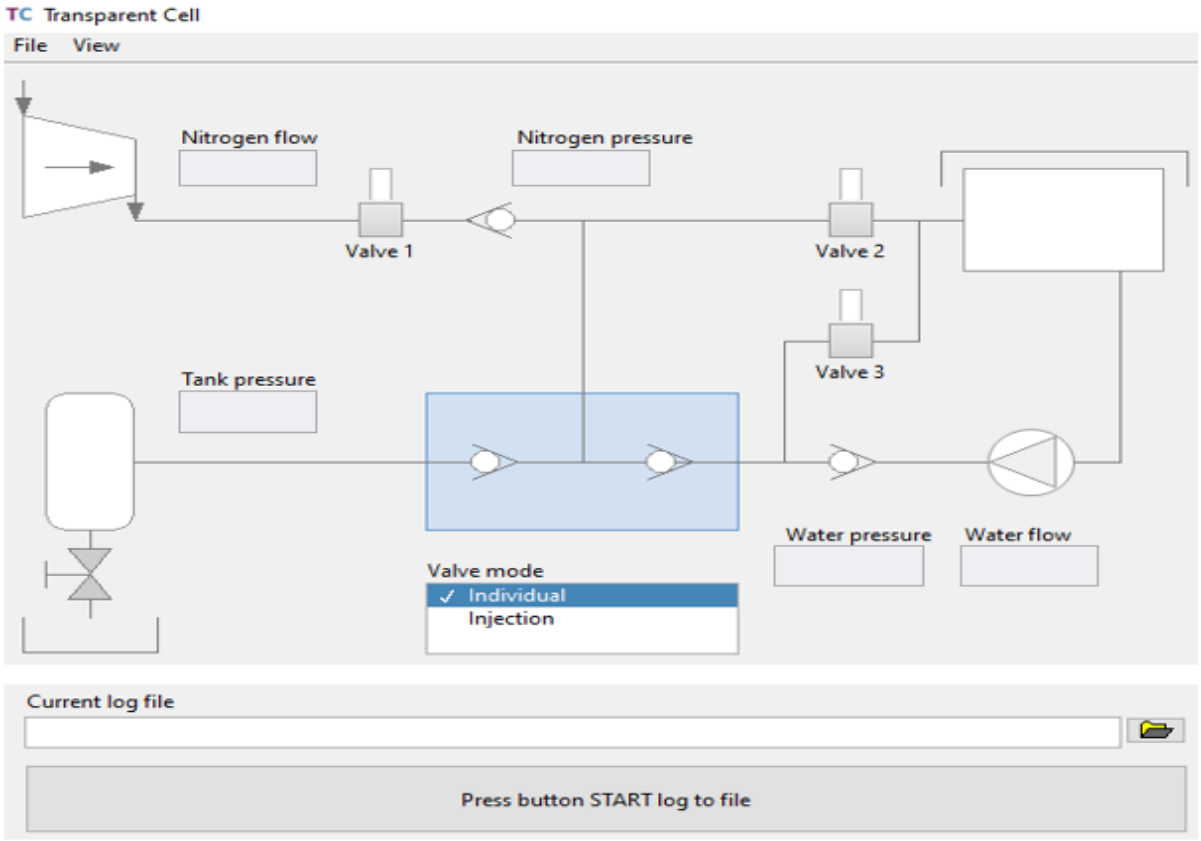

Figure 3.19: Controlling program for the LP setup

close certain valves. The selection of the modes depends on the experiment done.

This program also records and logs the pressure (3 data sets) and flowrate (2 data sets) data throughout the setup. Note that "Nitrogen flow", "Nitrogen pressure", and "Water pressure" in **Figure 3.19** refer to the high-rate gas flow meter, the pressure transmitter between valves 1 & 2**,** and the pressure transmitter below valve 3 respectively (see **Figure 3.17)**. The flow rate data is recorded in the units relative to the flow meter units' specifications, in this case L/min. The pressure is recorded in barg. Another data set that is recorded but is not seen on the program's main page is the time in second (measurements are recorded every 0.1 second). Hence, six sets of data are recorded. For the experiments conducted in this thesis, the "Water flow" and "Water pressure" data sets, indicating the flow rate of water and the water pressure respectively, are disregarded. This reduces the data sets of interest to four (Tank pressure, Nitrogen flow, Nitrogen pressure, and time)

After the experiment is done, the logged data is saved and exported to an Excel file for further analysis.

3.2.4. LP setup layout

Figure 3.20 shows the P & ID for the low-pressure setup. The water flow meter, the water pump, and the water tank (shown in the setup's P & ID) are three components that are not used in the experiments conducted in this setup, since water is not used as a working fluid. The line connecting those three components (highlighted in red on the P & ID) is noy used.

The $F2F_{cyc}$ completion is represented through the LP setup in the following way: the metallic air tank represents the pressurized formation near the injection fracture, the middle of the transparent cell represents the liner, and the downstream side of the production valve represents the formation near the production fracture.

3.2.5. Leakage test methodology and experimental procedure

Leakage test for the production valve

The "injection" mode in the Transparent cell software is first selected. This enables the opening of valves 1 & 3 at the same time (**Figure 3.21**). Air flows into the middle of the transparent cell. The injection valve opens, and the air fills up and pressurizes the metallic air tank. The pressure in the tank reaches 7.13 barg rapidly. The production valve closes since the injected air pushes the valve's ball against the valve's seat, closing the opening. Therefore, the pressure in the middle of the transparent cell (the pressure upstream the production valve read by the pressure transmitter "Nitrogen pressure") equalizes with the tank pressure at 7.13 barg and

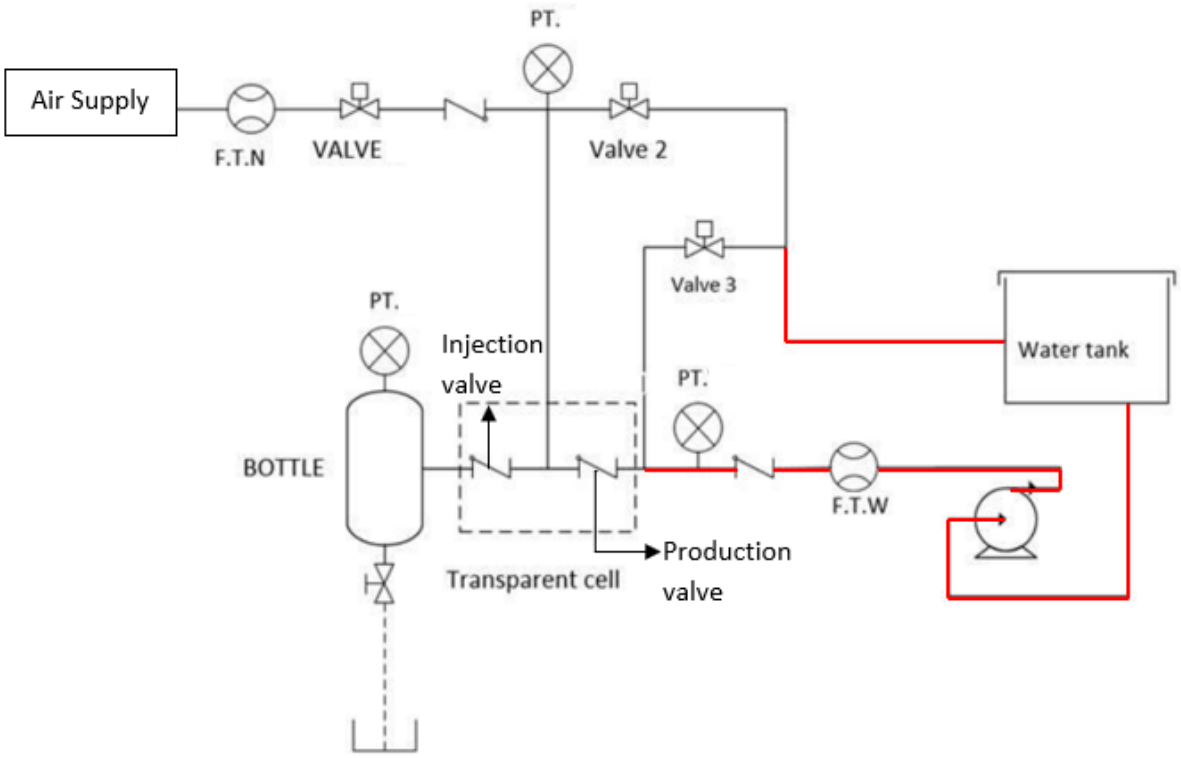

Figure 3.20: Piping and instrumentation diagram for the LP setup. The labelling of the injection and production valves is shown

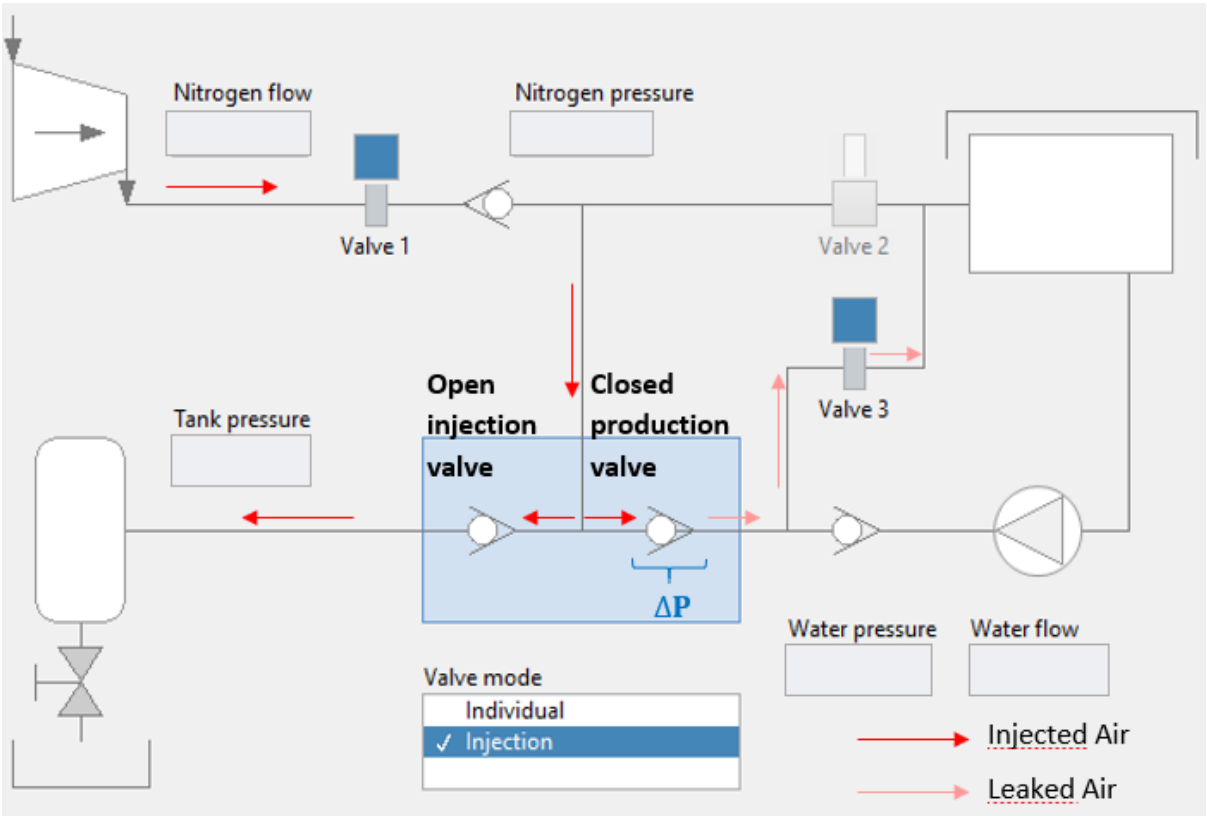

Figure 3.21: Injection mode setting in the "Transparent cell" software, and the path of injected and leaked air through the production valve

stays at that value as long as injection is on-going. The pressure downstream the production valve is 1 bara since valve 3 is open to the atmosphere. Hence, the differential pressure that exists across the production valve is 7.13 bar. The differential pressure created across the closed production valve in the LP setup represents the differential pressure in the $F2F_{cyc}$ method between the liner and the formation near the production fracture during injection.
However, this procedure only allows evaluating the leakage performance of the production valve under one differential pressure across it (7.13 bar).

Leakage test for the injection valve

After injection stops, the "individual" mode on the transparent cell software is selected. It allows operating on individual valves alone. To test the leakage through a closed injection valve, valve 2 is opened (**Figure 3.22**). Opening valve 2 to the atmosphere creates a differential pressure across the injection valve which pushes its ball towards the valve's seat, closing the valve. This differential pressure is represented by the difference between the tank pressure and the atmospheric pressure. As the injection valve leaks in its closing position, the tank pressure decreases and the leakage rate is assessed against different differential pressures. The leakage rate through the injection valve is calculated through the tank depressurization with time. The differential pressure created across the closed injection valve in the LP setup represents the differential pressure between the formation near the injection fracture and the liner in the $F2F_{cyc}$ method during production.

Alternative method to assess leakage performance of the production valve

An alternative method (**Figure 3.23**) had been proposed to create several differential pressures across the production valve at which leakage rates can be assessed:

1. Select the "injection" mode in the software and re-inject air (valves 1 & 3 are opened). Air fills up the metallic air tank again and the production valve closes ("Nitrogen pressure = "Tank Pressure" = 7.13 barg, and the differential pressure across the valve is at 7.13 bar).
2. Stop injection (this closes valves 1 & 3)
3. Select "individual" mode and open valve 3 alone to the atmosphere.

The injection valve is kept in its open position since no differential pressure is applied across it, and the air in the metallic air tank is not large enough to push the ball towards the injection

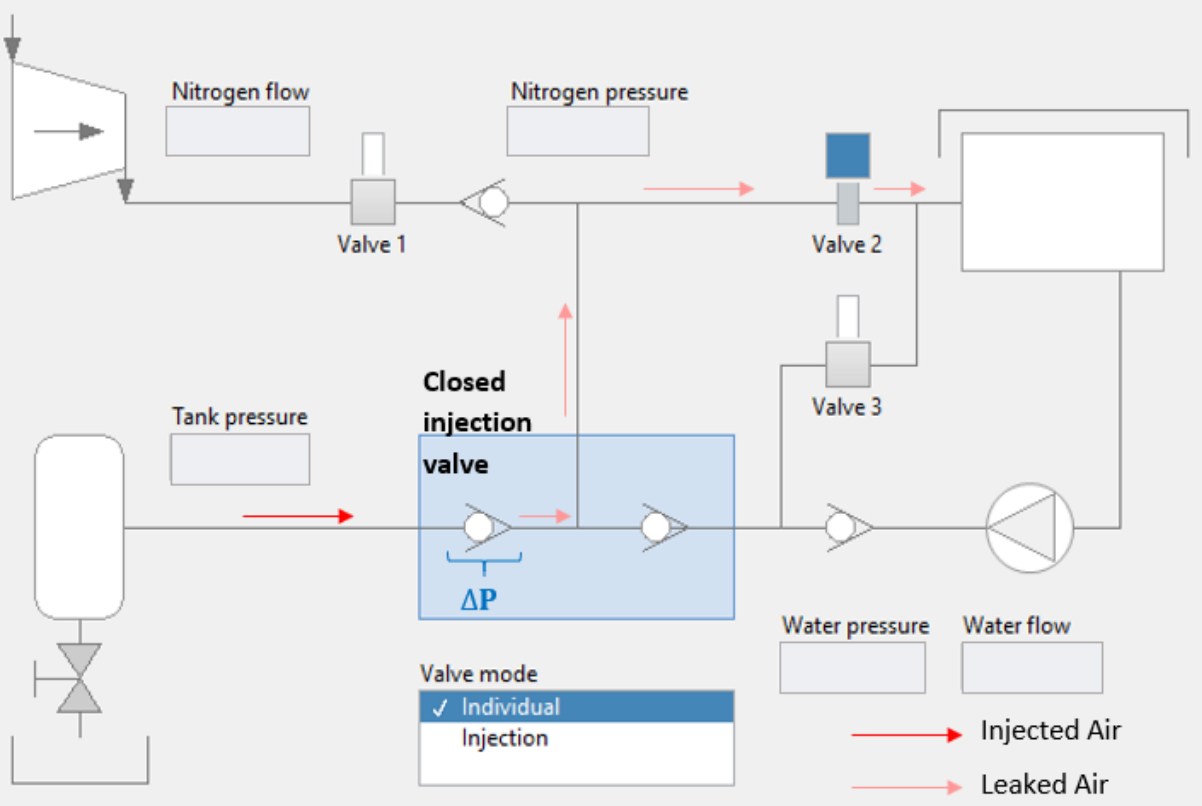

Figure 3.22: Individual mode setting in the "Transparent cell" software allowing the opening of valve 2, and the path of injected and leaked air through the injection valve

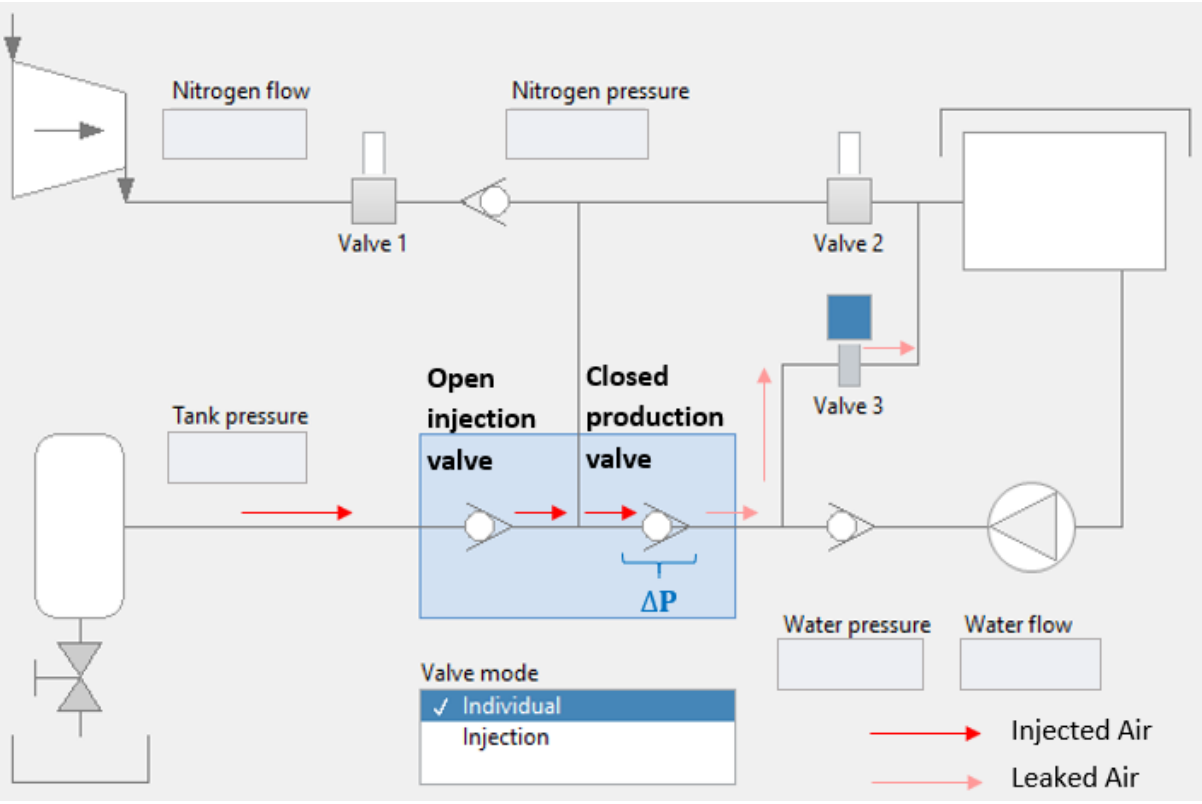

Figure 3.23: Individual mode setting in the Transparent cell software allowing the opening of valve 3, and the path of injected and leaked air through the production valve

valve's seat. Therefore, "Nitrogen pressure" is always equal to the "Tank pressure" when the production valve is closed. The leakage through the closed production valve is then estimated using data of the tank depressurization with time, since the pressure upstream the production valve ("Nitrogen Pressure") is equal to the "Tank pressure". The "Nitrogen pressure" decreases with time, so several pressure differentials now exist across the production valve as Valve 3 is opened to the atmosphere.

Leakage test methodology

For all the tests, the pressure at which air flows out from the lab facility air supply was 7.13 barg (8.13 bara). While assessing the leakage performance of the injection and production valves, the pressure downstream the valve of interest was always at atmospheric conditions (1 bara). The performance of both valves during the leakage tests had been studied at differential pressures of: 7, 6.5, 6, 5.5, 5, 4.5, 4, 3.5, 3, 2.5, 2, 1.5, and 1 bar.

The depressurization of the metallic air tank versus time was used to calculate the continuous leakage rates through the valves. The leakage rates were calculated at standard conditions. Every tank pressure value (barg) refers to a differential pressure that exists across the valve (bar). For example, a tank pressure value of 6 barg indicates a pressure differential of 6 bar across the injection or production valve. The calculated leakage rates are then selected at the differential pressures of interest.

4. Measurement and calculation of experimental parameters

4.1. Pressure measurements

The pressure in the LP and HP setups was measured through gauge pressure transmitters that have an accuracy of $\pm$ 0.1% of their calibrated range.

The calibrated range of the pressure transmitters is 0-10 barg for the LP setup, and 0-250 barg for the HP setup. This gives an accuracy of $\pm$ 0.01 barg and $\pm$ 0.25 barg for the LP and HP setup respectively. Hence, the differential pressures calculated (in bar) across the injection and production valves are $\pm$ 0.01 bar (δP_{LP}) and $\pm$ 0.25 bar (δP_{HP}) accurate.

4.2. Measurement through rotameter

In the HP setup, leakage rate measurements, as part of the leakage tests, were carried out using the rotameter. The flow rates measured by the rotameter in L/min were converted to scf/min, in which they were reported.

An illustration of how leakage rate values were read from the rotameter is found in *Appendix 7*.

The gas rotameter can detect flow ranging from 0.4 L/min to 5 L/min only. Any leakage rate in the HP and LP setup that fall below that range cannot be quantified (the ball inside the rotameter can only be seen fidgeting below the 0.4 L/min line).

The rotameter has an accuracy of $\pm$ 5 % of full scale, so the error associated with all the values read from the rotameter (δq_{ro}) is $\pm$ 0.25 L/min or $\pm$ 0.00883 scf/min.

4.3. Measurement through gas flow meter

The gas flow meter has been used in the leakage and closing rate tests in the HP setup. The gas flow meter has an accuracy of $\pm$ 5 % full scale (maximum gas flow meter scale value is 3 L/min). Therefore, the gas flow meter is $\pm$ 0.15 L/min or $\pm$ 0.005298 scf/min (δq_{gf}) accurate for all measured values.

4.4. Leakage rate calculation

4.4.1. Low-pressure setup

The depressurization of the metallic air tank versus time was used to calculate the leakage rates through the valves. The “Tank pressure” data (which records the pressure inside the tank during the leakage test) was converted to a dataset in absolute pressure (bara and pascal). As the

injection or production valves leak, the metallic air tank depressurizes. The ideal gas law was used to convert pressures inside the air tank to masses (Eq. **4.1**). The difference in the air mass inside the tank between two points in time is converted into a leakage rate (Eq. **4.2**) through the valve of interest. **Table 4.1** shows the given parameters for the leakage rate calculations in the LP setup.

Table 4.1: Given parameters for leakage rate calculations in the LP setup

Parameters (units)	Values
Metallic air tank volume (m^3)	0.001
Air molar mass (g/mol)	28.97
Ambient temperature (Kelvin)	293.15
Universal gas constant (J/K.mol)	8.314
Air density at standard conditions (kg/m^3)	1.225

$$m_{air} = a\left(\frac{P_m * V * M_{air}}{R * T}\right) \tag{4.1}$$

In which:

m_{air} : mass of air inside the tank (kg)

P_m : measured pressure inside the air tank (Pa or $kg.m^{-1}.s^{-2}$)

V : volume of air tank (m^3)

M_{air} : molar mass of air (g/mol)

R : Universal gas constant (J/K.mol or $kg.m^2.s^{-2}.K^{-1}.mol^{-1}$)

T : temperature (K)

a : factor to convert the mass from gram to kilogram (10^{-3})

$$q_{air,LP} = \frac{\frac{\Delta m_{air}}{\rho_{air}}}{\Delta t} * b \tag{4.2}$$

In which:

$q_{air,LP}$: air leakage rate at standard conditions in the LP setup (scf/min)

Δm_{air} : difference in mass of air inside the tank between times t_1 & t_2 (kg)

ρ_{air} : Air density at standard conditions (kg/m^3)

Δt : time increment (s)

b : factor to convert from is sm^3/min to scf/min (1878.9)

Limitations

The "Transparent cell" software records data every 0.1 seconds (high frequency), so the "Tank pressure" data is noisy. Hence, the calculated leakage rate (calculated with a Δt of 0.1s and then larger Δts) values were very noisy. Hence, the "tank pressure versus time" plot was fitted with a polynomial curve for the leakage tests conducted for the injection and production valves (best-fit polynomial curves shown in *Appendix 8*)

Equations **4.3 & 4.4** show the fifth-degree polynomial equations representing the tank depressurization versus time for the leakage tests done on the injection and production valves respectively.

$$P_f(t) = -5.923 * 10^{-19}\,(t^5) + 1.249 * 10^{-14}\,(t^4) - 1.081 * 10^{-10}\,(t^3) + 5.644 * 10^{-7}\,(t^2) - 2.527 * 10^{-3}\,(t) + 8.381 \quad (4.3)$$

$$P_f(t) = -3.983 * 10^{-15}\,(t^5) + 1.711 * 10^{-11}\,(t^4) - 2.762 * 10^{-8}\,(t^3) + 2.329 * 10^{-5}\,(t^2) - 1.662 * 10^{-2}\,(t) + 10.522 \quad (4.4)$$

In which:

P_f : pressure calculated through the polynomial fit (bara)

t : time recorded by the software (s)

The errors between the measured "Tank pressure" values and the pressures calculated through the polynomial fit are calculated through Eq. **4.5**. The error values fall below 0.8 % for the leakage test done on the injection valve (**Figure 4.1)** and below 1 % for the leakage test performed on production valve (**Figure 4.2)**. Therefore, the polynomial curves have an acceptable accuracy to describe the depressurization of the tank.

$$\epsilon = \frac{P_m - P_f}{P_m} * 100 \quad (4.5)$$

In which:

ϵ : error (%)

P_m : measured metallic air tank pressure (bara)

P_f : pressure calculated through the polynomial fit (bara)

Pressures calculated through the polynomial equations are then used for the mass calculations (Eq. **4.6**) and hence leakage rate calculations (Eq. **4.2**). The values P_f will be used instead of P_m.

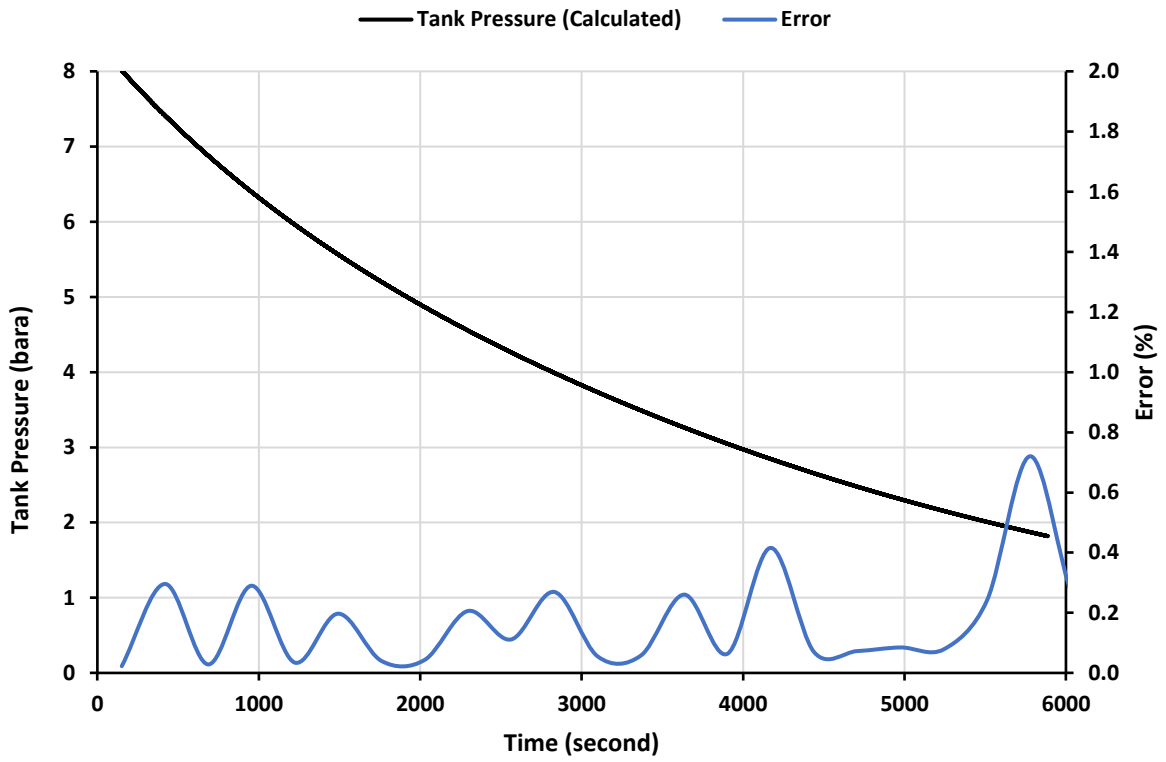

Figure 4.1: Error between the measured "Tank pressure" data and the calculated pressures using the polynomial equation *(Eq.4.3)* for the leakage test done on the injection valve

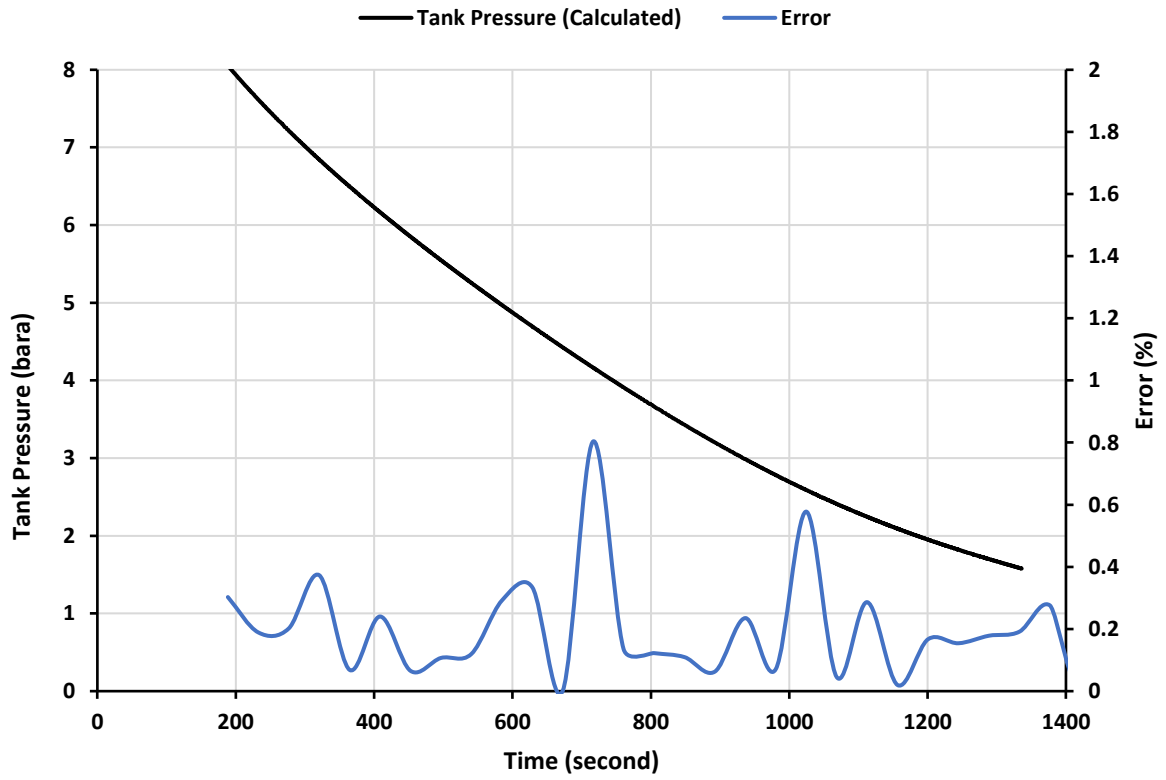

Figure 4.2: Error between the measured "Tank pressure" data and the calculated pressures using the polynomial equation *(Eq.4.4)* for the leakage test done on the production valve

$$m_{air} = a\left(\frac{P_f * V * M_{air}}{R * T}\right) \quad (4.6)$$

Leakage rate error propagation

As mentioned in **section 4.1**, the pressure transmitters in the LP setup have an accuracy of $\pm$ 0.1% of their calibrated range (calibrated range is 10 barg), so the error associated to all calculated differential pressures across the valves (in bar) is $\delta P_{LP} = \pm$ 0.01 bar.

In Eq. **4.6** all parameters except for the pressure are constant, hence it can be written as:

$$m_{air} = P_f * c_1 \quad (4.7)$$

Pressure values should be expressed in pascal, so the error associated to the mass is:

$$\delta m_{air} = (\delta P_{LP} * 10^5) * c_1 \quad (4.8)$$

In which:

δm_{air} : error associated to calculated mass values (kg)

δP_{LP} : error associated to pressure measurements in LP setup (barg)

c_1 : $a\ (V * M_{air})/(R * T)$

The factor 10^5 in Eq**. 4.8** is used to convert the error associated to pressure from barg to pascal.

The error associated to all calculated mass values is constant, $\delta m_{air} = \pm\ 1.189 * 10^{-5}$ kg.

In Eq. **4.2**, all parameters are constant except for the mass, so it can be written as:

$$q_{air,LP} = \Delta m_{air} * c_2 \quad (4.9)$$

The error associated to the leakage rates is then:

$$\delta q_{air,LP} = \left(\sqrt{\left(\delta m_{air_{,t_1}}\right)^2 + \left(\delta m_{air_{,t_2}}\right)^2}\right) . c_2 \quad (4.10)$$

Hence,

$$q_{air,LP} = (\Delta m_{air} * c_2) \pm \delta q_{air} \quad (4.11)$$

In which:

$\delta q_{air,LP}$: error associated to the air leakage rate in LP setup

$\delta m_{air_{,t_1}}$: error associated to the calculated mass of air at a time t_1

$\delta m_{air_{,t_2}}$: error associated to the calculated mass of air at a time t_2

c_2 : $b\ /\ (\rho_{air} * \Delta t)$

Note that $\Delta m_{air} = m_{air_{,t_1}} - m_{air_{t2}}$, and $\delta m_{air_{,t_1}} = \delta m_{air_{,t_2}} = \pm\, 1.189 * 10^{-5}$ kg.

Specifying Δt used to calculate leakage rates

An increment Δt = 0.1s was used at first to calculate the leakage rates (using Eq. **4.2**). The results showed that the leakage rates are smaller than the error $\delta q_{air,LP}$ associated to them ($\pm$ 0.258 scf/min, calculated through Eq. **4.10**).

Therefore, the time increment for leakage rate calculations should be increased to get $\delta q_{air,LP}$ values smaller than calculated leakage rates. To avoid the process of "trial and error", an error value equivalent to 10% of the smallest leakage rate (the leakage rate at the lowest differential pressure, 1 bar) was set as an acceptable error value associated to the leakage rates. This value was then used to calculate the time increment, using Eq. **4.12** (derived from Eq. **4.10**). The obtained time increment was then used to re-calculate the leakage rates. **Figure 4.3** shows a flow chart to clearly visualize the steps.

$$\Delta t = \left[\sqrt{2}(\delta m_{air})\right] * \frac{b}{\rho_{air}\, \delta q_{air,LP}} \tag{4.12}$$

Table 4.2 summarizes the leakage rates for the injection and production valves at a differential pressure of 1 bar, the 10% error associated to all calculated leakage rates, and the corresponding Δt values calculated.

Table 4.2: Leakage rates at a differential pressure of 1 bar, the error associated to the leakage rates, and the time increment used to re-calculate leakage rates for the injection and production valves

	$q_{air,LP}$ (scf/min)	$\delta q_{air,LP}$ (scf/min)	Δt (s)
Injection valve	0.00096	$\pm$ 0.000096	268
Production valve	0.00583	$\pm$ 0.000583	44

Tables 4.3 shows the percent difference (P.D) between the leakage rates calculated at a timestep of 268 second and 0.1 second for the injection valve. **Table 4.4** shows the percentage difference between the leakage rates calculated at a timestep of 44 second and 0.1 second for the production valve. In this section, the percent difference is calculated by Eq. **4.13**.

$$P.D = \frac{q_{air,LP_{\Delta t}} - q_{air,LP_{\Delta t=0.1}}}{q_{air,LP_{\Delta t=0.1}}} * 100 \tag{4.13}$$

Table 4.3: Percent difference between the leakage rates calculated at timesteps of 0.1 & 268 seconds for the largest and smallest pressure drops used across the injection valve

Injection valve			
	Δt = 0.1s	Δt = 268s	Difference
ΔP (bar)	$q_{air,LP}$ (scf/min)	$q_{air,LP}$ (scf/min)	(%)
7	0.00431	0.00440	2.08
1	0.00096	0.00099	3.11

Table 4.4: Percent difference between the leakage rates calculated at timesteps of 0.1 & 44 seconds for the largest and smallest pressure drops used across the production valve

Production valve			
	Δt = 0.1s	Δt = 44s	Difference
ΔP (bar)	$q_{air,LP}$ (scf/min)	$q_{air,LP}$ (scf/min)	(%)
7	0.01875	0.01950	4.01
1	0.00583	0.00584	0.12

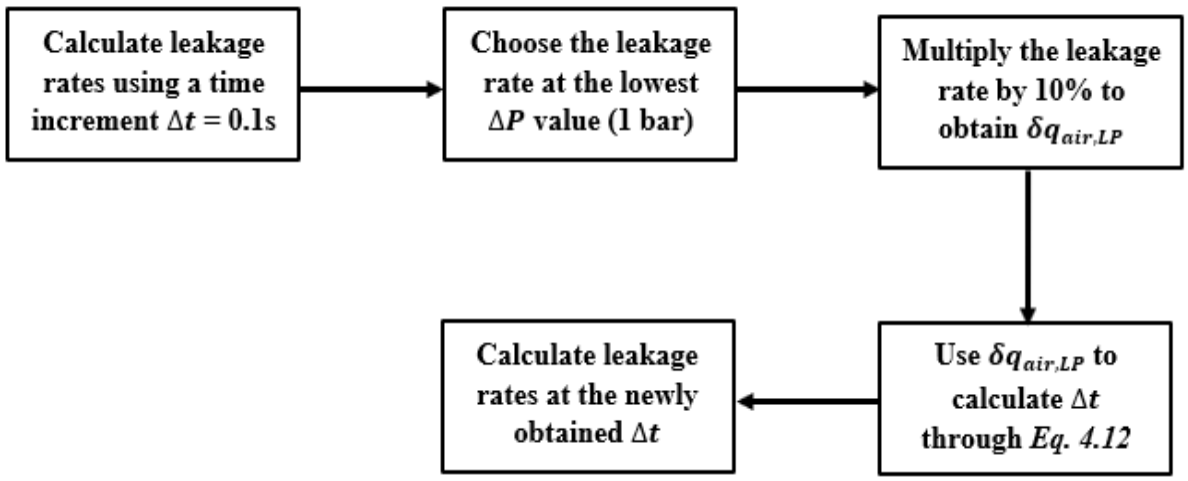

Figure 4.3: Flow chart representing steps to calculate Δt

The percent differences (shown for the largest (7 bar) and smallest (1 bar) ΔP used across the valves) are small for both valves. Therefore, the leakage rate values calculated at the new timesteps (268 and 44 seconds for the injection and production valves respectively) are representative of the leakage performance of the valves and are used in further analysis in this thesis.

4.4.2. High-pressure setup

As discussed in **section 3.1.2**, the pressure regulator of the nitrogen tank does not allow to increase the pressure incrementally from 0 to 7 barg. Leakage rates through the injection and production valves were measured by the rotameter (L/min then converted to scf/min, $q_{N_{2,ro}}$). at differential pressures starting from 7 bar. The maximum pressure differential that can be created across the injection and production valves in the LP setup is 7.13 bar.

To compare the leakage performance of the injection and production valves at the same differential pressures in the HP and LP setups, the measured rates in the HP setup were plotted against their respective differential pressures. A best-fit polynomial curve fitted to the values was used to mathematically extrapolate leakage rate values towards the low-pressure range ($\Delta P \leq 7$ bar). The best-fit polynomial curves were forced to pass through the origin.

Equations **4.13 & 4.14** show the fifth- and fourth-degree polynomial equations resulting from the best-fit line to the plot established for the injection and production valves respectively.

$$q_{N_2,f}(\Delta P) = +1.5316 * 10^{-11} (\Delta P)^5 - 5.5137 * 10^{-9}(\Delta P)^4 + 8.1283 * 10^{-7} (\Delta P)^3 - 6.1567 * 10^{-5} (\Delta P) + 2.4518 * 10^{-3} (\Delta P) \quad (4.14)$$

$$q_{N_2,f}(\Delta P) = -1.6244 * 10^{-10} (\Delta P)^4 + 1.5969 * 10^{-7}(\Delta P)^3 - 2.3579 * 10^{-5} (\Delta P)^2 + 1.2924 * 10^{-3} (\Delta P) \quad (4.15)$$

In which:

$q_{N_{2,f}}$: nitrogen leakage rate calculated through the polynomial fit (scf/min)

ΔP : pressure differential across the valve (bar)

Note that the values extrapolated to the low-pressure range have no error associated to them since they were not measured.

5. Results and Discussion

5.1. Leakage tests in HP setup

In this section, results from the rotameter measurements are presented and then used for further analysis and discussion. Note that all best-fit lines were forced to pass through the origin.

Figures 5.1 & 5.2 show the plots for the measured leakage rates through the rotameter versus differential pressures associated to the leakage rates, across the injection and production valves respectively. Note that leakage rates through the production valve at ΔP of 7 and 10 bar could not be read by the rotameter since they fell under its minimum 0.4 L/min flow limit (or 0.014126 scf/min).

After a ΔP of 100 bar and 75 bar for the injection and production valves respectively, the leakage rates decrease with increasing differential pressures. These pressure differentials are referred to as critical differential pressures (ΔP_c) from this point forward in this report.

To assess the leakage performance of the valves at the low-pressure range (which falls below the critical differential pressures for both valves), the leakage rates measured at and before ΔP of 100 bar (for the injection valve) and 75 bar (for the production valve) were used to get the best-fit line needed to extrapolate leakage rates to the low-pressure range.

For the injection valve, the best-fit line that resulted in Eq. **4.14** is shown in **Figure 5.3**.

For the production valve, three data points (leakage rates at ΔP of 20, 50, and 75 bar) were not enough to establish an accurate best-fit line. To establish a the best-fit line that can accurately describe the trend the measured data points follow, four or more points were needed. Hence, an additional measurement at a ΔP of 65 bar was done (**Table 5.1)** (this data point was just used for the purpose of establishing an accurate best-fit line to extrapolate leakage rates to the low-pressure range and is not shown elsewhere in the report). The best fit line that resulted in Eq. **4.15** is shown in **Figure 5.4**.

Table 5.1: Additional leakage rate measurement at a differential pressure of 65 bar across the production valve

Production valve			
Rotameter			
ΔP **(bar)**	$q_{N_{2,ro}}$ **(scf/min)**	δP_{HP} **(bar)**	δq_{ro} **(scf/min)**
65	0.0256	$\pm$ 0.25	$\pm$ 0.00883

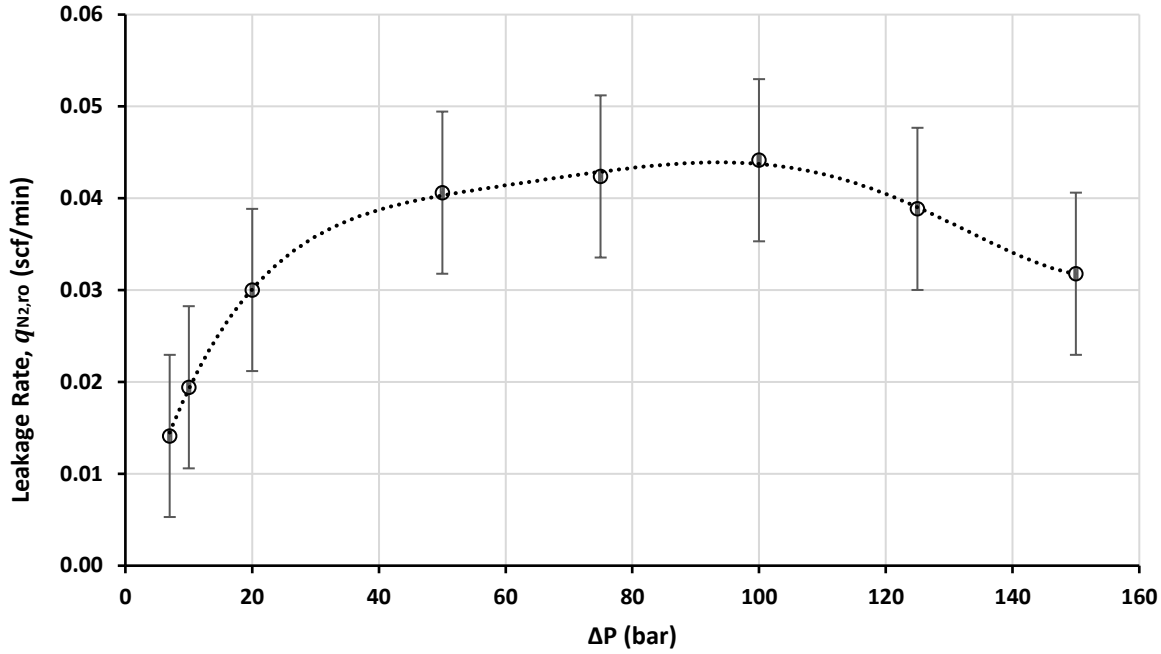

Figure 5.1: Measured leakage rates versus differential pressure across the injection valve in the HP setup. Y error bars ± 0.00883 scf/min and X error bars ± 0.25 bar. Black dotted line represents a fit through the data points

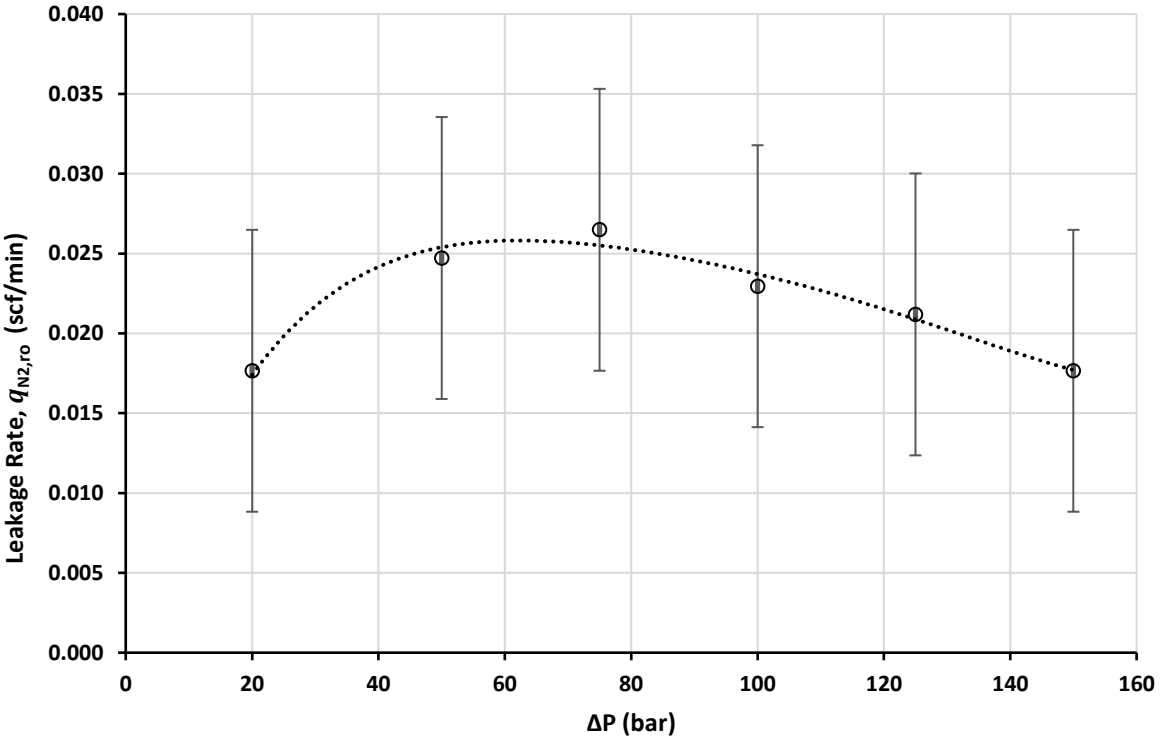

Figure 5.2: Measured leakage rates versus differential pressure across the production valve in the HP setup. Y error bars ± 0.00883 scf/min and X error bars ± 0.25 bar. Black dotted line represents a fit through the data points

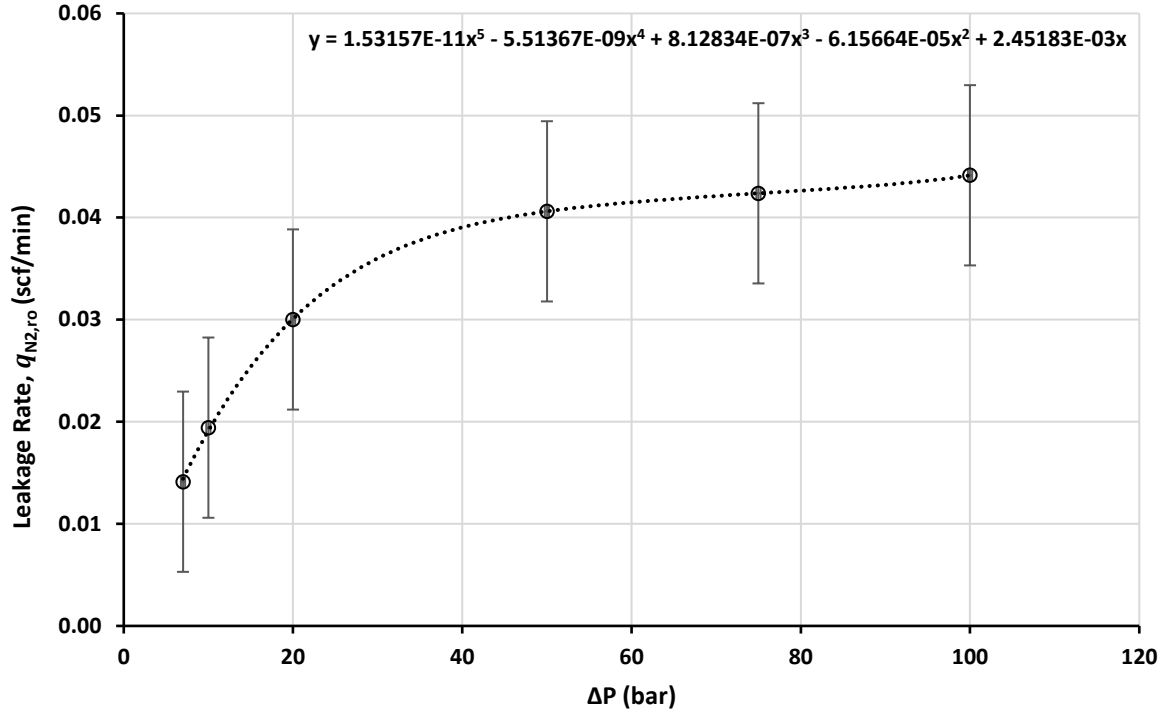

Figure 5.3: Measured leakage rates versus differential pressure (Δ*P* up until 100 bar) across the injection valve in the HP setup. Y error bars ± 0.00883 scf/min and X error bars ± 0.25 bar. The best-fit polynomial line (dotted black line) represents *Eq. 4.14* which is also shown on the plot

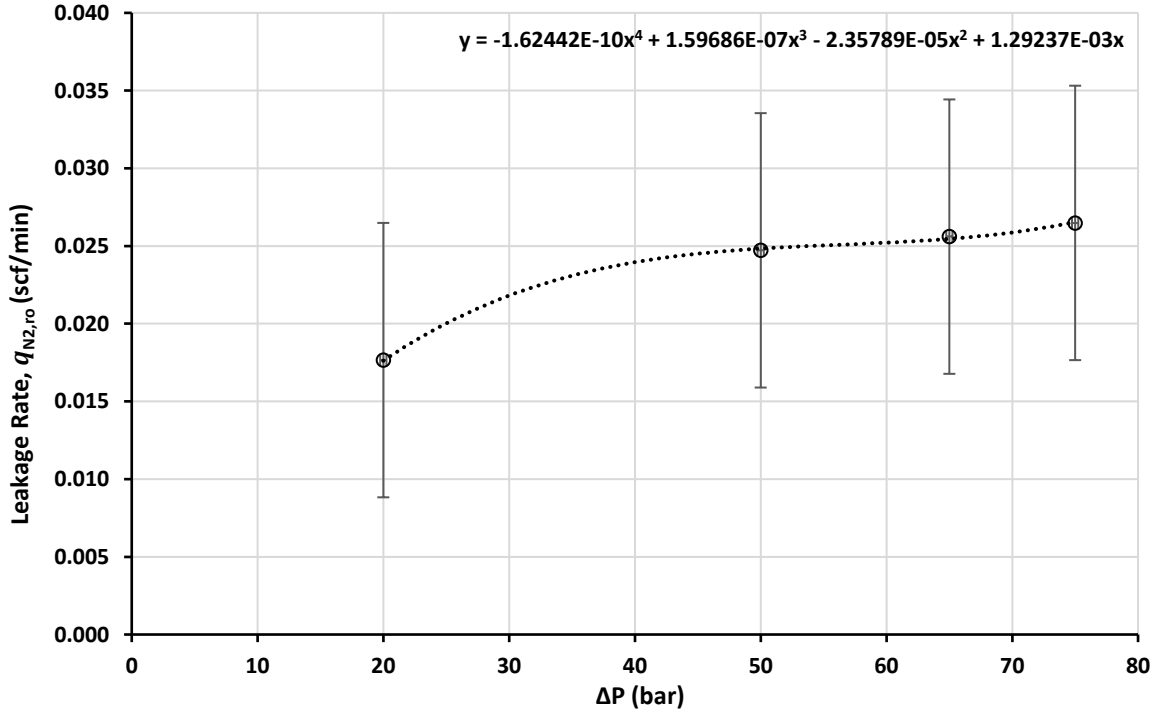

Figure 5.4: Measured leakage rates versus differential pressure (ΔP up until 75 bar) across the production valve in the HP setup. Y error bars ± 0.00883 scf/min and X error bars ± 0.25 bar. The best-fit polynomial line (dotted black line) represents *Eq. 4.15* which is also shown on the plot

Tables 5.2 & 5.3 show the leakage rates through the injection and production valves respectively, measured through the rotameter ($q_{N_2,ro}$) and calculated ($q_{N_2,f}$) through Eqs. **4.14** (for the injection valve) **& 4.15** (for the production valve).

Leakage rates at $\Delta P \geq 7$ were also calculated through Eqs. **4.14 & 4.15** for the injection and production valves respectively. This was done to calculate the percent difference (P.D) between the measured and calculated values. A low P.D indicates that the polynomial equations can be used to safely extrapolate the leakage rates to low pressure range.

In this section, the P.D is calculated using Eq. **5.1** and is shown in **Tables 5.2 & 5.3**.

$$P.D = \frac{\left|q_{N_2,ro} - q_{N_2,f}\right|}{q_{N_2,ro}} * 100 \tag{5.1}$$

Table 5.2: Measured and calculated leakage rates through the injection valve in the HP setup, percent difference between the two, and error associated to the measured leakage rates and pressure measurements

Injection valve					
	Rotameter			Equation 4.14	Difference
ΔP (bar)	$q_{N_2,ro}$ (scf/min)	δP_{HP} (bar)	δq_{ro} (scf/min)	$q_{N_2,f}$ (scf/min)	(%)
1.0	[-]	[-]	[-]	0.00239	[-]
1.5	[-]	[-]	[-]	0.00354	[-]
2.0	[-]	[-]	[-]	0.00466	[-]
2.5	[-]	[-]	[-]	0.00576	[-]
3.0	[-]	[-]	[-]	0.00682	[-]
3.5	[-]	[-]	[-]	0.00786	[-]
4.0	[-]	[-]	[-]	0.00887	[-]
4.5	[-]	[-]	[-]	0.00986	[-]
5.0	[-]	[-]	[-]	0.01082	[-]
5.5	[-]	[-]	[-]	0.01175	[-]
6.0	[-]	[-]	[-]	0.01266	[-]
6.5	[-]	[-]	[-]	0.01355	[-]
7.0	0.01413	$\pm$ 0.25	$\pm$ 0.00883	0.01441	2.024
10	0.01942	$\pm$ 0.25	$\pm$ 0.00883	0.01912	1.557
20	0.03002	$\pm$ 0.25	$\pm$ 0.00883	0.03008	0.206
50	0.04061	$\pm$ 0.25	$\pm$ 0.00883	0.04061	0.017

75	0.04238	± 0.25	± 0.00883	0.04238	0.004
100	0.044144	± 0.25	± 0.00883	0.044143	0.002
125	0.03885	± 0.25	± 0.00883	[-]	[-]
150	0.03178	± 0.25	± 0.00883	[-]	[-]

Table 5.3: Measured and calculated leakage rates through the production valve in the HP setup, percent difference between the two, and error associated to the measured leakage rates and pressure measurements

Production valve					
	Rotameter			**Equation 4.15**	**Difference**
ΔP (bar)	**$q_{N_2,ro}$ (scf/min)**	**δP_{HP} (bar)**	**δq_{ro} (scf/min)**	**$q_{N_2,f}$ (scf/min)**	**(%)**
1.0	[-]	[-]	[-]	0.00127	[-]
1.5	[-]	[-]	[-]	0.00189	[-]
2.0	[-]	[-]	[-]	0.00249	[-]
2.5	[-]	[-]	[-]	0.00309	[-]
3.0	[-]	[-]	[-]	0.00367	[-]
3.5	[-]	[-]	[-]	0.00424	[-]
4.0	[-]	[-]	[-]	0.00480	[-]
4.5	[-]	[-]	[-]	0.00535	[-]
5.0	[-]	[-]	[-]	0.00589	[-]
5.5	[-]	[-]	[-]	0.00642	[-]
6.0	[-]	[-]	[-]	0.00694	[-]
6.5	[-]	[-]	[-]	0.00745	[-]
7.0	[-]	[-]	[-]	0.00795	[-]
10	[-]	[-]	[-]	0.01072	[-]
20	0.01766	± 0.25	± 0.00883	0.01767	0.056
50	0.02472	± 0.25	± 0.00883	0.02462	0.420
75	0.02649	± 0.25	± 0.00883	0.02652	0.143
100	0.02295	± 0.25	± 0.00883	[-]	[-]
125	0.02119	± 0.25	± 0.00883	[-]	[-]
150	0.01766	± 0.25	± 0.00883	[-]	[-]

Although the P.D seems to increase with decreasing differential pressures for the injection valve, the values are still small and acceptable. **Figures 5.5 & 5.6** show the plot for the measured and extrapolated leakage rates versus the differential pressures across the injection valve and production valves respectively.

A comparison between the measurements through the rotameter and the newly installed gas flow meter is found in *Appendix 9*. The comparison shows that the rotameter was an adequate tool for measuring the leakage rates through the valves.

5.2. Closing rate tests in HP setup

The air rate needed to close both the injection and production valve (when the ball is pushed towards the valve's seat) is in the order of 0.1766 scf/min (or 5 L/min, equivalent to the air rate supplied by the lab facility air supply).

In this section, measurements from the gas flow meter are used to assess the closing performance of the injection and production valves. The closure of the valve happens rapidly, so the air leaked prior to the valve's closure was hard to detect by the rotameter.

Figures 5.7 & 5.8 show the results of the closing rate tests done on the injection and production valves respectively. The "Air Rate" data has two parts. The first part represents the rate of the air leaked prior to the closure of the valves ($q_{air,HP}$, the peak). The second part represents the air leakage rate through the valves after their closure (horizontal line, which are close to the nitrogen leakage rates through the closed injection and production valves at a ΔP of 7 bar, shown in **section 5.1**). A differential pressure of 7.13 bar was established across the valves after their closure since the lab facility air supply supplies air at a pressure of 7.13 barg or 8.13 bara. For the closing rate tests, the first part of the graph is of interest.

The leaked air prior to the closure of the valves and the air rate needed to close the valves are shown in **Table 5.4**.

Table 5.4: Leaked air prior to the closure of the production and injection valves during the closing rate test

Valve	$q_{air,HP}$ (scf/min)	Rate needed for valve closure (scf/min)
Injection	0.11725	0.1766
Production	0.11702	0.1766

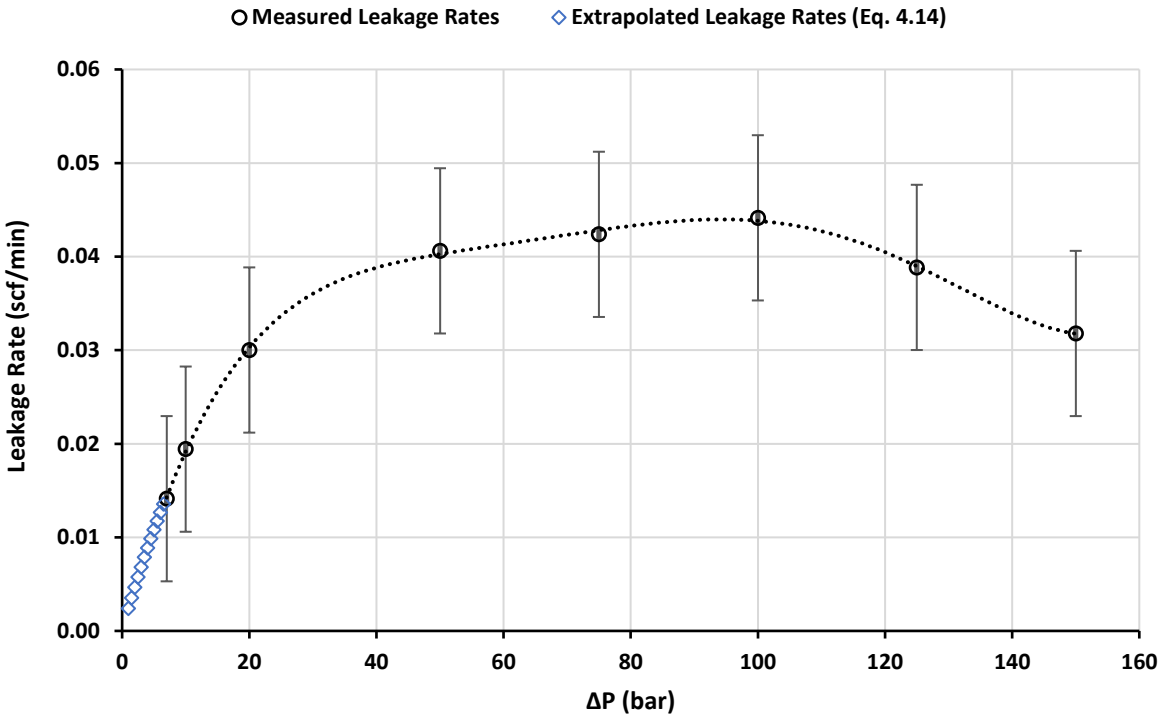

Figure 5.5: Measured (black) and extrapolated (blue) leakage rates versus differential pressure (bar) across the injection valve in the HP setup. Y error bars ± 0.00883 scf/min and X error bars ± 0.25 bar. Black dotted line represents a fit through the measured data points

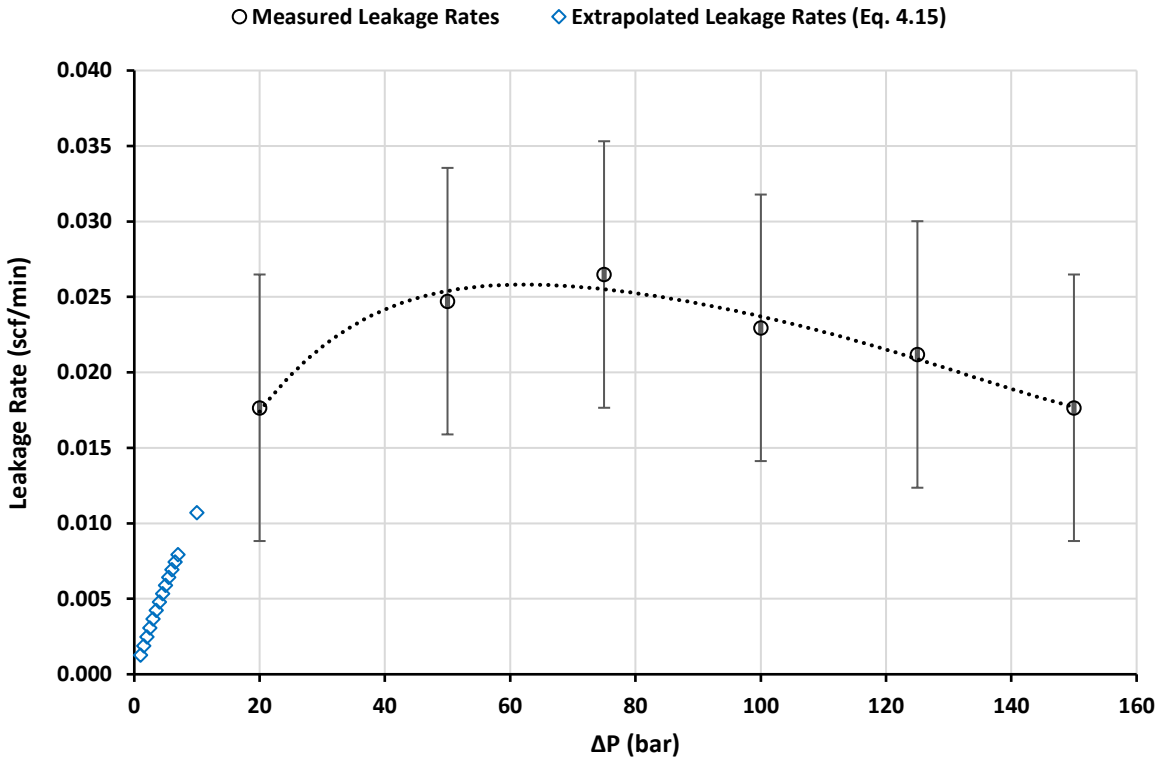

Figure 5.6: Measured (black) and extrapolated (blue) leakage rates versus differential pressure (bar) across the production valve in the HP setup. Y error bars ± 0.00883 scf/min and X error bars ± 0.25 bar. Black dotted line represents a fit through the measured data points

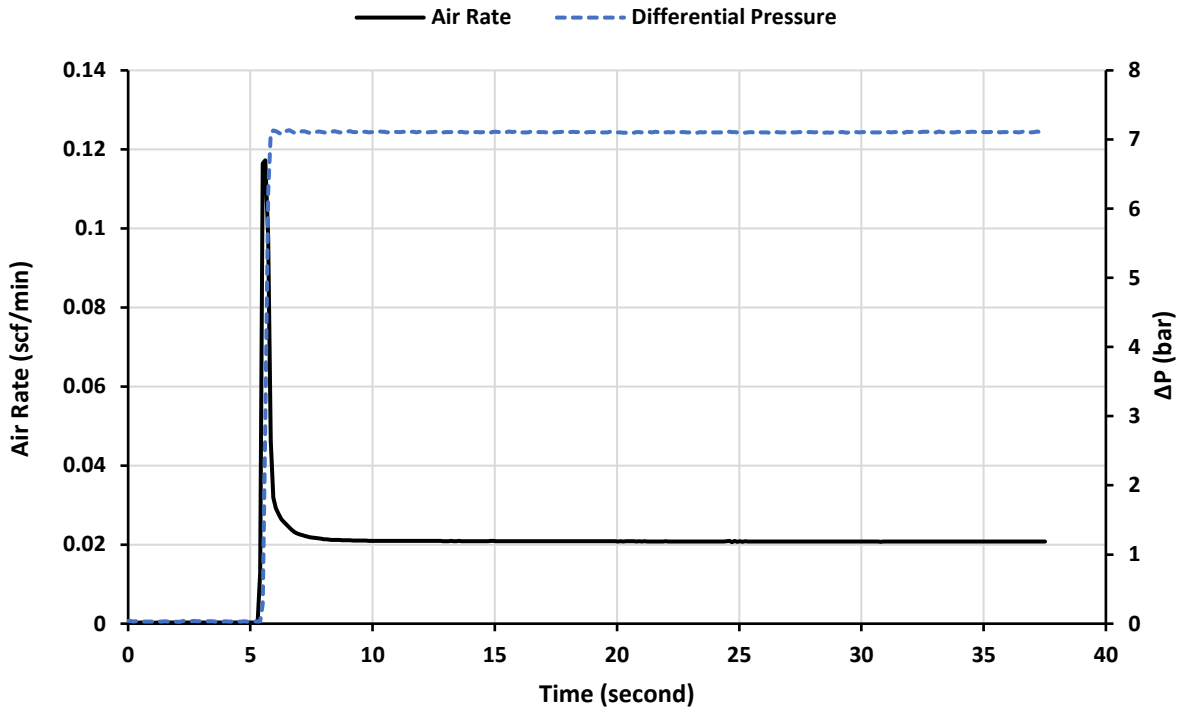

Figure 5.7: Closing rate test for the injection valve. The peak in "Air Rate" shows the air leakage rate prior to the valve's closure, and the horizontal line shows the air leakage rate after the valve's closure. The differential pressure established across the valve after its closure is also shown (dotted blue line)

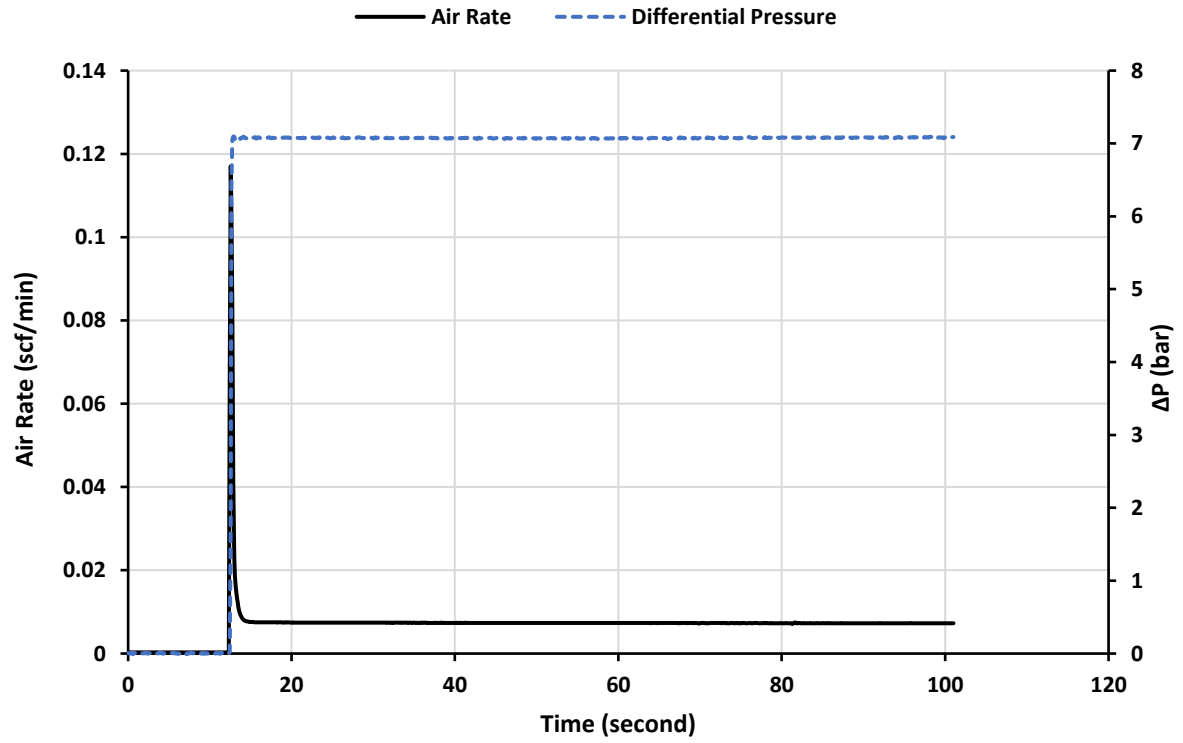

Figure 5.8: Closing rate test for the production valve. The peak in "Air Rate" shows the air leakage rate prior to the valve's closure, and the horizontal line shows the air leakage rate after the valve's closure. The differential pressure established across the valve after its closure is also shown (dotted blue line)

The time between starting the log file in the monitoring program of the HP setup and opening the valves needed to carry out the closing rate test (**section 3.1.6**) was different when carrying out the tests on the injection and production valves. This is the reason the peak ($q_{air,HP}$) occurred at different times in **Figures 5.7 & 5.8**. This does not affect the results.

5.3. Leakage tests in LP setup

Table 5.5 shows the calculated leakage rates through the injection and production valves respectively. **Figures 5.9 & 5.10** show the leakage rates associated with the differential pressures across the injection and production valves respectively. Note that all best-fit lines were forced to pass through the origin.

Table 5.5: Calculated leakage rates through the injection and production valves in the LP setup, the error associated to the pressure measurements, and the error associated to the leakage rates

	Injection valve			**Production valve**		
ΔP **(bar)**	$q_{air,LP}$ **(scf/min)**	δP_{LP} **(bar)**	$\delta q_{air,Lp}$ **(scf/min)**	$q_{air,LP}$ **(scf/min)**	δP_{LP} **(bar)**	$\delta q_{air,Lp}$ **(scf/min)**
1.0	0.00099	$\pm$ 0.01	$\pm$ 0.000096	0.00584	$\pm$ 0.01	$\pm$ 0.000586
1.5	0.00121	$\pm$ 0.01	$\pm$ 0.000096	0.00795	$\pm$ 0.01	$\pm$ 0.000586
2.0	0.00146	$\pm$ 0.01	$\pm$ 0.000096	0.00894	$\pm$ 0.01	$\pm$ 0.000586
2.5	0.00165	$\pm$ 0.01	$\pm$ 0.000096	0.00981	$\pm$ 0.01	$\pm$ 0.000586
3.0	0.00186	$\pm$ 0.01	$\pm$ 0.000096	0.01052	$\pm$ 0.01	$\pm$ 0.000586
3.5	0.00212	$\pm$ 0.01	$\pm$ 0.000096	0.01114	$\pm$ 0.01	$\pm$ 0.000586
4.0	0.00247	$\pm$ 0.01	$\pm$ 0.000096	0.01177	$\pm$ 0.01	$\pm$ 0.000586
4.5	0.00270	$\pm$ 0.01	$\pm$ 0.000096	0.01254	$\pm$ 0.01	$\pm$ 0.000586
5.0	0.00296	$\pm$ 0.01	$\pm$ 0.000096	0.01366	$\pm$ 0.01	$\pm$ 0.000586
5.5	0.00327	$\pm$ 0.01	$\pm$ 0.000096	0.01444	$\pm$ 0.01	$\pm$ 0.000586
6.0	0.00364	$\pm$ 0.01	$\pm$ 0.000096	0.01658	$\pm$ 0.01	$\pm$ 0.000586
6.5	0.00407	$\pm$ 0.01	$\pm$ 0.000096	0.01804	$\pm$ 0.01	$\pm$ 0.000586
7.0	0.00440	$\pm$ 0.01	$\pm$ 0.000096	0.01950	$\pm$ 0.01	$\pm$ 0.000586

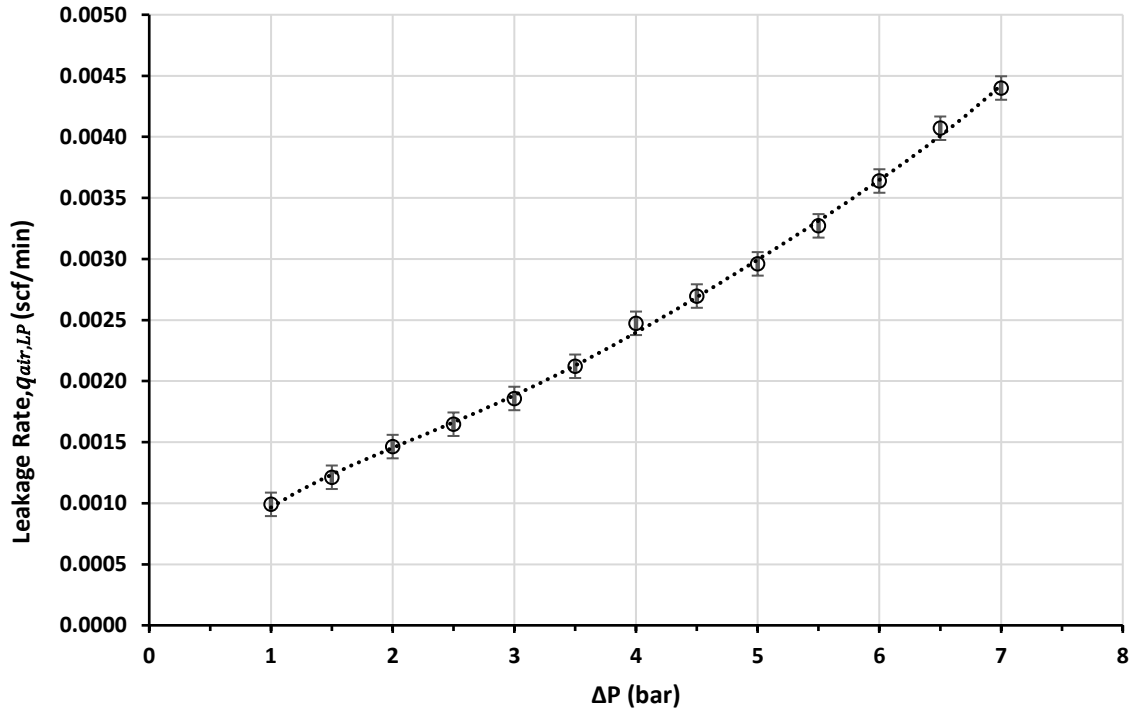

Figure 5.9: Calculated leakage rates versus differential pressures across the injection valve in the LP setup. Y error bars ± 0.000096 scf/min and X error bars ± 0.01 bar. A best-fit line (dotted black line) is fitted to the data

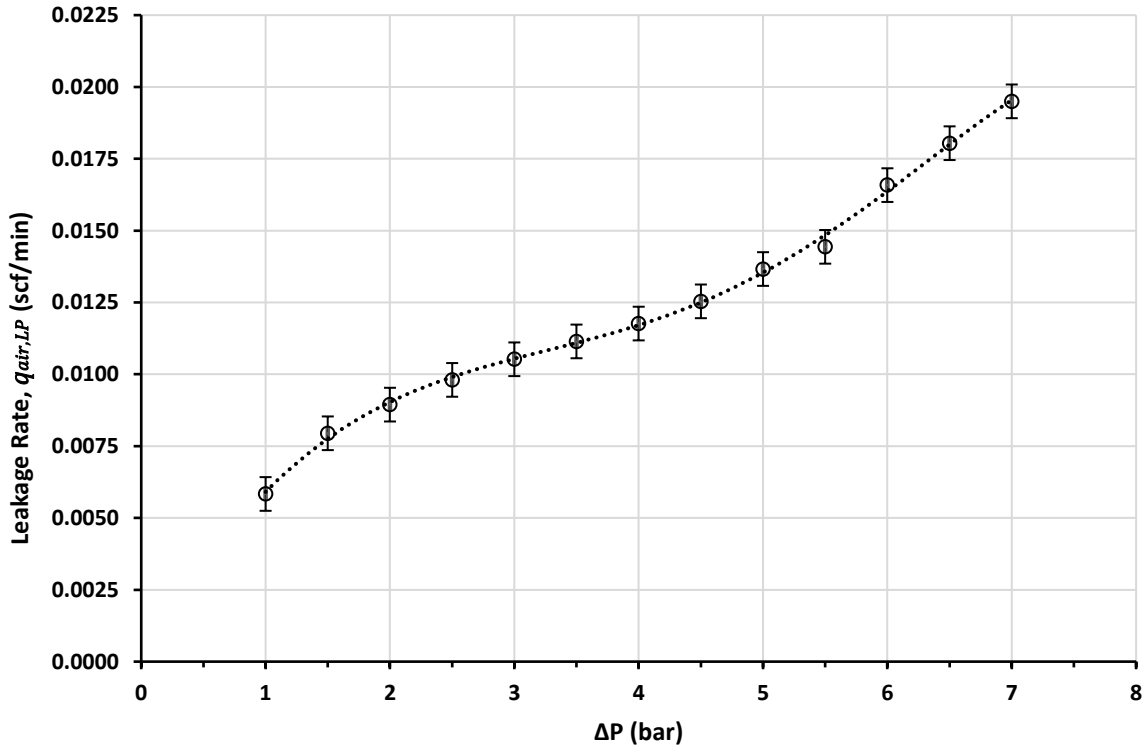

Figure 5.10: Calculated leakage rates versus differential pressures across the production valve in the LP setup. Y error bars ± 0.000586 scf/min and X error bars ± 0.01 bar. A best-fit line (dotted black line) is fitted to the data

5.4. Dimensionless Analysis

Figures 5.11, 5.12, 5.13 & 5.14 show the comparison of leakage rates through the injection and production valves in the HP setup, the LP setup, between the injection valves of the HP and LP setups, and between the production valves of the HP and LP setups respectively. One factor that was speculated to affect the outcome of the leakage tests results was the seat and ball roughness. Therefore, a dimensionless analysis was carried out to analyze the results obtained and determine the effect of the seat and ball roughness on leakage rates. **Table 5.6** shows the parameters that characterize leakage through valves. All best-fit lines showed in the figures were forced to pass through the origin.

In this section, the differential pressures across the valves (ΔP) and the leakage rates (q) are expressed in pascal (Pa) and sm^3/s respectively.

Table 5.6: Parameters that characterize leakage through valves used to obtain the dimensionless parameters

Parameters (units)	
$\boldsymbol{q}$ (sm^3/s)	Leakage rate
$\boldsymbol{\Delta P}$ (Pa)	Differential pressure
$\boldsymbol{\varepsilon_a}$ (m)	Valve seat roughness
$\boldsymbol{\varepsilon_b}$ (m)	Ball roughness
$\boldsymbol{\rho}$ (kg/m^3)	Fluid density (standard conditions)
$\boldsymbol{\mu}$ (Pa.s)	Fluid viscosity (standard conditions)
$\boldsymbol{D_a}$ (m)	Valve seat diameter
$\boldsymbol{D_b}$ (m)	Ball diameter

Using Buckingham's theorem, the dimensionless pi terms obtained are the following (the derivation of the π-terms is found in the *Appendix 10*):

$$\pi_1 = \frac{\rho q}{\mu D_b} \tag{5.2}$$

$$\pi_2 = \frac{\rho \Delta P D_b^2}{\mu^2} \tag{5.3}$$

$$\pi_3 = \frac{\varepsilon_a + \varepsilon_b}{D_a} \tag{5.4}$$

In which:

π_1 : dimensionless leak flow

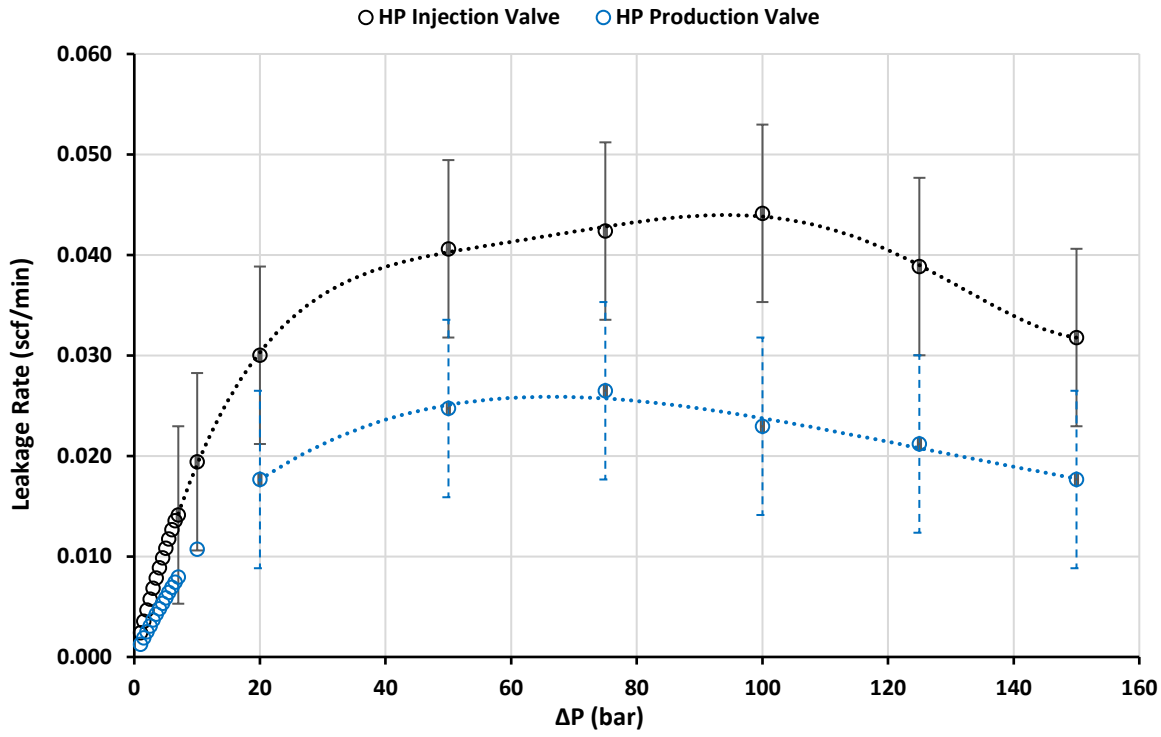

Figure 5.11: Comparison between the leakage rates through the injection valve and production valve in the HP setup. Y error bars ± 0.00883 scf/min and X error bars ± 0.25 bar. Black and blue dotted lines represent fits through the measured data points

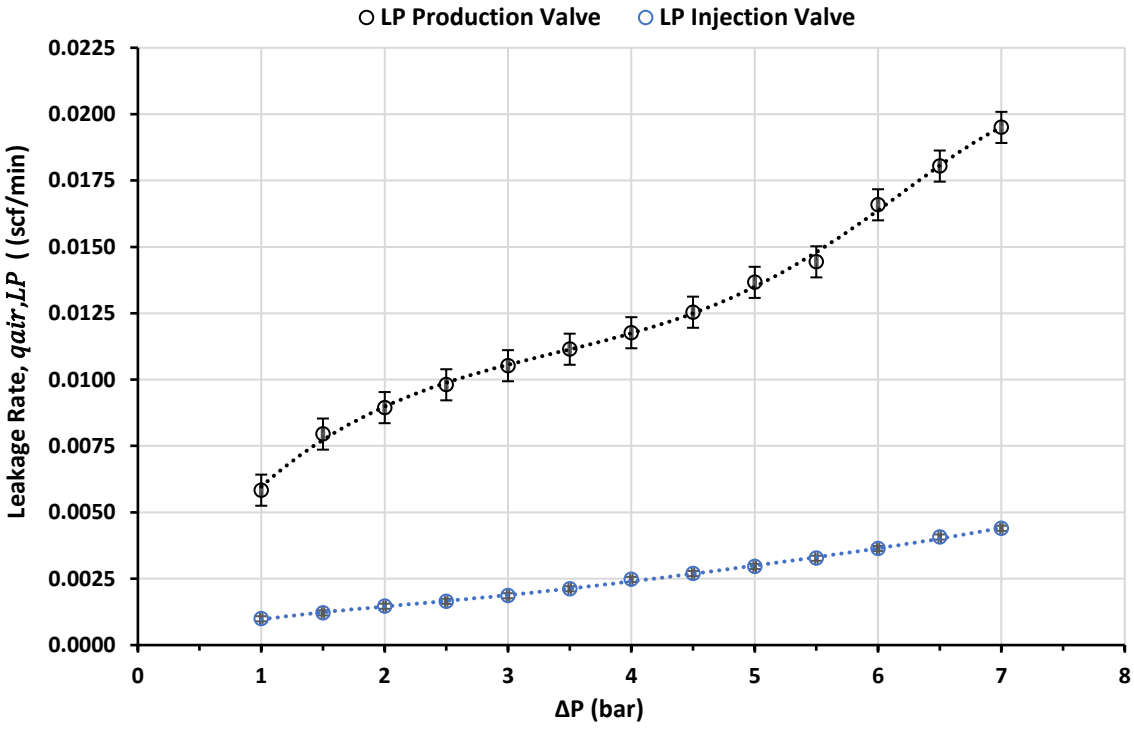

Figure 5.12: Comparison between the leakage rates through the injection valve and production valve in the LP setup. Black Y error bars ± 0.000586 scf/min, blue Y error bars ± 0.000096 scf/min and X error bars ± 0.01 bar. Black and blue dotted lines represent fits through the measured data points

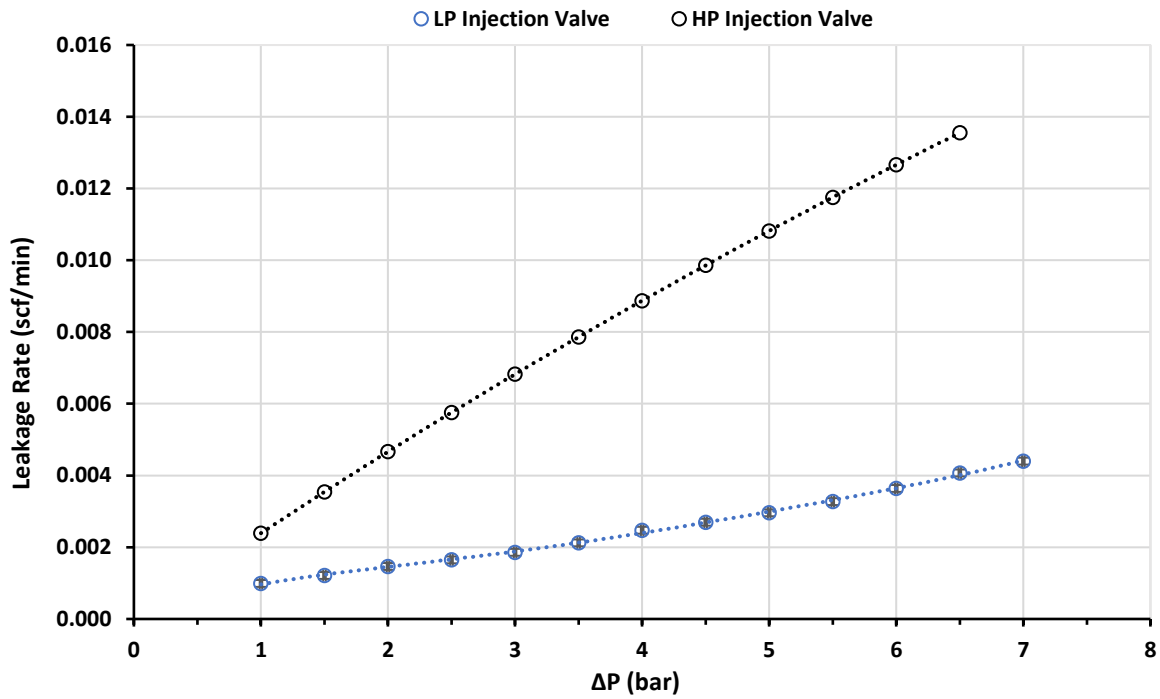

Figure 5.13: Comparison between the leakage rates through the injection valve in the LP setup and injection valve in the HP setup. Black Y error bars ± 0.000096 scf/min, and black X error bars ± 0.01 bar (for the LP injection valve). "HP injection valve" data represent the extrapolated leakage rates to the low-pressure range. Black and blue dotted lines represent fits through data points

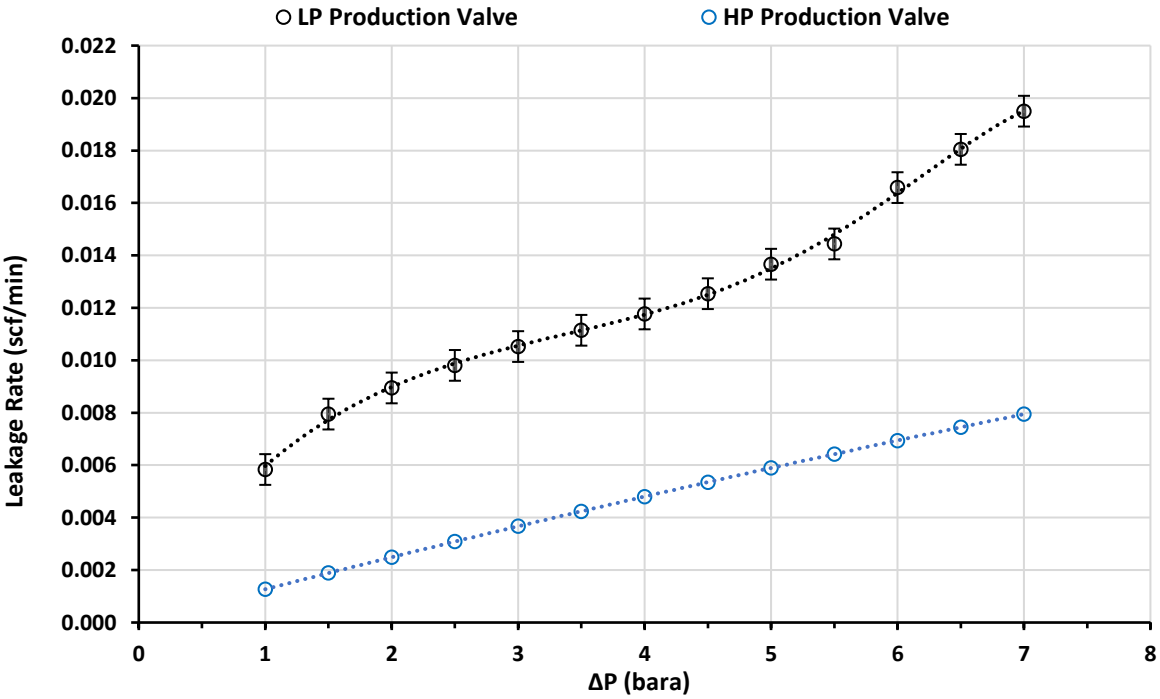

Figure 5.14: Comparison between the leakage rates through the production valve in the LP setup and production valve in the HP setup. Black Y error bars ± 0.000586 scf/min, and black X error bars ± 0.01 bar (for the LP production valve). "HP production valve" data represent the extrapolated leakage rates to the low-pressure range. Black and blue dotted lines represent fits through data points

π_2 : dimensionless pressure drop

π_3 : dimensionless relative roughness, $\varepsilon_a + \varepsilon_b$ represent the mean roughness of the valve

Nitrogen gas and air were used as the working fluids for leakage tests in the HP and LP setups respectively. The viscosity (μ) of Nitrogen and air was calculated using Sutherland's Formula (Eq. **5.5**). The factor 10^{-3} converts the viscosity from cP (centipoise) to Pa.s (pascal second)

$$\mu = 10^{-3}\left[\mu_o * \left(\frac{a}{b}\right) * \left(\frac{T}{T_o}\right)^{1.5}\right] \tag{5.5}$$

In which:

μ : viscosity of the fluid (Pa.s)

μ_o : reference viscosity at reference temperature T_o (cP)

T : input temperature (degrees Rankine)

T_o : reference temperature (degrees Rankine)

C : Sutherland's constant

a : $0.555T_o + C$

b : $0.555T + C$

The reference temperature T_o was chosen to be the temperature at standard conditions. In this thesis, leakage rates have been calculated and measured at standard conditions, so the $T = T_o$ = 506.67 degrees Rankin (15 degrees Celsius). **Table 5.7** shows the values of the parameters to calculate the viscosity of the working fluids at standard conditions, and their densities (ρ) at standard conditions.

Table 5.7: Parameters to calculate the viscosity of the working fluids and their densities at standard conditions

Fluid	Sutherland's Constant (C)	a/b	T/T_o	μ_o (cP)	μ (Pa.s)	ρ (kg/m^3)
Nitrogen	111	1	1	0.01744	$1.744 * 10^{-5}$	1.165
Air	120	1	1	0.01802	$1.802 * 10^{-5}$	1.225

5.4.1. Calculation of dimensionless π- terms for HP setup

Calculation of π_1 and π_2

Table 5.8 shows the given parameters needed to calculate the dimensionless leak flow (π_1) and the dimensionless pressure drop (π_2) for the injection and production valves in the HP setup. The same silicon nitride ball with a diameter D_b was used for the leakage tests done for

both valves.

Table 5.8: Parameters to calculate the dimensionless leak flow and the dimensionless pressure drop in the HP setup

ρ (kg/m^3)	μ (Pa.s)	D_b(m)	$\frac{\rho}{\mu D_b}$	$\frac{\rho D_b^2}{\mu^2}$
1.165	$1.744 * 10^{-5}$	0.00625	$1.069 * 10^{7}$	$1.496 * 10^{5}$

The leakage rate (q, sm^3/s) was calculated using $q_{N_2,ro}$ and $q_{N_2,f}$ (both in scf/min), by multiplying the leakage rates in scf/min by a conversion factor d = $4.72 * 10^{-4}$. The differential pressure is converted from bar to pascal.

Equation **5.6** calculates the error associated to the dimensionless leak flow ($\delta\pi_1$). Equation **5.7** calculates the error associated to the dimensionless pressure drop ($\delta\pi_2$). The derivation of the equations is found in *Appendix 11*.

Note that the leakage rates extrapolated to the low-pressure range have no error associated to them since they were not measured.

$$\delta\pi_1 = \pm\left[\delta q_{ro} * d\left(\frac{\rho}{\mu D_b}\right)\right] \tag{5.6}$$

$$\delta\pi_2 = \pm\left[\delta P_{HP} * 10^5\left(\frac{\rho D_b^2}{\mu^2}\right)\right] \tag{5.7}$$

Table 5.9 shows an example on calculating π_1 and π_2 for the injection and production valves respectively, along with the errors associated to the values. The calculations were shown for one extrapolated and one measured leakage rate. **Figure 5.15** shows the log-log dimensionless plot of π_1 versus π_2 for the injection and production valves.

Table 5.9: Example on calculating π_1 and π_2 for the injection and production valves shown for one extrapolated (at $\Delta P = 6.0 * 10^5$ Pa) and one measured (at $\Delta P = 20 * 10^5$ Pa) leakage rate

	Injection valve		**Production valve**	
Parameters (units)	**ΔP (Pa)**		**ΔP (Pa)**	
	$6.0 * 10^5$	**$20 * 10^5$**	**$6.0 * 10^5$**	**$20 * 10^5$**
$q_{N_2,ro}$ (scf/min)	[-]	0.03002	[-]	0.0177
$q_{N_2,f}$ (scf/min)	0.01266	[-]	0.00694	[-]
q (sm^3/s)	$5.98 * 10^{-6}$	$1.42 * 10^{-5}$	$3.28 * 10^{-6}$	$8.33 * 10^{-6}$

$\boldsymbol{\pi_1}$	62.55	148.27	34.28	87.22
$\boldsymbol{\pi_2}$	$8.61 * 10^{10}$	$2.87 * 10^{11}$	$8.61 * 10^{10}$	$2.87 * 10^{11}$
$\boldsymbol{\delta\pi_1}$	[-]	44.5	[-]	44.5
$\boldsymbol{\delta\pi_2}$	[-]	$3.74 * 10^{9}$	[-]	$3.74 * 10^{9}$

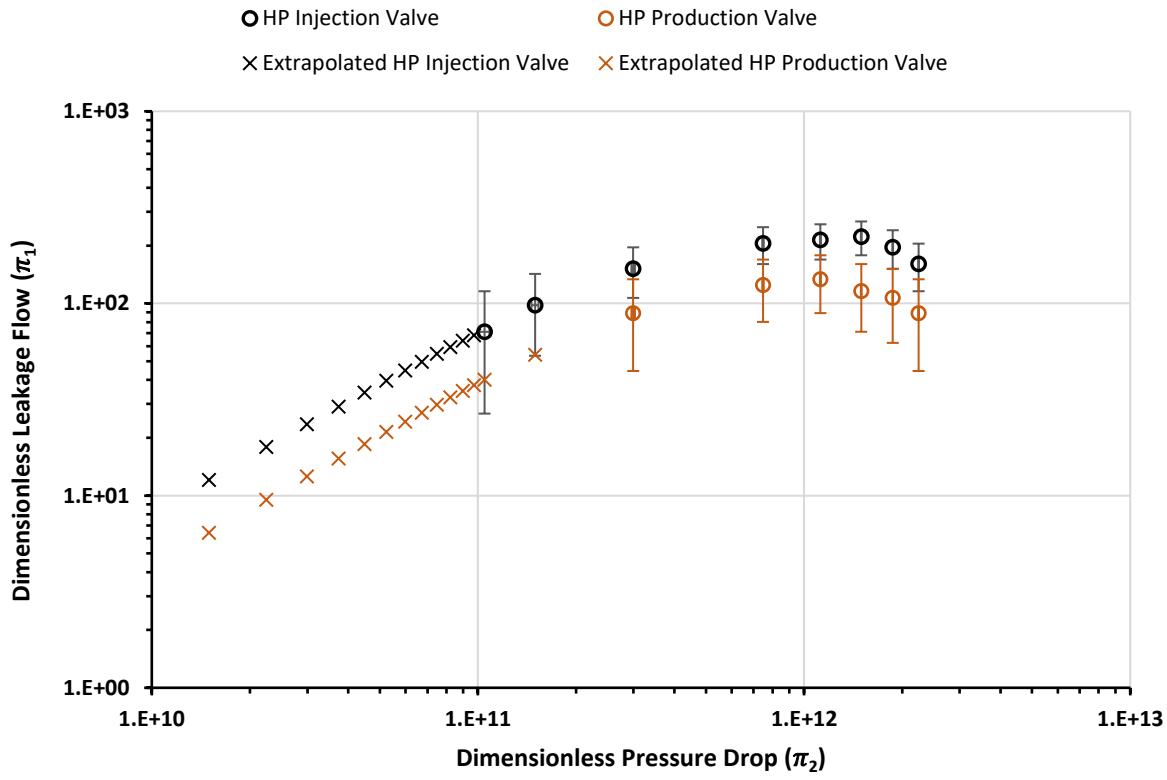

Figure 5.15: Log-log plot of dimensionless leakage flow versus the dimensionless pressure drop for the injection (black) and production (orange) valves. The black and orange Y error bars $\pm$ 44.5 and the black and orange X error bars $\pm$ $3.74 * 10^9$

Examination of π_3

The surface roughness of the seat of the HP injection and production valves (ε_a) could not be measured. This was because the roughness meter used could not be aligned with the valve's sealing surface to get any roughness value. Therefore, π_3 could not be measured. In this section and from this point forward in this report, π_3 and E/D refer to the dimensionless relative roughness and are used interchangeably.

A plot presented by Zarea et al. (1999), using the same dimensionless parameters and π-terms as in this thesis, was used to estimate π_3, The plot shows the dimensionless leakage flow at specific dimensionless pressure drops in ball-type check valves with different mean roughness. This plot was used because Zarea et al. (1999) was working with a similar valve geometry.

First, the points from Zarea et al. (1999) plot were plotted on a graph (**Figure 5.16**) using

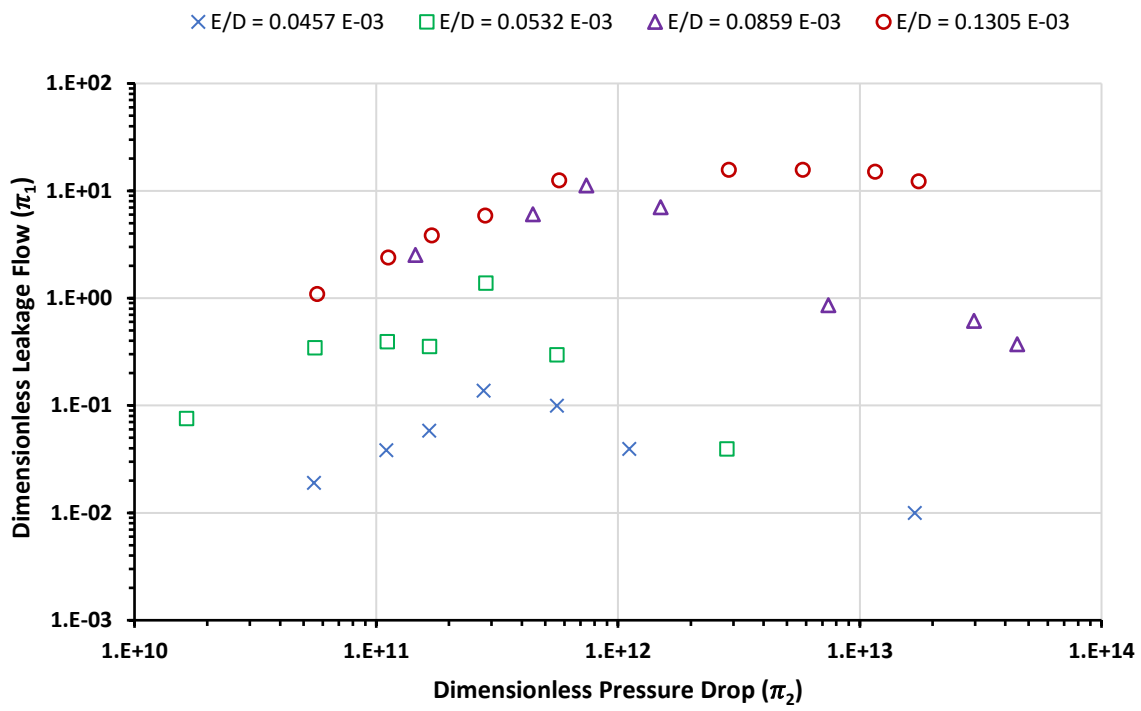

Figure 5.16: Log-log plot of dimensionless leakage flow versus the dimensionless pressure drop from Zarea et al. (1999), modified. The different labels indicate the calculated dimensionless relative roughness of the different ball-type check valves tested

"WebPlotDigitizer". Second, the critical dimensionless pressure drop (π_{2_c}) for the four different dimensionless relative roughness were extracted from the plot (**Table 5.10**). Third, the dimensionless relative roughness were plotted versus the critical dimensionless pressure drop, and a best fit-line was fitted through the data points (**Figure 5.17**).

Table 5.10: Different cases of the calculated dimensionless relative roughness of the valves and the critical dimensionless differential pressure drop extracted for each case

E/D	π_{2_c}
$4.57 * 10^{-5}$	$2.78 * 10^{11}$
$5.32 * 10^{-5}$	$2.83 * 10^{11}$
$8.59 * 10^{-5}$	$7.39 * 10^{11}$
$1.31 * 10^{-4}$	$2.65 * 10^{12}$

Equation **5.8** is the second-degree polynomial equation resulting from the best-fit line to the data points.

$$\pi_3 = -2.3804 * 10^{-29} \left(\pi_{2_c}\right)^2 + 1.0399 * 10^{-16} \left(\pi_{2_c}\right) + 2.2127 * 10^{-5} \quad (5.8)$$

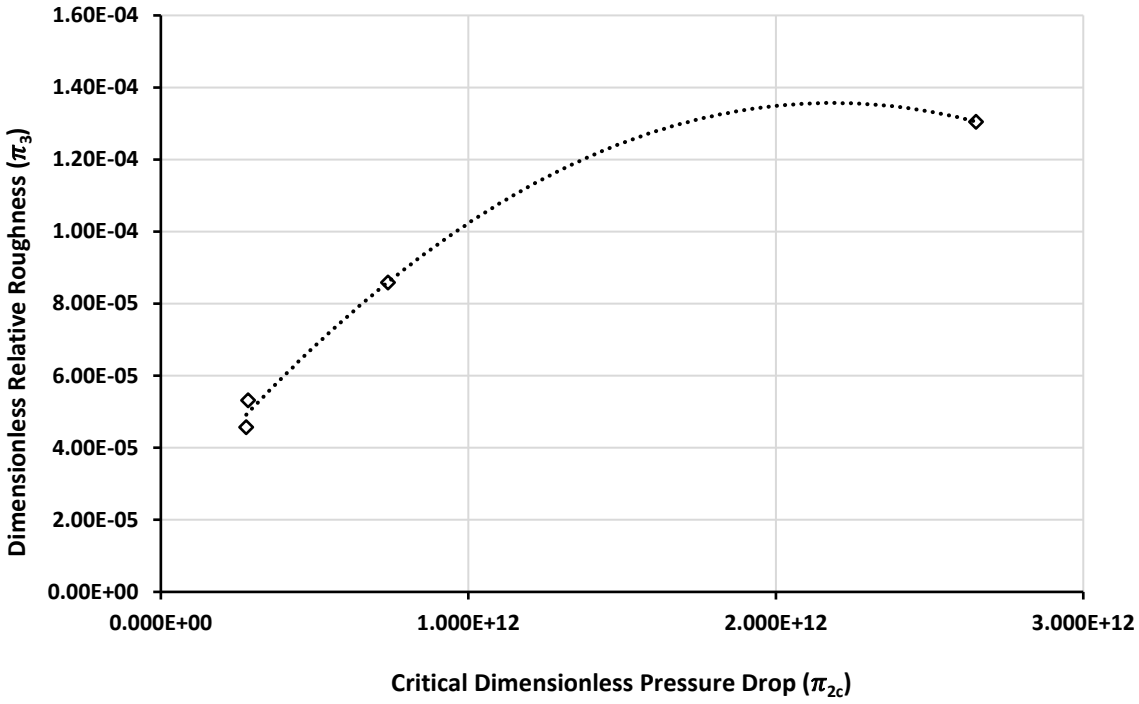

Figure 5.17: Dimensionless relative roughness versus critical dimensionless pressure drop (values extracted from Zarea et al. (1999) plot). The black dotted line shows the second-degree polynomial equation fitted through the data points

Fourth and finally, the measured critical dimensionless pressure drops for the injection and production valves were used to estimate the dimensionless relative roughness of both valves through Eq. **5.8**.

According to **section 5.1**, the critical differential pressures for the injection and production valves (used to calculate π_{2_c}through Eq. **5.3**) are at 100 and 75 bar respectively. The results for π_3 estimations for the HP injection and production valves (using Eq. **5.8**) are shown in **Table 5.11**.

Table 5.11: Calculated dimensionless relative roughness of the injection and production valves

Valve	ΔP_c (Pa)	π_{2_c}	π_3
Injection	$100 * 10^5$	$1.5 * 10^{12}$	$2.31 * 10^{-4}$
Production	$75 * 10^5$	$1.12 * 10^{12}$	$1.685 * 10^{-4}$

Consequently, Eq. **5.9** (derived from Eq. **5.4**) calculates the surface roughness of the seat of the injection and production valves (**Table 5.12**). Procedure of obtaining the roughness of the silicon nitride ball (ε_b) used in both valves in the HP setup is found in *Appendix 12*.

$$\varepsilon_a = (\pi_3 * D_a) - \varepsilon_b \tag{5.9}$$

Table 5.12: Diameters of the HP valves' seats, the silicon nitride ball's roughness, the estimated dimensionless relative roughness, and the calculated roughness of the valves' seats

Valve	D_a (m)	ε_b (m)	π_3	ε_a
Injection	0.00445	$3 * 10^{-7}$	$2.317 * 10^{-4}$	0.729
Production	0.00437	$3 * 10^{-7}$	$1.684 * 10^{-4}$	0.435

5.4.2. Calculation of dimensionless π- terms for LP setup

Calculation of π_1 and π_2

The parameters needed to calculate the dimensionless leak flow (π_1) and the dimensionless pressure drop (π_2) for the injection and production valves in the LP setup are shown in **Table 5.13**. The two stainless steel balls used in the leakage tests have the same diameter D_b.

Table 5.13: Parameters to calculate the dimensionless leak flow and the dimensionless pressure drop in the LP setup

ρ (kg/m^3)	μ (Pa.s)	D_b(m)	$\frac{\rho}{\mu D_b}$	$\frac{\rho D_b^2}{\mu^2}$
1.225	$1.802 * 10^{-5}$	0.007	$9.711 * 10^{6}$	$1.849 * 10^{5}$

The leakage rate (q, sm^3/s) was calculated using $q_{air,LP}$ (scf/min), by multiplying $q_{air,LP}$ by the conversion factor d = $4.72 * 10^{-4}$. The differential pressure is converted from bar to pascal. Equation **5.10** calculates the error associated to the dimensionless leak flow ($\delta\pi_1$). Equation **5.11** calculates the error associated to the dimensionless pressure drop ($\delta\pi_2$). The derivation of the equations is found in *Appendix 11*.

$$\delta\pi_1 = \pm\left[\delta q_{air,LP} * d\left(\frac{\rho}{\mu D_b}\right)\right] \tag{5.10}$$

$$\delta\pi_2 = \pm\left[\delta P_{LP} * 10^5\left(\frac{\rho D_b^2}{\mu^2}\right)\right] \tag{5.11}$$

$\delta q_{air,LP}$ is different for each valve (refer to **section 4.4.1**). The calculated $\delta\pi_1$ and $\delta\pi_2$ for the injection and production valves are shown in **Table 5.14**.

Table 5.15 shows an example on calculating π_1 and π_2 for the injection and production valves respectively. **Figure 5.18** shows the dimensionless log-log plot of π_1 versus π_2 for the LP injection and production valves.

Table 5.14: Calculated error associated to the dimensionless leak flow and dimensionless pressure drop values for the injection and production valves in the LP setup

Valve	$\delta q_{air,LP}$ (scf/min)	δP_{LP} (bar)	$\delta\pi_1$	$\delta\pi_2$
Injection	$\pm$ 0.000096	$\pm$ 0.01	0.44	$1.85 * 10^8$
Production	$\pm$ 0.000586	$\pm$ 0.01	2.69	$1.85 * 10^8$

Table 5.15: Example on calculating π_1 and π_2 for the injection and production valves at $\Delta P = 6.0 * 10^5$ Pa in the LP setup

	Injection valve	Production valve
Parameters (units)	**ΔP (Pa)**	**ΔP (Pa)**
	$6.0 * 10^5$	**$6.0 * 10^5$**
$q_{air,LP}$ (scf/min)	0.0036	0.0166
q (sm^3/s)	$1.72 * 10^{-6}$	$7.83 * 10^{-6}$
π_1	16.68	76.01
π_2	$1.11 * 10^{11}$	$1.11 * 10^{11}$

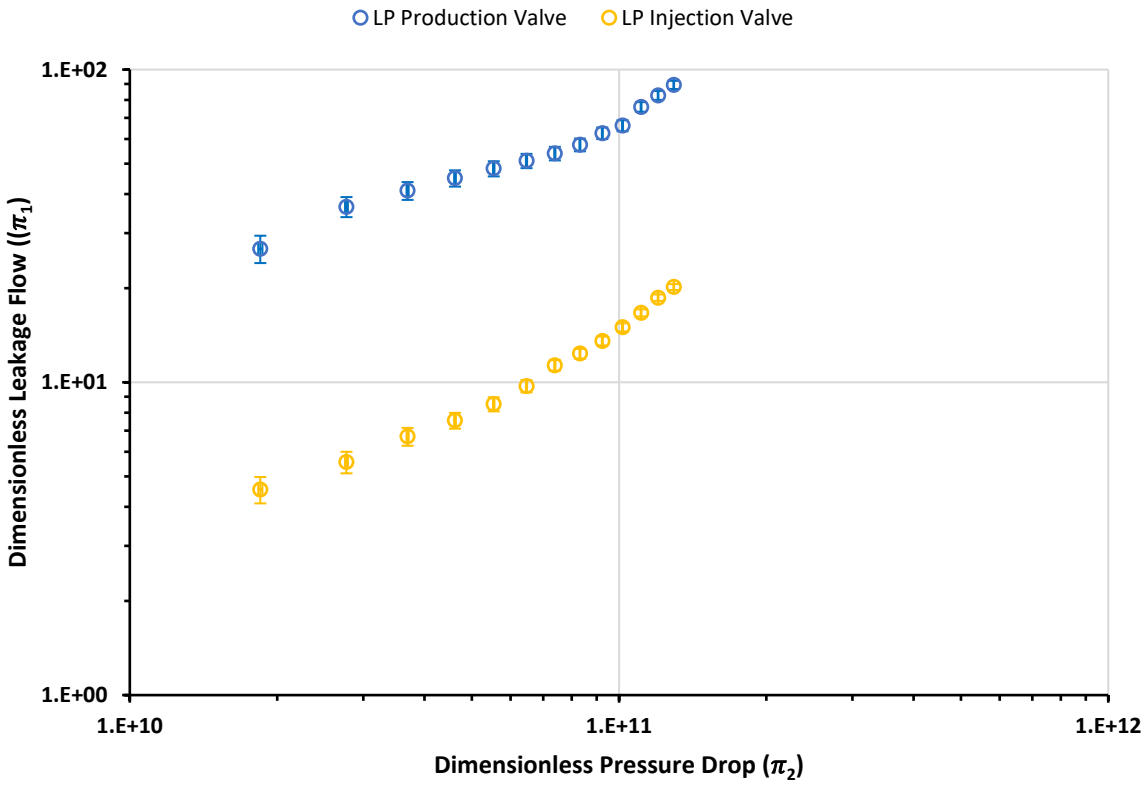

Figure 5.18: Log-log plot of dimensionless leakage flow versus the dimensionless pressure drop for the injection (yellow) and production (blue) valves. The blue and orange Y error bars show $\delta\pi_1$ of the injection and production valves respectively. Blue and orange X error bars show $\delta\pi_2$

Examination of π_3

The surface roughness of the seat of the LP injection and production valves (ε_a) could not be measured. The roughness meter used could not be aligned with the valve's sealing surface to carry out any roughness measurements. Therefore, π_3 could not be measured. The maximum differential pressure established across the valves in the LP setup is 7.13 bar, so no critical differential pressure is attained. Hence, a critical dimensionless pressure drop could not be calculated to estimate π_3, as done in **section 5.4.1**. The stainless steel balls for the injection and production valves have the same properties. The procedure of obtaining the roughness of balls (ε_b) is found in *Appendix 12.*

Table 5.16: Diameters of the LP valves' seats and the stainless-steel balls' roughness

Valve	D_a (m)	ε_b (m)	π_3	ε_a
Injection	0.00437	$5 * 10^{-7}$	[-]	[-]
Production	0.00437	$5 * 10^{-7}$	[-]	[-]

5.5. Analysis and comparison with literature study

Before comparing the results of the experiments to the literature study, it is important to point out that the leakage performance of the injection and production ball-type valves in the HP (silicon nitride ball and metallic seat) and LP (metallic ball and acrylic plastic seat) setups comply with NORSOK's acceptance criteria for leakage rates through a closed valve.

Leakage rates measured or calculated fell below 15 scf/min (the leak rate acceptance criteria for gas), deeming the sealing performance of the valves to be effective.

In the closing rate tests in the HP setup, the injection and production valves were able to close and maintain a seal thereafter. The leaked air rate prior to the closure of valves also fell below 15 scf/min.

Figures 5.13 & 5.14 show the comparison of leakage rates between the injection valves of the HP and LP setups, and between the production valves of the HP and LP setups respectively. The injection valve in the HP setup leaked more than the one in the LP setup, but the production valve in the LP setup leaked more than the one in the HP setup. Therefore, no definite conclusion can be drawn on the effect of the valve seat material on its sealing capability. Moreover, as roughness was not measured experimentally, it is not possible to determine if the difference in leakage performance is due to manufacturing differences. A dimensionless analysis was carried out to analyze the results obtained and determine the effect of the seat and

ball roughness on leakage rates. **Table 5.17** shows the summary of the seat diameter, ball and seat roughness, and the dimensionless relative roughness of each valve in both setups.

Table 5.17: Summary of the dimensionless relative roughness parameters

Valve	D_a (m)	ε_b (m)	ε_a	E/D (or π_3)
LP Production	0.00437	$5 * 10^{-7}$	[-]	[-]
HP Production	0.00437	$3 * 10^{-7}$	0.435	$1.684 * 10^{-4}$
LP Injection	0.00437	$5 * 10^{-7}$	[-]	[-]
HP Injection	0.00445	$3 * 10^{-7}$	0.729	$2.317 * 10^{-4}$

Figure 5.19 shows the dimensionless log-log plot of π_1 versus π_2 for the injection and production valves in both setups. The dimensionless relative roughness (π_3 or E/D) is also shown for the injection and production valves of the HP setup (estimated values)

Figure 5.20 shows the dimensionless log-log plot of π_1 versus π_2 for the measured and calculated leakage rates in the experiments conducted in this thesis and the leakage rates measured by Zarea et al. (1999).

According to Zarea et al. (1999) data points, the increasing dimensionless relative roughness of valves yield increasing dimensionless leakage flow values (**Figure 5.20**). A set of data points plotting higher than others indicate that they have a higher dimensionless relative roughness.

The estimated E/D of the HP injection valve is greater than the one for the HP production valve (**Table 5.17**), and it is backed up by how the HP data points plot. The calculated injection valve's seat roughness was greater than the one calculated for the production valve. The HP injection and production valves are tested using the same silicon nitride ball. The difference in the seat diameter of both valves is too small that it should have little-to-no effect on the E/D of the valves. Hence, the only factor affecting the E/D is the roughness of the seat, which in turn, affects the leakage rates through the valves (**Figure 5.11**).

The LP production valve data points plot higher than the LP injection valve data points on the log-log plot. The ball used in both valves have the same roughness, and the seat diameter of both valves is the same. Therefore, the only parameter affecting E/D is the roughness of the seat, which seems larger for the production valve. This in turn affects the leakage rates through the valves, where the production valve leaks more than the injection one (**Figure 5.12**).

The HP injection valve data points plots higher than those of the LP injection valve. The valves have a slightly different seat diameter. This should have little-to-no effect on the E/D. The reason the HP injection valve has a higher E/D is that it has a larger valve mean roughness

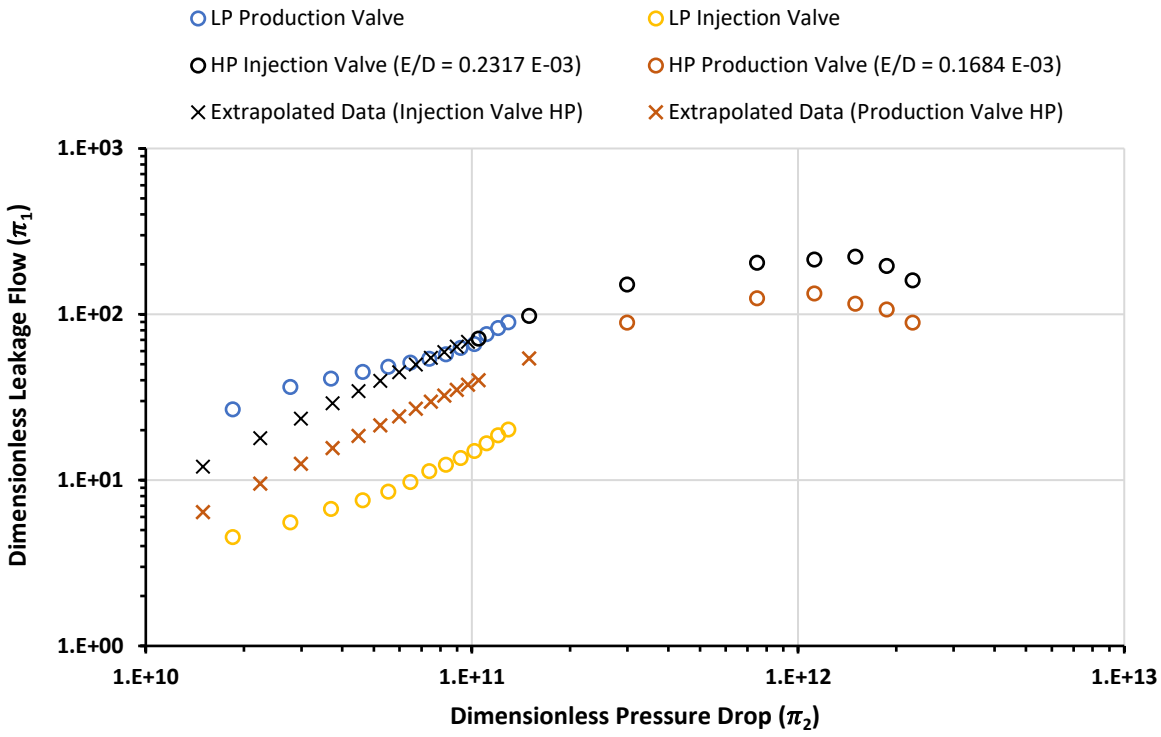

Figure 5.19: Dimensionless leakage flow versus dimensionless pressure drop for the injection and production valves in both setups

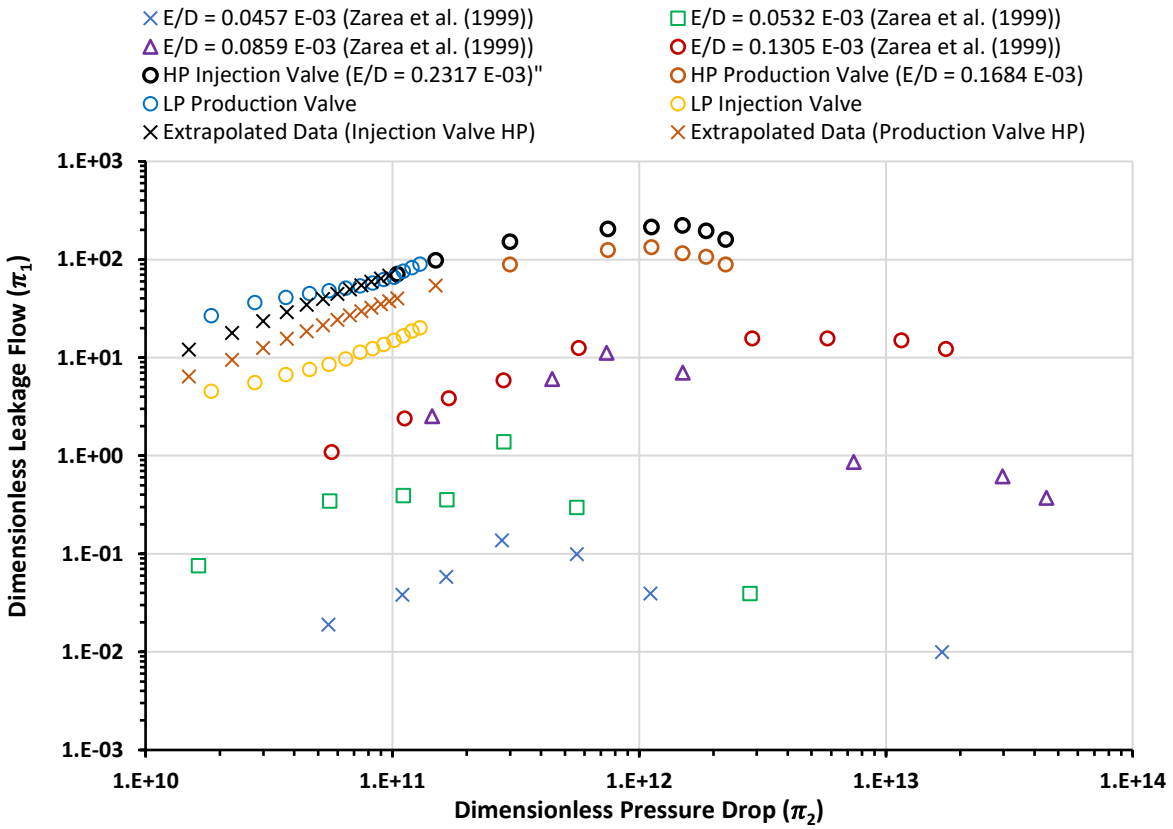

Figure 5.20: Dimensionless leakage flow versus dimensionless pressure drop from both Zarea et al. (1999) (modified) and the HP and LP injection and production valves

($\varepsilon_a + \varepsilon_b$) than the LP injection valve. The larger valve mean roughness translates into higher leakage rates through the HP injection valve, compared to the LP one (**Figure 5.13**)

The LP and HP production valves have the same seat diameter, but they have a different valve mean roughness ($\varepsilon_a + \varepsilon_b$). The LP production valve data points plot higher than those of the HP production valve, indicating that the mean roughness of the former could be higher the latter. The larger valve mean roughness translates into higher leakage rates through the LP production valve, compared to the HP one (**Figure 5.14**).

When comparing leakage rates through the valves within the same setup, the roughness of the valve's seat affected the leakage rate. When comparing leakage rates through the valves of different setups, the valve's mean roughness affected the leakage rates through the valves. Hence, the valve's seat roughness and the roughness of the ball in ball-type check valves are important factors to consider when assessing leakage rates.

Note that the valves of the HP and LP setup were manufactured in different places, so there was no control over the difference in roughness for each of the seal surface. It seems the valves of the LP setup were not polished the same way, but it is unfortunately not possible to confirm this.

Figure 5.21 shows leakage rates through one valve tested in the work of Zarea et al. (1999) (using air as a working fluid) at certain differential pressures. In the experiment conducted by Zarea et al. 1999, a critical differential pressure, after which leakage rates decrease with increasing differential pressure, was not reached.

The leakage rates through the injection and production HP valves decreased with increasing differential pressures after a critical differential pressure of 100 bar and 75 bar was established across the injection and production valves respectively.

The reason for this could be because the maximum pressure differential used in the Zarea et al. 1999 experiments was too low (90 psi or 6.122 bar). This can be confirmed with the results obtained with the LP setup in which no critical differential pressure was reached.

The results seem to indicate that when using gas as a working fluid, a good seal between the ball and the valve's seat (therefore lower leakage rates at higher pressure differentials thereafter) is established at high differential pressures across the valves.

5.6. Correspondence between test results and $F2F_{cyc}$ method

In the $F2F_{cyc}$ method, due to the closing delays of and leakages across the check valves, there will be losses in volumetric efficiency. When the well is set from production to injection,

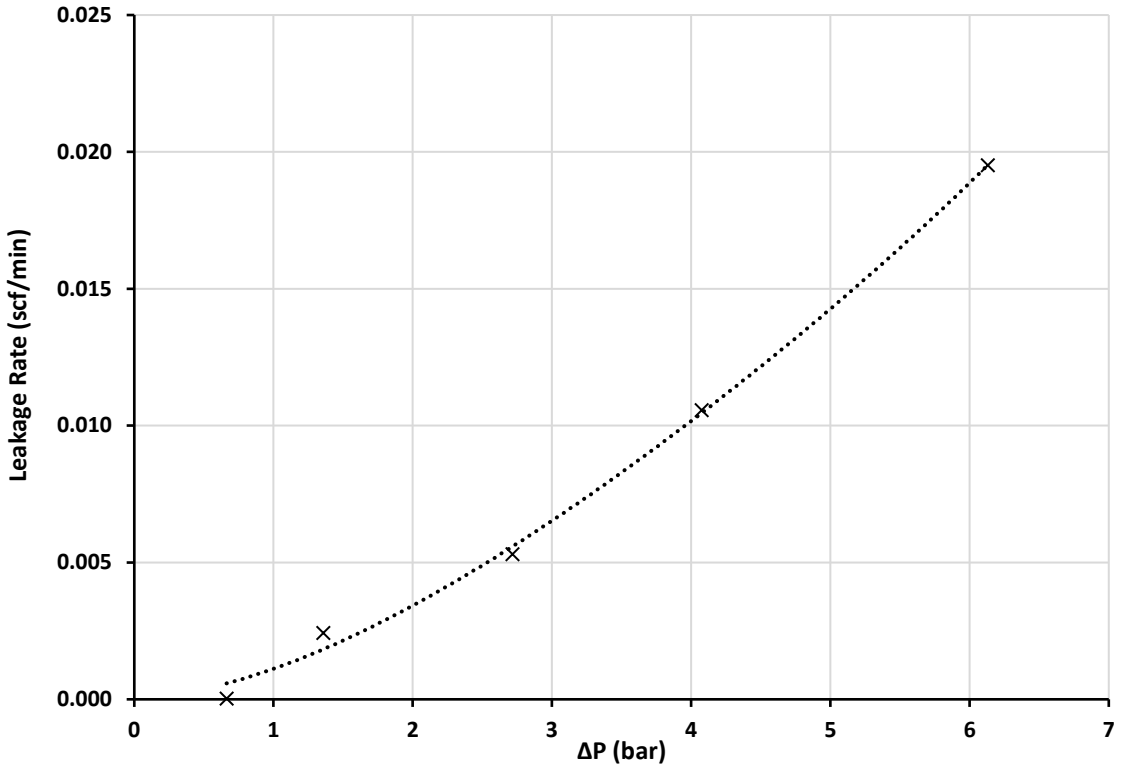

Figure 5.21: Leakage rates (using air as the working fluid) through one ball-type check valve (D_b= 34.925 mm, ε_b = 0.1747 μm, D_a = 25 mm, ε_a= 0.843 μm) from Zarea et al. 1999 (modified)

closing delay of the production valve will result in some flowback into the production fractures prior to their valve closure. Leakages through the closed production valve results in unwanted loss of injection fluid, which can be detrimental to the injection fluid's utilization plan in an EOR project. When the well is set from injection to production, closing delay of the injection valve will result in some flow back of the injected fluid into the liner. Leakages through the closed injection valve results in some leak flow from the injection fractures into the liner. This will affect the pressure maintenance in the injection fractures negatively, and more injection fluid will be needed in next injection periods to increase the pressure of the injection fractures. This in turn will have a negative effect on recoveries.

In this thesis, leakage rates (prior to the valve's closure and after the valve's closure, as part of the closing rate and leakage tests respectively) through the injection and production ball-type check valves fell below 15scf/min, which is NORSOK's valve leak rate acceptance criteria for gas. The low leakage rates through the closed valves indicate that a good seal exists between the ball and the valve seats, limiting the volumetric losses in the $F2F_{cyc}$ method. A critical differential pressure across the valves is also reached, where the gas leakage rates exhibit a reduction effect with higher pressure differentials. Hence, the ball-type check valves will

reduce their leakage at greater differential pressures. This is highly important when it comes to assessing the performance of the ball-type check valves in the $F2F_{cyc}$ EOR method, as this can be crucial to the utilization of the injection fluid, recovery factors, and the economics of the project.

The valve's seat roughness and the ball roughness are important factors to consider when employing ball-type check valves in a $F2F_{cyc}$ project, since they can have considerable effects on leakage rates through the closed valves. Choosing adequate valve mean roughness and setting a maximum limit on the value that can be reached (during the lifetime of an EOR project) is an important aspect in limiting the volumetric losses, therefore improving the economics of the $F2F_{cyc}$ method.

6. Conclusions and recommendations

The performance of the injection and production ball-type check valves to be employed in the $F2F_{cyc}$ method was experimentally quantified through closing rate and leakage tests. Leakage rates at certain pressure differentials through the closed silicon nitride ball and metallic seat (in the high-pressure setup, using nitrogen gas as a working fluid) and the metallic ball and acrylic plastic seat check valves (in low-pressure setup, using air as a working fluid) fell below the NORSOK's leak rate acceptance criteria for gas (15 scf/min). In the closing rate tests in the HP setup, the valves were able to close and then maintain a seal, and the leaked air prior to their closure also fell below 15 scf/min.

It was noticed that leakage rates at the same differential pressures across the valves within the same setup were different. As the geometry of the valves is almost identical, this indicates that the differences in performance could be due to manufacturing and the resulting roughness of the conical seat area. A dimensionless analysis was carried out to try to verify this claim and compared against published data. It was observed that probably the roughness of the high-pressure production valve is lower than the roughness of the high-pressure injection valve. It was also observed that the roughness of the low-pressure production valve is higher than the roughness of the low-pressure injection valve. However, it was not possible to verify these statements with measurements.

The leakage rates through the HP injection and production valves reached a critical differential pressure after which the valves continued leaking at a lower rate at greater differential pressures. This indicates that a good seal between the ball and the valve's seat is established. This phenomenon was not shown in the LP setup, since the maximum differential pressure that can be established (7.13 bar) was not high enough to reach a critical differential pressure. Results from the high-pressure leakage tests experiments showed that a good seal between the ball and the valve's seat is established when using gas as a working fluid at high differential pressures across the valves.

Some recommendations for future work to expand the scope of the assessment of the performance of the ball-type check valves are listed.

To further provide more ground for the dimensionless plot established to be used for further studies, the following is recommended:

1. Utilization of different gas working fluids in the HP setup with different densities or viscosities to study the leakage rates through the same valves used in this thesis. This

will prove the applicability of the dimensionless plot established in this thesis.

2. Conduct experiments to measure the leakage performance of ball-type check valves (with conical seats) with several known valve and ball roughness in the HP setup.
3. Expanding the scope of the dimensionless plot will help estimate leakage rates through valves at certain differential pressures without the need of conducting experiments.

To further utilize the LP setup, the following is recommended:

1. Making changes to the setup so that a gas flow meter can be installed downstream the transparent cell.
2. Assess leakage rates through the valves by using sand, as to mimic the effect sand production has on the sealing capability of the ball.

7. References

Azhar, R. (2016). *Cyclic Same-Well Enhanced Oil Recovery-Gas EOR Assessment for a Horizontal Multi-Fractured Well* (Master's Thesis, NTNU).

EIA, U. (2021). How much shale (tight) oil is produced in the United States? https://www.eia.gov/tools/faqs/faq.php?id=847&t=6

EIA, U. (2015). World Shale Rescource Assessments. Analysis and Projections. https://www.eia.gov/analysis/studies/worldshalegas/

Jacobs, T. (2015). Unconventional Resources Will Require Unconventional EOR. *Journal of Petroleum Technology*, *67*(09), 68-70. https://doi.org/10.2118/0915-0068-jpt

Luo, G., Ehlig-Economides, C., & Nikolaou, M. (2019). Managing miscible fluid injection and tight oil production from a single fractured horizontal well. *Journal of Petroleum Science and Engineering*.

Luo, G., Ehlig-Economides, C., & Nikolaou, M. (2021). Advantage of miscible fluid injection and tight oil production through a single-well alternating production-injection procedure over other single-well EOR methods. *Journal of Petroleum Science and Engineering*, *199*, 108091. https://doi.org/10.1016/j.petrol.2020.108091

Mydland, S., Yusra, I., Whitson, C. H., Dahouk, M. M., & Carlsen, M. L. (2020). Gas EOR Processes in Tight Unconventionals. SPE Improved Oil Recovery Conference. OnePetro.

Norsk olje og gass. (n.d.). *117 recommended guidelines for well integrity*. Retrieved June 16, 2022.

Sanchez-Rivera, D., Mohanty, K., & Balhoff, M. (2015). Reservoir simulation and optimization of Huff-and-Puff operations in the Bakken Shale. *Fuel*, *147*, 82-94.

Zarea, S., Rojas-Solorzano, L., & Kabboul, F. (1999, April). Run life enlargement methodology for ball-and-seat check valves used in artificial lift pumping units. In *Latin American and Caribbean Petroleum Engineering Conference*. OnePetro.

Zhu, P., Balhoff, M. T., & Mohanty, K. K. (2015). Simulation of fracture-to-fracture gas injection in an oil-rich shale. SPE Annual Technical Conference and Exhibition

8. Appendices

Appendix 1: Geometry of pressure cell (with the valve holder inside)

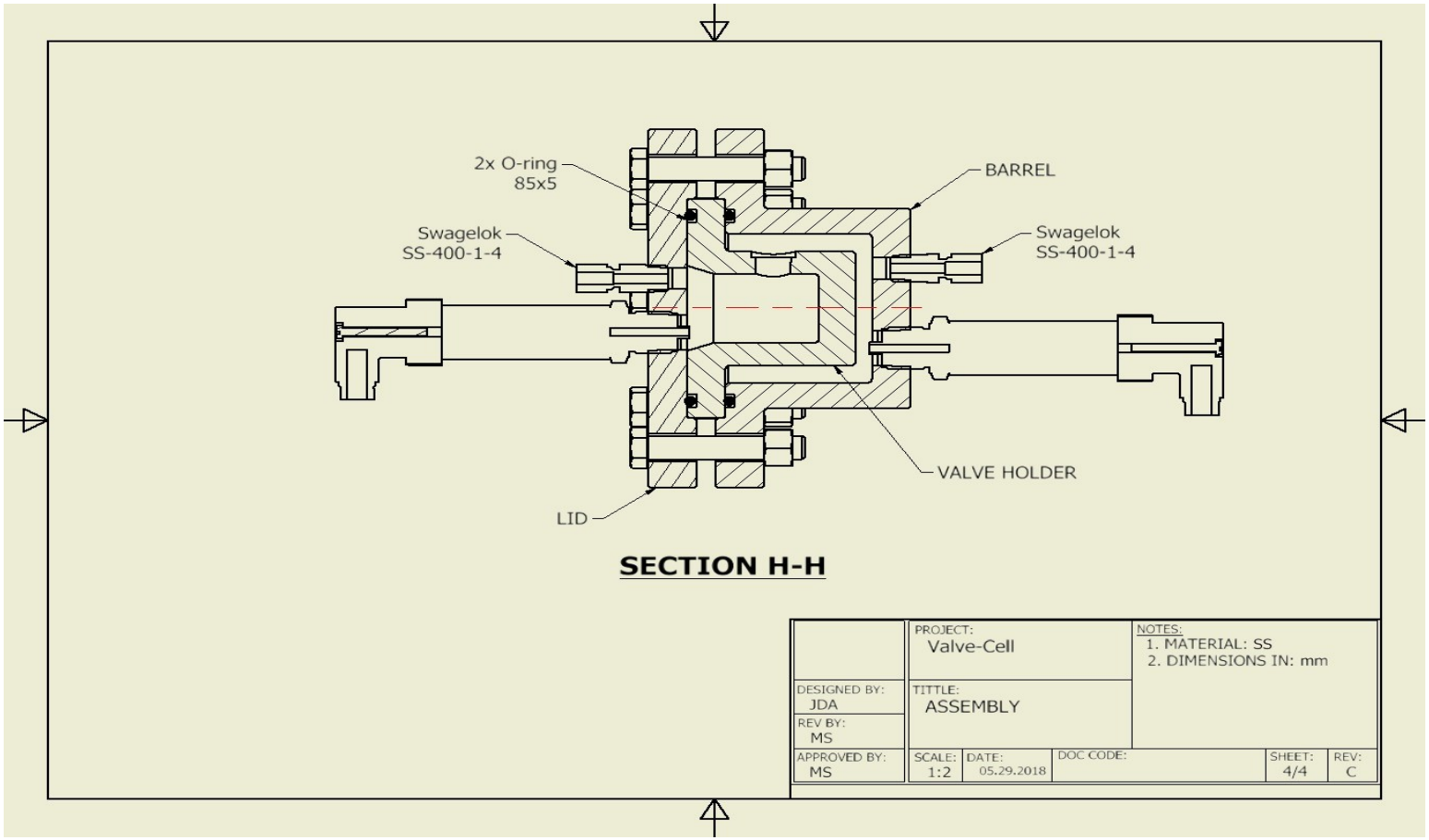

Appendix 2: Geometry of the injection valve in the high-pressure (HP) setup

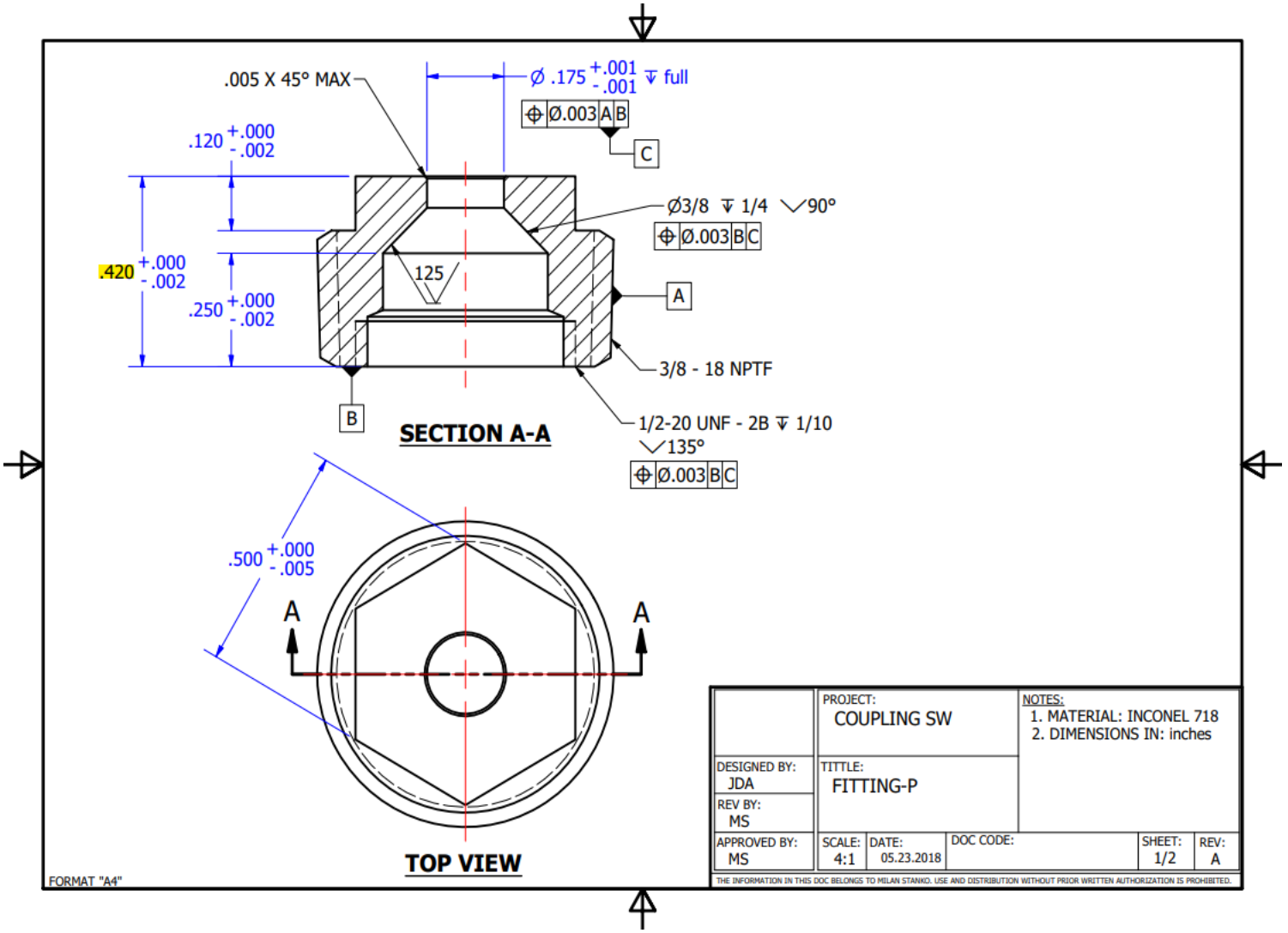

Appendix 3: Geometry of the production valve in the high-pressure (HP) setup

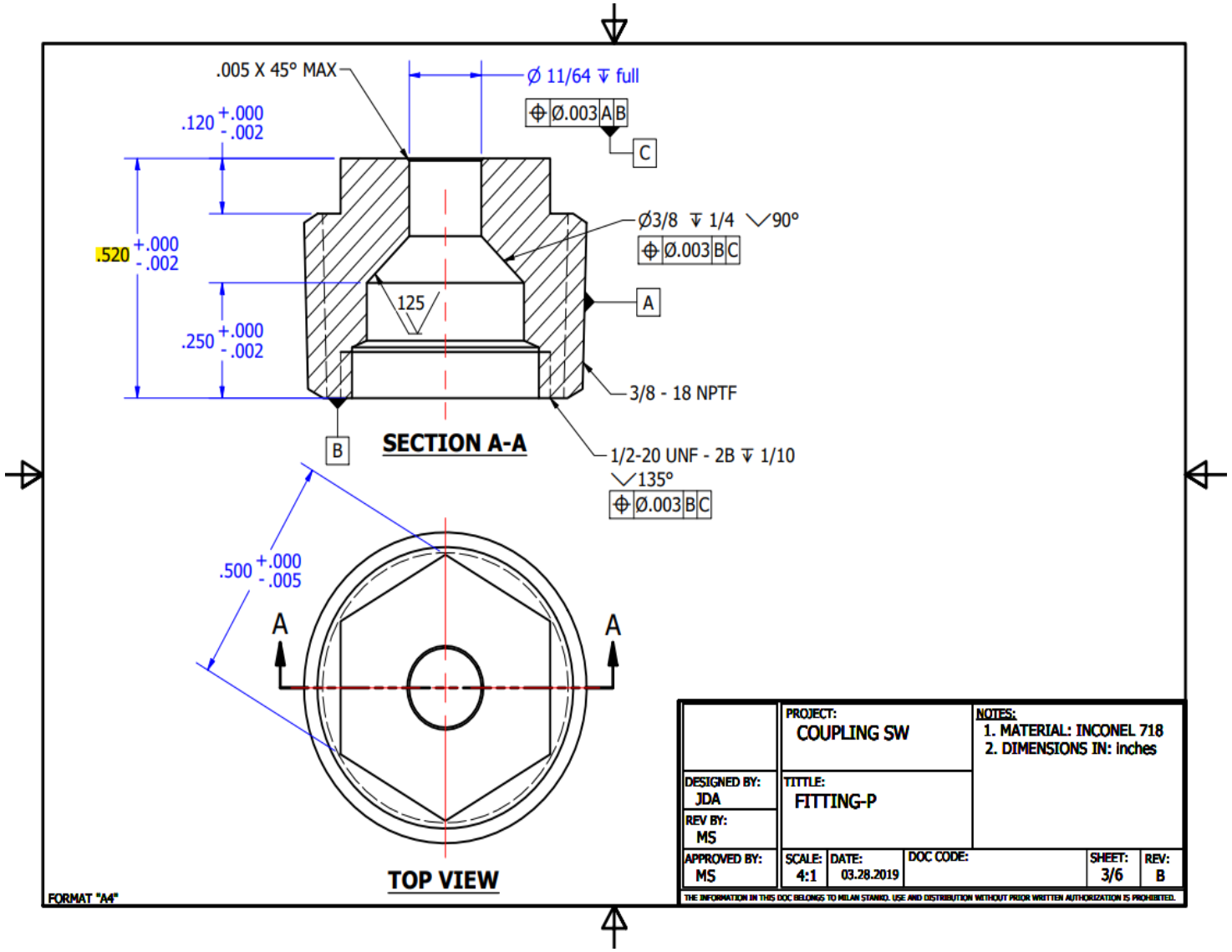

Appendix 4: Nitrogen tank pressure regulator

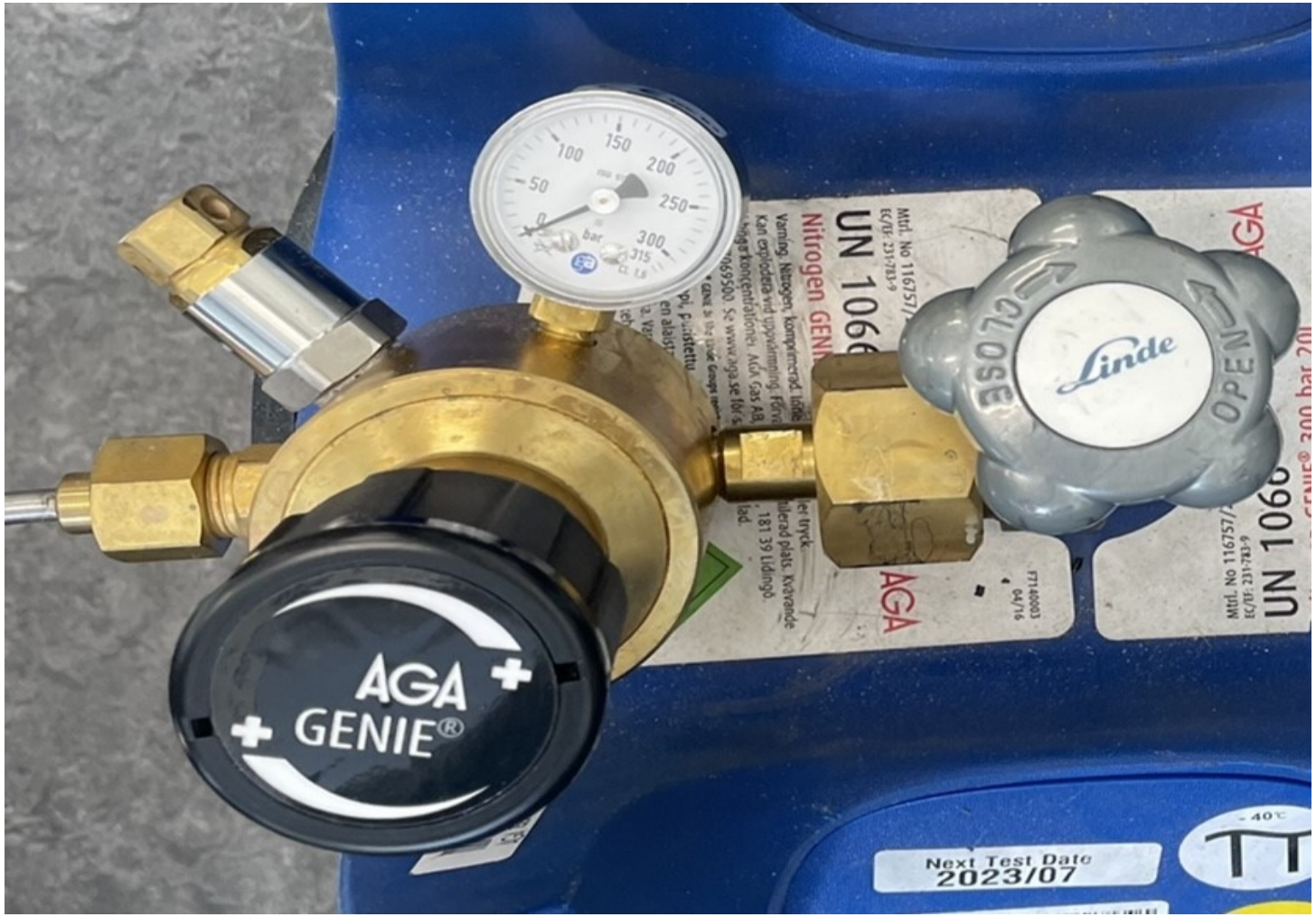

Appendix 5: Geometry of the injection valve within the transparent cell

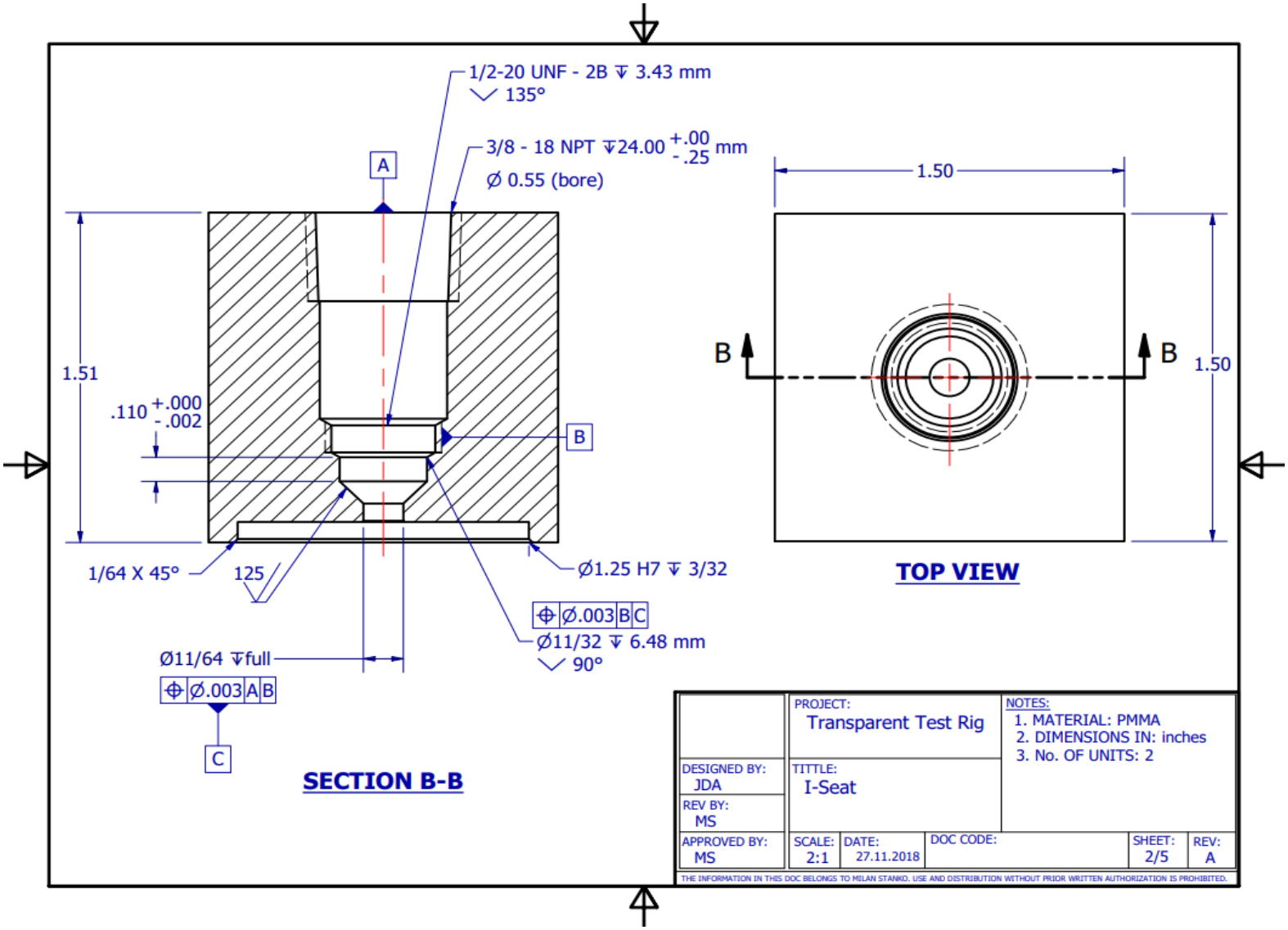

Appendix 6: Geometry of the production valve within the transparent cell

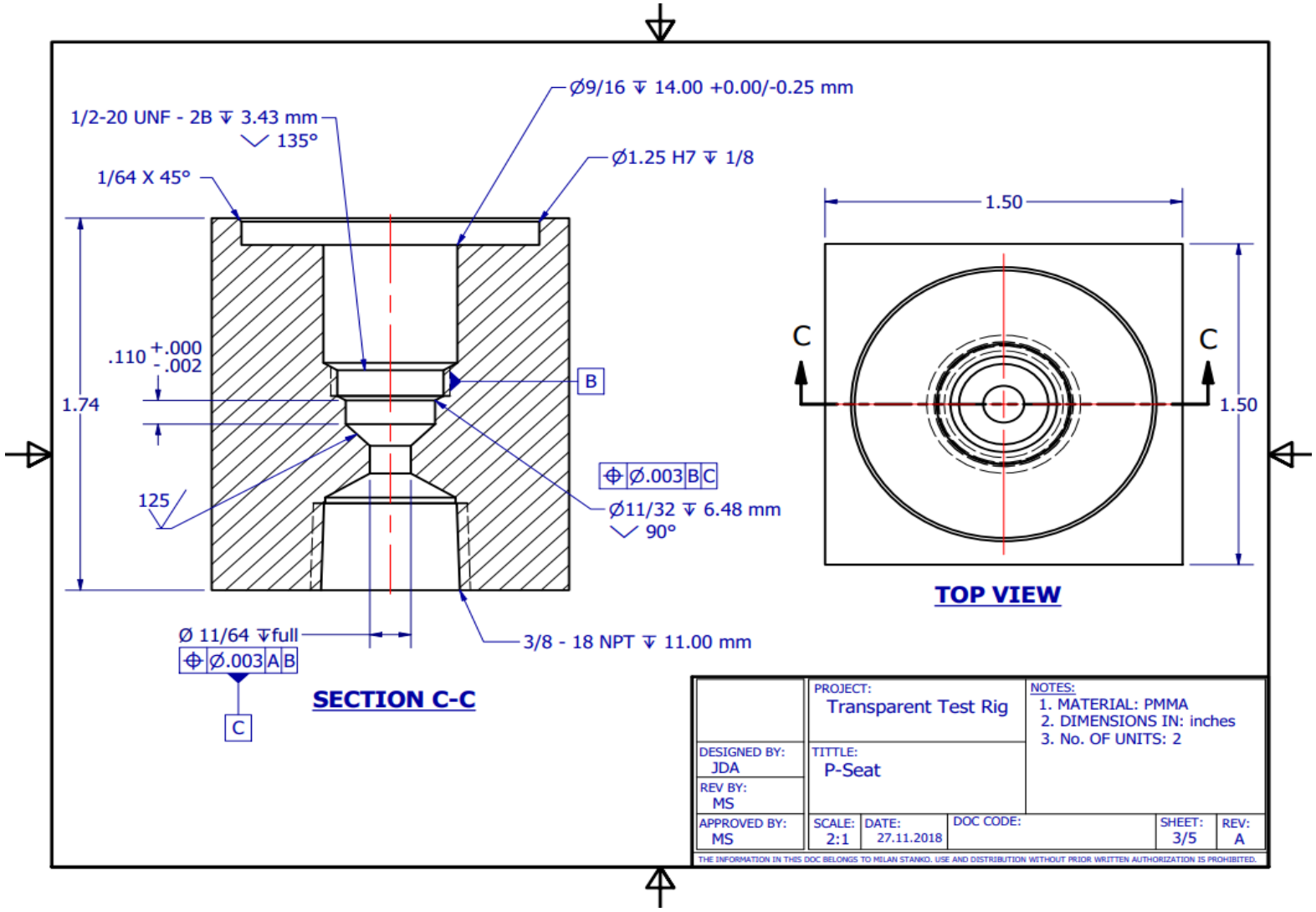

Appendix 7: Reading values from the rotameter

Figure A7.1 shows the rotameter used in the experiments and **Figure A7.2** shows a sketch of a part of the rotameter (highlighted in black in **Figure A7.1**), in which the reading of measured values is explained.

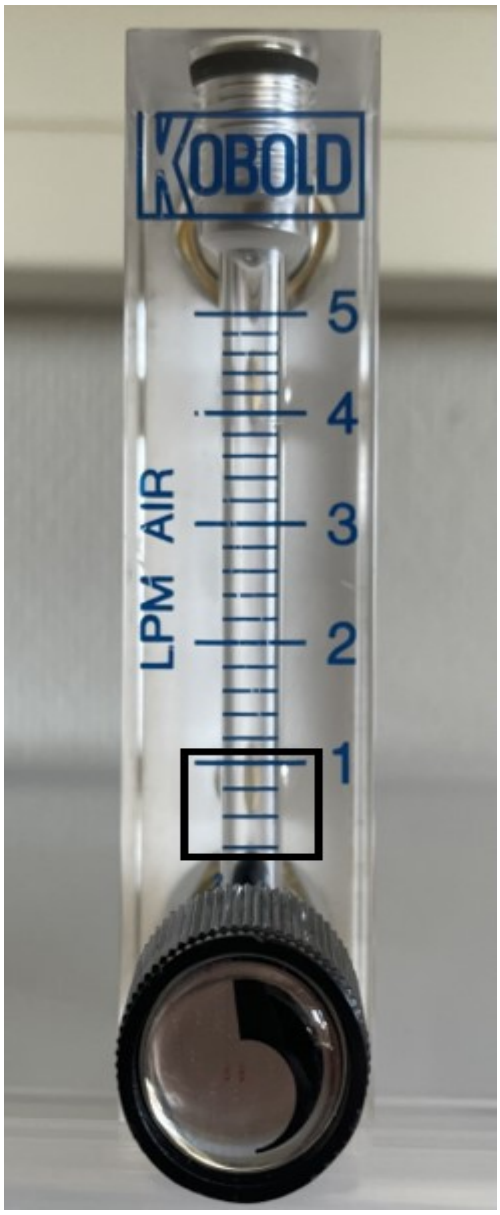

Figure A7.1: Rotameter

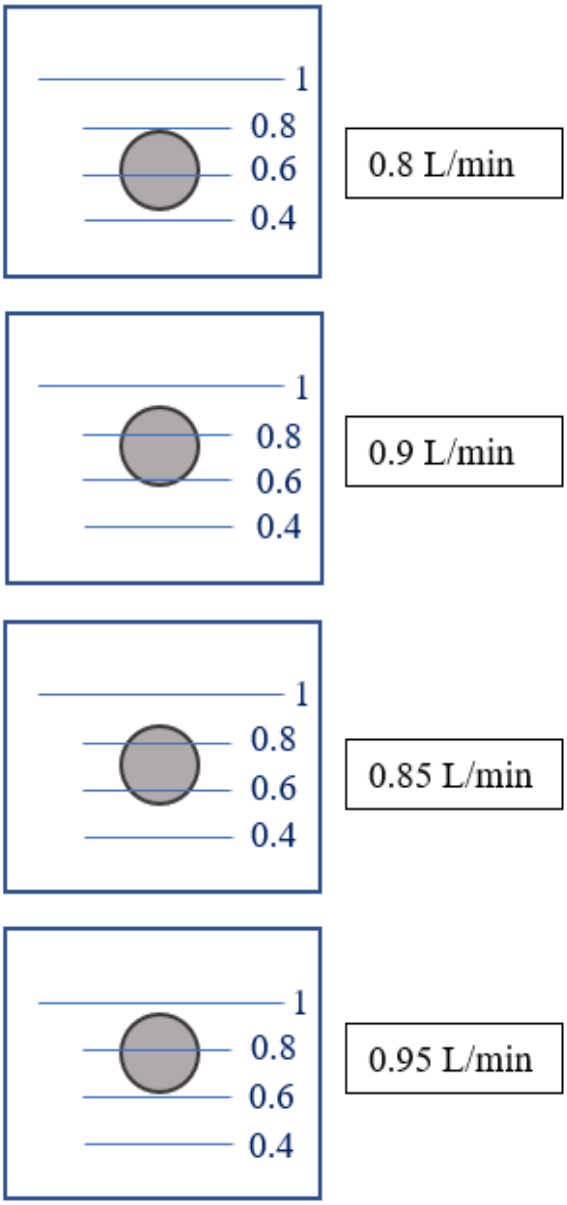

Figure A7.2: Measurements through rotameter

Appendix 8: Best-fit polynomial curves for metallic air tank pressure versus time (tank depressurization)

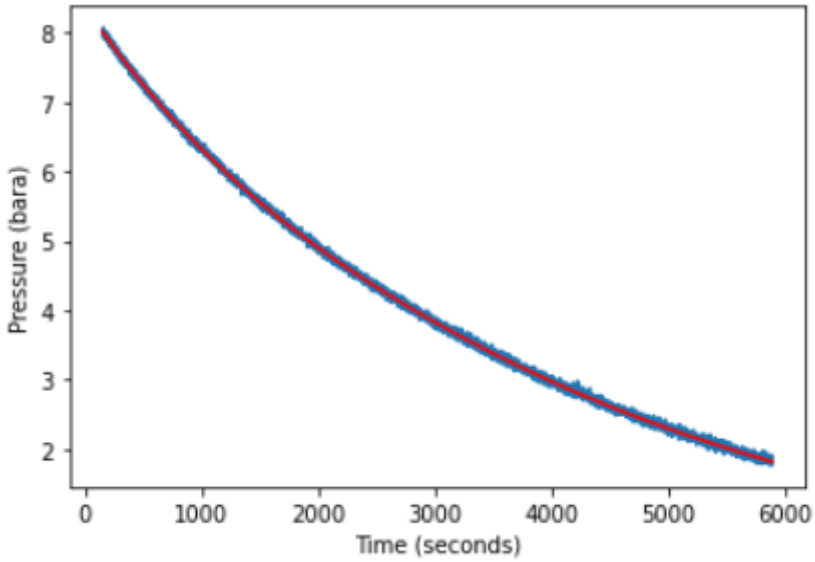

Figure A8.1 Tank depressurization (bara) vs. time (second) from the time of opening "valve 2" during injection valve leakage test, and a fifth-degree polynomial fit (in red)

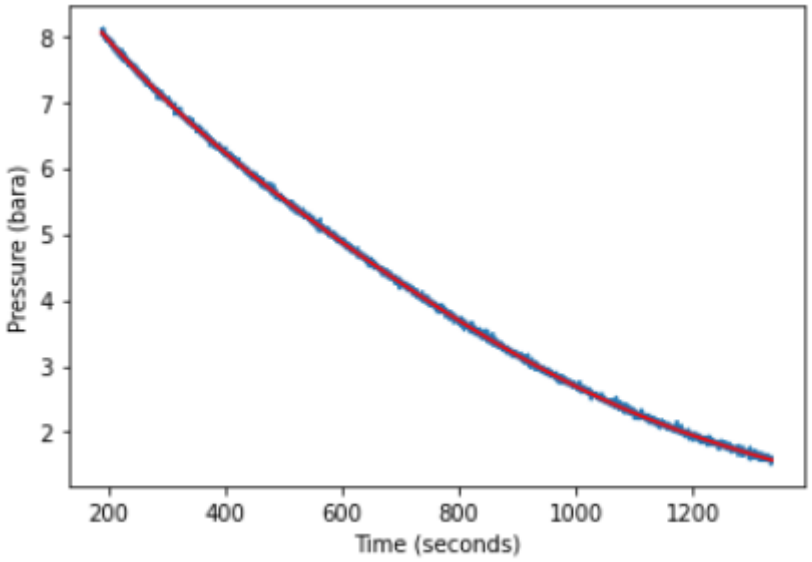

Figure A8.2 Tank depressurization (bara) vs. time (second) from the time of opening "valve 2" during production valve leakage test, and a fifth-degree polynomial fit (in red)

Appendix 9: Comparison between rotameter and gas flow meter measurements in HP setup

Leakage test through the production valve in the HP setup is used as an example to compare leakage rates measured through rotameter and the gas flow meter.

After the differential pressure of interest stabilizes and is established across the valve, the leakage rate measured by the flow meter fluctuates over that ΔP interval. Therefore, an average leakage rate is calculated. The coefficient of variation (CoV) is calculated to show the extent of variability (fluctuation) of the measured data with respect to the average leakage rate calculated. A low CoV indicates that the average leakage rate is representative of the leakage performance of the valve over that interval.

The gas flow meter has an accuracy of $\pm$ 5 % full scale (maximum gas flow meter scale value is 3 L/min). Therefore, the gas flow meter is $\pm$ 0.15 L/min or $\pm$ 0.005298 scf/min accurate for all measured values. The error as a percentage of leakage rate is calculated by dividing δq_{gf} by $q_{N_2,gf}$ (scf/min) at each differential pressure.

Table A9.1 shows the leakage rates measured using the gas flow meter at the ΔP of interest established across the production valve.

Table A9.1: The leakage rates measured using the gas flow meter at the ΔP of interest established across the production valve, the average leakage rate over that ΔP the CoV, the error associated to leakage rate measurements through the gas flow meter, the error associated to pressure measurements, and the error as a percentage of leakage rate

Production valve					
Gas flow meter					
ΔP (bar)	$q_{N_2,gf}$ (scf/min)	CoV (%)	δP_{HP} (bar)	δq_{gf} (scf/min)	Error (%)
7	0.00759	0.1575	$\pm$ 0.25	$\pm$ 0.005298	69.80
10	0.01115	0.5196	$\pm$ 0.25	$\pm$ 0.005298	47.52
20	0.02007	0.8316	$\pm$ 0.25	$\pm$ 0.005298	26.39
50	0.03020	0.0873	$\pm$ 0.25	$\pm$ 0.005298	17.54
75	0.03116	0.8314	$\pm$ 0.25	$\pm$ 0.005298	17.00
100	0.02944	0.1959	$\pm$ 0.25	$\pm$ 0.005298	17.99
125	0.02407	0.5621	$\pm$ 0.25	$\pm$ 0.005298	22.01
150	0.01988	0.9524	$\pm$ 0.25	$\pm$ 0.005298	26.65

The CoV (%) is so small that all that the calculated average leakage rates are considered representative of the leakage performance of the production valve over each ΔP interval. As

one goes further away from the maximum scale value (3 L/min), the error as a % of flow increases (since the error value in scf/min is constant for all measured flow rates). Since the error as a percentage of leakage rate exceeds the CoV at all differential pressures, then δq_{gf} is used as the error associated to leakage rate measurements.

Table A9.2 shows the leakage rates measured through the rotameter at the differential pressures of interest across the production valve. Note that leakage rates at ΔP of 7 and 10 bar could not be read by the rotameter since they fell under its minimum 0.4 L/min flow limit (or 0.014126 scf/min).

Table A9.2: The leakage rates measured through the rotameter at the differential pressures of interest across the production valve, the error associated to leakage rate measurements through the rotameter, and the error associated to pressure measurements

Production Valve			
Rotameter			
ΔP (bar)	$q_{N_2,ro}$ (scf/min)	δP_{HP}(bar)	δq_{ro} (scf/min)
7	[-]	[-]	[-]
10	[-]	[-]	[-]
20	0.01766	$\pm$ 0.25	$\pm$ 0.005298
50	0.02472	$\pm$ 0.25	$\pm$ 0.005298
75	0.02649	$\pm$ 0.25	$\pm$ 0.005298
100	0.02295	$\pm$ 0.25	$\pm$ 0.005298
125	0.02119	$\pm$ 0.25	$\pm$ 0.005298
150	0.01766	$\pm$ 0.25	$\pm$ 0.005298

Figure A9.1 shows the leakage rates measured by the rotameter and the gas flow meter, versus the differential pressures across the production valve.

A best-fit line was fitted to the measured gas flow meter leakage rates at and before the critical differential pressure of 75 bar, to extrapolate leakage rates to the low-pressure range (**Figure A9.2**). The best-fit line resulted in Eq. **A9.1**. Best-fit lines are forced through the origin.

$$q_{N_2,gf} = 8.4050 * 10^{-8} (\Delta P)^3 - 1.8176 * 10^{-5} (\Delta P)^2 + 1.3055 (\Delta P) \quad \text{(A9.1)}$$

Tables A9.3 shows the leakage rates through the production valve, measured through the gas flow meter and calculated ($q_{N_2,f}$) through Eq. **A9.1.** Leakage rates at the differential pressures greater than 7 bar were also calculated through Eq. **A9.1** This was done to calculate the percent

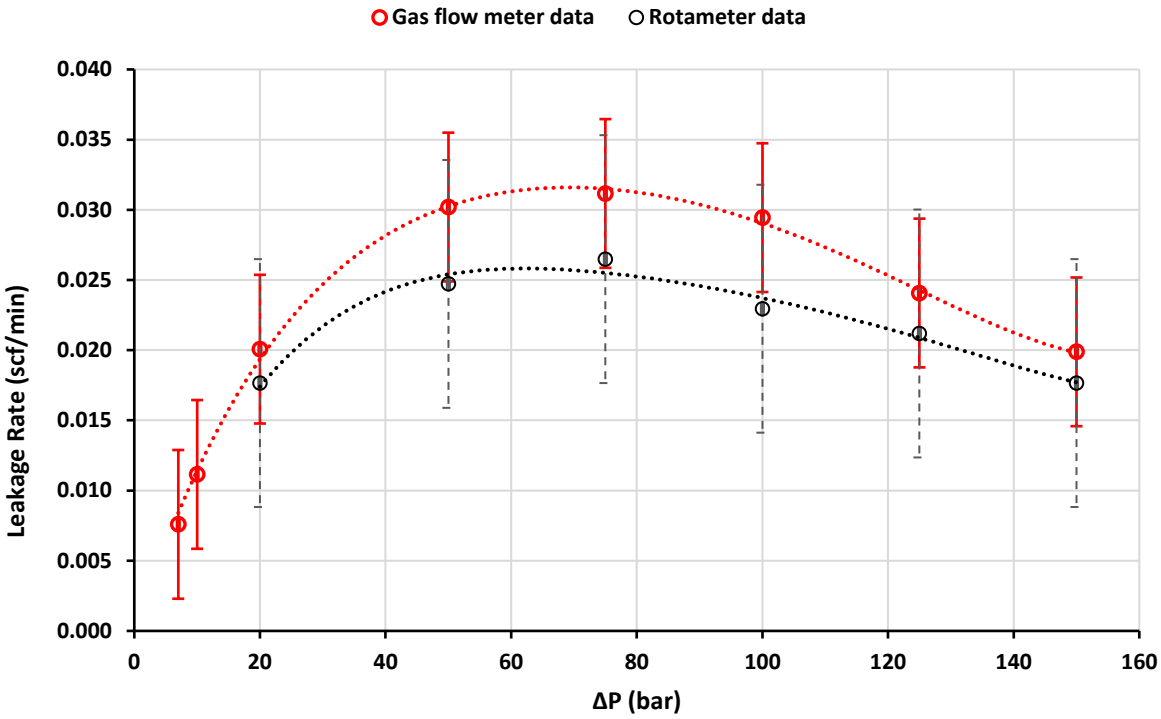

Figure A9.1: Leakage rates measured by the rotameter (black) and the gas flow meter (red), versus the differential pressures across the production valve. The red error bars represent δq_{gf} and δP along the Y and X direction respectively. The black, dashed error bars represent δq_{gf} and δP along the Y and X direction respectively. The dotted red and black curves represent a fit for the measured data points.

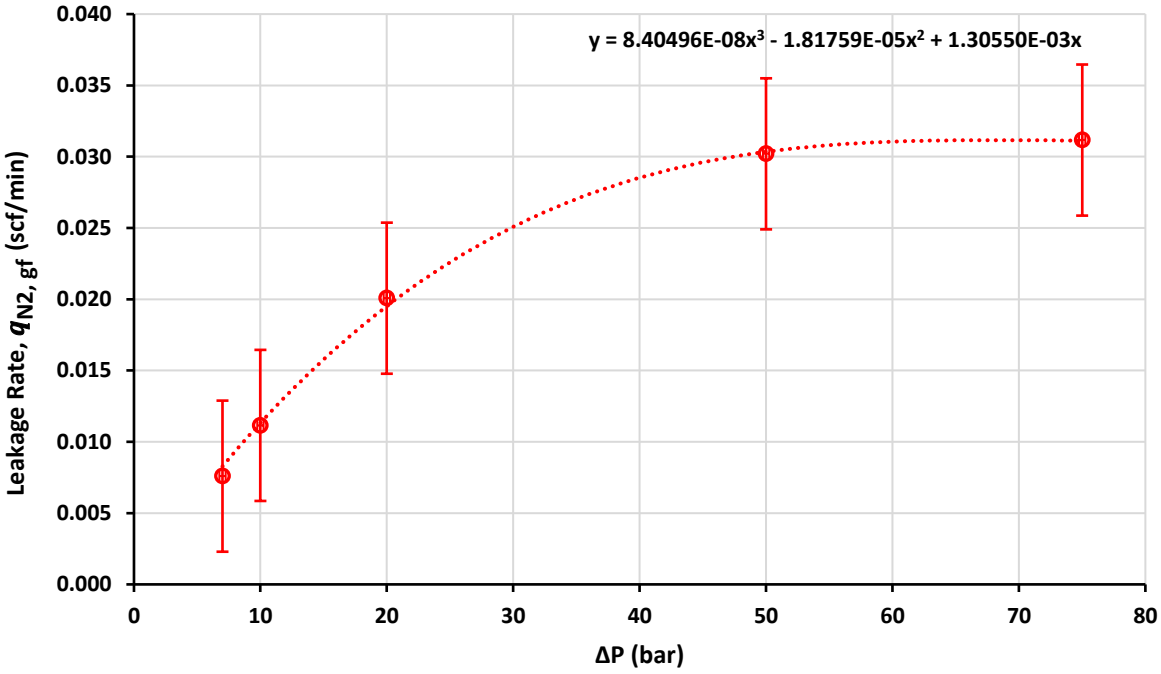

Figure A9.2: Measured leakage rates versus differential pressure (ΔP up to 75 bar) across the production valve in the HP setup. Y error bars ± 0.005298 scf/min and X error bars ± 0.25 bar. The best-fit polynomial line (dotted red line) represents *Eq. A9.1* which is also shown on the plot.

difference between the measured and calculated values (at $\Delta P \geq 7$). A low P.D indicates that the polynomial equations can be used to safely extrapolate the leakage rates to the low-pressure range. P.D is calculated using Eq. **A9.2** and is shown in **Table A9.3**

$$P.D = \frac{\left|q_{N_2,gf} - q_{N_2,f}\right|}{q_{N_2,gf}} * 100 \tag{A9.2}$$

Table A9.3: Measured and calculated leakage rates through the production valve in the HP setup, percent difference between the two, and error associated to the leakage rates and pressure measurements

Production valve					
	Gas flow meter			Equation A9.1	Difference
ΔP (bar)	$q_{N_2,gf}$ (scf/min)	δP_{HP} (bar)	δq_{gf} (scf/min)	$q_{N_2,f}$ (scf/min)	(%)
1.0	[-]	[-]	[-]	0.00239	[-]
1.5	[-]	[-]	[-]	0.00354	[-]
2.0	[-]	[-]	[-]	0.00466	[-]
2.5	[-]	[-]	[-]	0.00576	[-]
3.0	[-]	[-]	[-]	0.00682	[-]
3.5	[-]	[-]	[-]	0.00786	[-]
4.0	[-]	[-]	[-]	0.00887	[-]
4.5	[-]	[-]	[-]	0.00986	[-]
5.0	[-]	[-]	[-]	0.01082	[-]
5.5	[-]	[-]	[-]	0.01175	[-]
6.0	[-]	[-]	[-]	0.01266	[-]
6.5	[-]	[-]	[-]	0.01355	[-]
7.0	0.00759	$\pm$ 0.25	$\pm$ 0.005298	0.008277	9.040
10	0.01115	$\pm$ 0.25	$\pm$ 0.005298	0.011321	1.539
20	0.02007	$\pm$ 0.25	$\pm$ 0.005298	0.019512	2.794
50	0.03020	$\pm$ 0.25	$\pm$ 0.005298	0.030341	0.474
75	0.03116	$\pm$ 0.25	$\pm$ 0.005298	0.031131	0.105
100	0.02944	$\pm$ 0.25	$\pm$ 0.005298	[-]	[-]
125	0.02407	$\pm$ 0.25	$\pm$ 0.005298	[-]	[-]
150	0.01988	$\pm$ 0.25	$\pm$ 0.005298	[-]	[-]

The P.D seems to increase at a ΔP of 7 bar, but the best-fit line represents near perfectly leakage rates measured through the gas flow meter at other differential pressures.

Figure A9.3 shows the leakage rates extrapolated towards the low-pressure range ($1 \leq \Delta P \leq 7$). The first data set shows rates calculated using Eq. **A9.1** (using gas flow meter measured data), and the second data set shows the rates calculated using Eq. **4.15** (using the rotameter measured data**).** Note that at a ΔP of 7 bar, no extrapolated value exists for the "gas flow meter" data set, since the gas flow meter can measure the leakage rate at this differential pressure, while the rotameter cannot.

There were several findings in comparing the rotameter and gas flow meter data.

First, taking into account the error associated to the leakage rates for both data sets in **Figure A9.1**, it can be clearly seen that the leakage rates measured through the rotameter fall within the range of the leakage rates measured through the gas flow meter.

Second, the percent difference between the extrapolated data towards the low-pressure range using the rotameter and the gas flow meter measured data is very small (**Table A9.4** and **Figure A9.3**).

Table A9.4: Difference between extrapolated data using *Eq. A9.1* (using gas flow meter measured data) and *Eq. 4.15* (using the rotameter measured data)

Production Valve			
	Extrapolated data (Eq. A9.1)	**Extrapolated data (Eq. 4.15)**	**Difference**
ΔP (bar)	**$q_{N_2,f}$ (scf/min)**	**$q_{N_2,f}$ (scf/min)**	**(%)**
1.0	0.00129	0.00127	1.434
1.5	0.00192	0.00189	1.648
2.0	0.00254	0.00249	1.862
2.5	0.00315	0.00309	2.076
3.0	0.00376	0.00367	2.290
3.5	0.00435	0.00424	2.504
4.0	0.00494	0.00480	2.718
4.5	0.00551	0.00535	2.932
5.0	0.00608	0.00589	3.146
5.5	0.00664	0.00642	3.360
6.0	0.00720	0.00694	3.573
6.5	0.00774	0.00745	3.787
7.0	[-]	0.00795	[-]

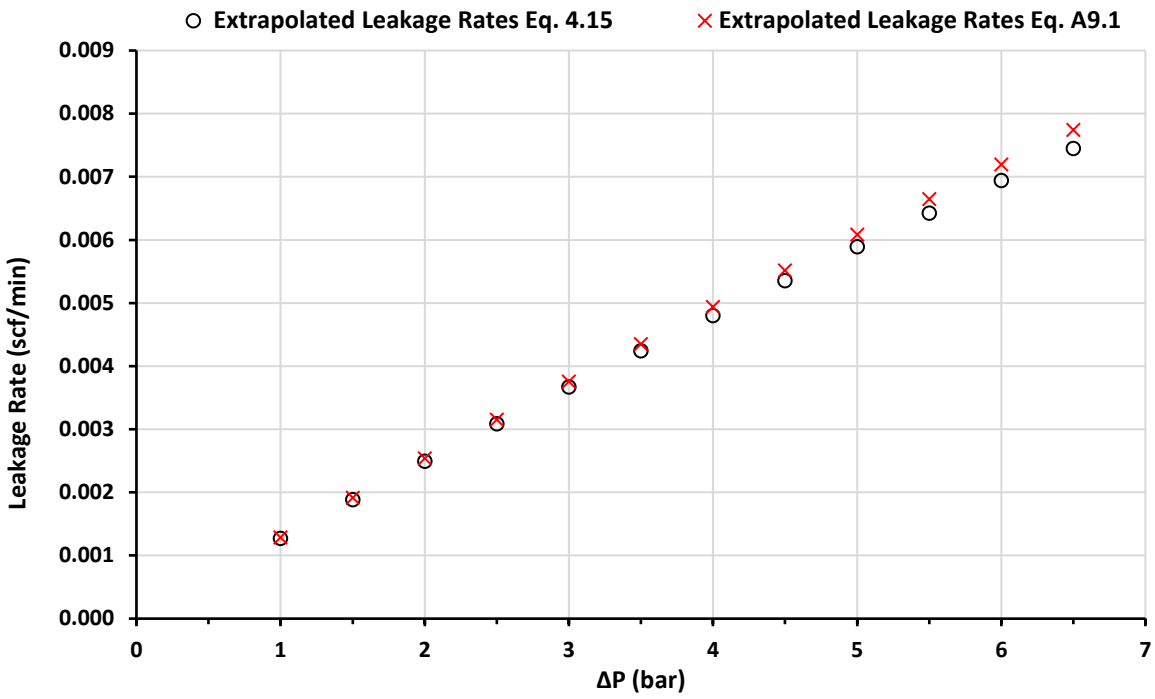

Figure A9.3: The leakage rates extrapolated towards the low-pressure range. Red crosses indicate the data set of leakage rates calculated using *Eq. A9.1*, and the black circles indicate the data set of leakage rates calculated using *Eq. 4.15* (using the rotameter measured data)

Third, at ΔP of 7 bar, the rotameter was unable to detect a leakage rate (its minimum flow detection limit is 0.4 L/min or 0.014126 scf/min), but the gas flow meter measured a leakage rate of 0.00759 scf/min. This shows that the rotameter was accurate not detecting a flow. Finally, the extrapolated leakage rate at ΔP of 7 bar using the gas rotameter measured data is 0.00795 scf/min (refer to **Table A9.4**). The measured leakage value at this differential pressure using the gas flow meter is 0.00759 scf/min (**Table A9.3**). This 4.7 % difference between the two values show that the extrapolated values using the rotameter measured data can be trusted to assess the leakage performance of the valves at the low-pressure range.

The comparison shows that the rotameter was an adequate tool for measuring the leakage rates in the HP setup.

Appendix 10: Derivation of the dimensionless parameters using Buckingham's Theorem

Parameters (units)	Dimensions (L, T, M)
$\boldsymbol{q}$ (m^3/s)	$L^3\,T^{-1}$
$\Delta\boldsymbol{P}$ (Pa)	$ML^{-1}T^{-2}$
$\boldsymbol{\varepsilon_a}$ (m)	L
$\boldsymbol{\varepsilon_b}$ (m)	L
$\boldsymbol{\rho}$ (kg/m^3)	ML^{-3}
$\boldsymbol{\mu}$ (Pa.s)	$ML^{-1}T^{-1}$
$\boldsymbol{D_a}$ (m)	L
$\boldsymbol{D_b}$ (m)	L

The number of repeating variables (r) is three, and they are taken to be ρ, μ, and D_b .The number of parameters (k) is 8. So, the number of π terms is 5 (k – r).

1st π-term

$\pi_1 = q\,\rho^a\mu^b D_b^c$

$L^0M^0T^0 = (L^3\,T^{-1})\,(ML^{-3})^a\,(ML^{-1}T^{-1})^b\,(L^c)$

$L \quad : 0 = 3 - 3a - b + c$

$M \quad : 0 = a + b$

$T \quad : 0 = -1 - b$

$a = 1, \quad b = -1, \quad and\ c = -1$

$$\boldsymbol{\pi_1 = \frac{\rho q}{\mu D_b}}$$

2nd π-term

$\pi_2 = \Delta P\,\rho^a\mu^b D_b^c$

$L^0M^0T^0 = (ML^{-1}T^{-2})\,(ML^{-3})^a\,(ML^{-1}T^{-1})^b\,(L^c)$

$L \quad : 0 = -1 - 3a - b + c$

$M \quad : 0 = 1 + a + b$

$T \quad : 0 = -2 - b$

$a = 1, \quad b = -2, \quad and\ c = 2$

$$\boldsymbol{\pi_2 = \frac{\Delta P \rho D_b^2}{\mu^2}}$$

3rd π-term

$\pi_3 = \varepsilon_a\, \rho^a \mu^b D_b^c$

$L^0 M^0 T^0 = (L)\ (ML^{-3})^a\ (ML^{-1}T^{-1})^b\ (L^c)$

$L \quad : 0 = 1 - 3a - b + c$

$M \quad : 0 = a + b$

$T \quad : 0 = -b$

$a = 0, \quad b = 0, \quad and\ c = -1$

$$\boldsymbol{\pi_3 = \frac{\varepsilon_a}{D_b}}$$

4th π-term

$\pi_3 = \varepsilon_b\, \rho^a \mu^b D_b^c$

$L^0 M^0 T^0 = (L)\ (ML^{-3})^a\ (ML^{-1}T^{-1})^b\ (L^c)$

$L \quad : 0 = 1 - 3a - b + c$

$M \quad : 0 = a + b$

$T \quad : 0 = -b$

$a = 0, \quad b = 0, \quad and\ c = -1$

$$\boldsymbol{\pi_4 = \frac{\varepsilon_b}{D_b}}$$

5th π-term

$\pi_3 = D_a\, \rho^a \mu^b D_b^c$

$L^0 M^0 T^0 = (L)\ (ML^{-3})^a\ (ML^{-1}T^{-1})^b\ (L^c)$

$L \quad : 0 = 1 - 3a - b + c$

$M \quad : 0 = a + b$

$T \quad : 0 = -b$

$a = 0, \quad b = 0, \quad and\ c = -1$

$$\boldsymbol{\pi_5 = \frac{D_a}{D_b}}$$

The π terms can be written in different forms, but the number of π terms (5) should always be respected. Note that π_3' is referred to as π_3 in the thesis.

$$\pi_3' = \frac{\pi_3 + \pi_4}{\pi_5} = \frac{\boldsymbol{\varepsilon_a + \varepsilon_b}}{\boldsymbol{D_a}}$$

Appendix 11: Derivation of the errors associated to the dimensionless π-terms

Error associated to the dimensionless leak flow for the HP setup

$$q = q_{N_2,ro} * d$$

The error associated to the measured leakage rates through the rotameter is δq_{ro}. Therefore, the error associated with the leakage rate q (sm^3/s) is:

$$\delta q = \delta q_{ro} * d$$

The dimensionless leak flow is expressed through the following equation:

$$\pi_1 = \frac{\rho q}{\mu D_b}$$

Hence, the error associated to the dimensionless leak flow is:

$$\delta\pi_1 = \pm\left[\delta q * \left(\frac{\rho}{\mu D_b}\right)\right]$$

Substituting for δq, we get:

$$\boldsymbol{\delta\pi_1 = \pm\left[\delta q_{ro} * d\left(\frac{\rho}{\mu D_b}\right)\right]}$$

Error associated to the dimensionless pressure drop for the HP setup

$$\delta\Delta P = \delta P_{HP} * 10^5$$

Where the factor 10^5 is used to convert the error associated to pressure measurements from bar to pascal. The dimensionless pressure drop is expressed through the following equation:

$$\pi_2 = \frac{\Delta P \rho D_b^2}{\mu^2}$$

Hence, the error associated to the dimensionless pressure drop is:

$$\pi_2 = \pm\left[\delta\Delta P\left(\frac{\rho D_b^2}{\mu^2}\right)\right]$$

Substituting for $\delta\Delta P$, we get:

$$\boldsymbol{\delta\pi_2 = \pm\left[\delta P_{HP} * 10^5\left(\frac{\rho D_b^2}{\mu^2}\right)\right]}$$

Error associated to the dimensionless leak flow for the HP setup

$$q = q_{air,LP} * d$$

The error associated to the calculated leakage rates through the tank depressurization is $\delta q_{air,LP}$. Therefore, the error associated with the leakage rate q (sm^3/s) is:

$$\delta q = \delta q_{air,LP} * d$$

The dimensionless leak flow is expressed through the following equation:

$$\pi_1 = \frac{\rho q}{\mu D_b}$$

Hence, the error associated to the dimensionless leak flow is:

$$\delta\pi_1 = \pm\left[\delta q * \left(\frac{\rho}{\mu D_b}\right)\right]$$

Substituting for δq, we get:

$$\boldsymbol{\delta\pi_1 = \pm\left[\delta q_{air,LP} * d\left(\frac{\rho}{\mu D_b}\right)\right]}$$

Error associated to the dimensionless pressure drop for the HP setup

$$\delta\Delta P = \delta P_{LP} * 10^5$$

Where the factor 10^5 is used to convert the error associated to pressure measurements from bar to pascal. The dimensionless pressure drop is expressed through the following equation:

$$\pi_2 = \frac{\Delta P \rho D_b^2}{\mu^2}$$

Hence, the error associated to the dimensionless pressure drop is:

$$\pi_2 = \pm\left[\delta\Delta P\left(\frac{\rho D_b^2}{\mu^2}\right)\right]$$

Substituting for $\delta\Delta P$, we get:

$$\boldsymbol{\delta\pi_2 = \pm\left[\delta P_{LP} * 10^5\left(\frac{\rho D_b^2}{\mu^2}\right)\right]}$$

Appendix 12: Conversion of R_a to R_t

Figure A12.1 shows the arithmetical average surface roughness (R_a) of specific ball grades. R_a is expressed in microinches (μ") in the table. Equation **A12.1** is used to convert R_a in microinches to micrometers (μm).

$$R_a(\mu m) = R_a(\mu")/40 \quad \text{(A12.1)}$$

To convert from R_a to R_t, the conversion table shown in **Figure A12.2** is used. R_t in this chart is expressed in microns (or micrometer).

HP valves silicon nitride ball

The 6.25 mm silicon nitride balls used in the HP setup are grade 5 (GR:5) balls (**Figure A12.3**). Therefore, the corresponding R_a is 0.8 μ" which equates to 0.02 μm. The minimum R_a (μm) that can be converted using the conversion table is 0.025 μm. Since the arithmetical average surface roughness of the silicon nitride ball is less than 0.025 μm, then the latter is used to get R_t. Hence, R_t read from the chart is 0.3 μm (or $3 * 10^{-7}$ m, ε_b).

LP valves stainless-steel balls

The 7 mm stainless-steel balls used in the LP setup are 440c grade 25 balls. Therefore, the corresponding R_a for grade 25 balls is 2 μ" (**Figure A12.1**) which equates to 0.05 μm. Using the conversion table in **Figure A12.2**, the R_t is 0.5 μm (or $5 * 10^{-7}$ m, ε_b).

Grade	Allowable Ball Diameter Variation	Deviation From Spherical Form	Surface Roughness Arithmetical Average	Basic Diameter Tolerance	Allowable Lot Diameter Variation
3	3 µ" .000003"	3 µ" .000003"	.5 µ" .0000005"	30 µ" +/-.00003"	5 µ" .000005"
5	5 µ" .000005"	5 µ" .000005"	.8 µ" .0000008"	50 µ" +/-.00005"	10 µ" .00001"
10	10 µ" .00001"	10 µ" .00001"	1.0 µ" .000001"	100 µ" +/-.0001"	20 µ" .00002"
15	15 µ" .000015"	15 µ" .000015"	1.0 µ" .000001"	100 µ" +/-.0001"	30 µ" .00003"
16	16 µ" .000016"	16µ" .000016"	1.0 µ" .000001"	100 µ" +/-.0001"	32 µ" .000032"
24	24 µ" .000024"	24 µ" .000024"	2.0 µ" .000002"	100 µ" +/-.0001"	48 µ" .000048"
25	25 µ" .000025"	25 µ" .000025"	2.0 µ" .000002"	100 µ" +/-.0001"	50 µ" .000048"
48	48 µ" .000048"	48 µ" .000048"	3.0 µ" .000003"	200 µ" +/-.0002"	96 µ" .000096"
50	50 µ" .000050"	50 µ" .000050"	3.0 µ" .000003"	300 µ" +/-.0003"	100 µ" .0001"
100	100 µ" .0001"	100 µ" .0001"	5.0 µ" .000005"	500 µ" +/-.0005"	200 µ" .0002"
200	200 µ" .0002"	200 µ" .0002"	8.0 µ" .000008"	1000 µ" +/-.001"	400 µ" .0004"
300	300 µ" .0003"	300 µ" .0003"		1000 µ" +/-.001"	600 µ" .0006"
500	500 µ" .0002"	500 µ" .0002"	2000 µ" +/-.002"	2000 µ" +/-.002"	
1000	1000 µ" .001"	1000 µ" .001"		2000 µ" +/-.002"	2000 µ" +/-.002"
2000	2000 µ" .002"	2000 µ" .002"	5000 µ" +/-.005"	2000 µ" +/-.002"	
3000	3000 µ" .003"	3000 µ" .003"		5000 µ" +/-.005"	6000 µ" +/-.006"

Figure A12.1: Arithmetical average surface roughness (R_a) for different ball grades

Surface Roughness Conversion Chart							
Ra micro-meters	Ra micro-inches	RMS	CLA (N)	Rt	N	Cut-Off Length	
						in.	mm
0.025	1	1.1	1	0.3	1	0.003	0.08
0.05	2	2.2	2	0.5	2	0.01	0.25
0.1	4	4.4	4	0.8	3	0.01	0.25
0.2	8	8.8	8	1.2	4	0.01	0.25
0.4	16	17.6	16	2.0	5	0.01	0.25
0.8	32	35.6	32	4.0	6	0.03	0.8
1.6	63	69.3	63	8.0	7	0.03	0.8
3.2	125	137.5	125	13	8	0.1	2.5
6.3	250	275	250	25	9	0.1	2.5
12.5	500	550	500	50	10	0.1	2.5
25.0	1000	1100	1000	100	11	0.3	8.0
50.0	2000	2200	2000	200	12	0.3	8.0

Figure A12.2: Conversion chart from R_a to R_t (microns)

2	2	002500000UN Lot# 101239 C 1/4" SILICON NITRIDE GR:5 CT:0915076 SH:973	23.4400	46.8

Figure A12.3: The grade of the silicon nitride ball used in the HP setup

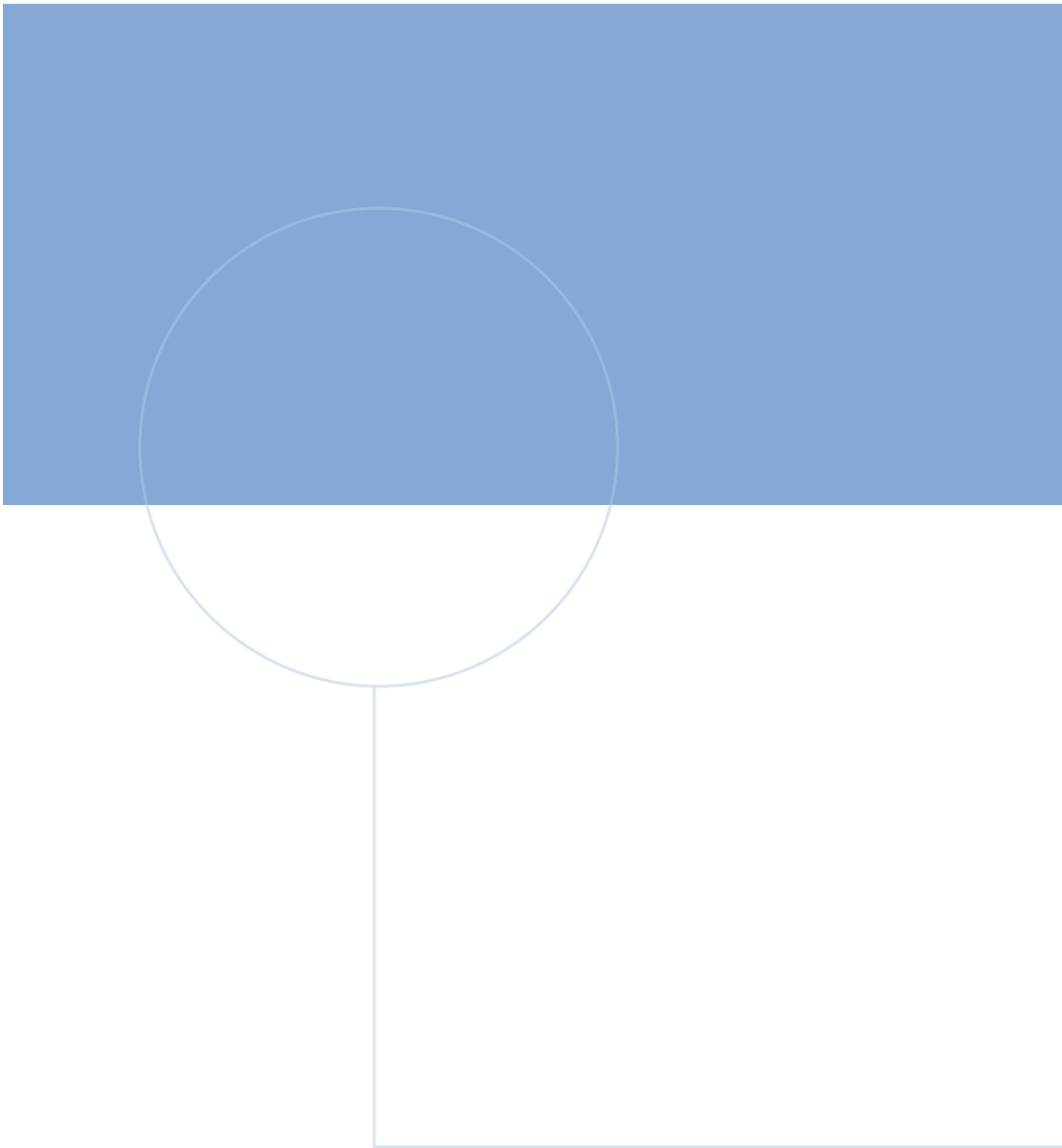

NTNU

Norwegian University of
Science and Technology